# ENRICHMENT OF MCF7 BREAST CANCER CELLS FROM LEUKOCYTES THROUGH CONTINUOUS FLOW DIELECTROPHORESIS

A THESIS SUBMITTED TO
THE GRADUATE SCHOOL OF NATURAL AND APPLIED SCIENCES
OF
MIDDLE EAST TECHNICAL UNIVERSITY

BY

ZEYNEP ÇAĞLAYAN

IN PARTIAL FULFILLMENT OF THE REQUIREMENTS
FOR
THE DEGREE OF MASTER OF SCIENCE
IN
ELECTRICAL AND ELECTRONICS ENGINEERING

DECEMBER 2018

Approval of the thesis:

**ENRICHMENT OF MCF7 BREAST CANCER CELLS FROM LEUKOCYTES THROUGH CONTINUOUS FLOW DIELECTROPHORESIS**

submitted by **ZEYNEP ÇAĞLAYAN** in partial fulfillment of the requirements for the degree of **Master of Science in Electrical and Electronics Engineering Department, Middle East Technical University** by,

Prof. Dr. Halil Kalıpçılar
Dean, Graduate School of **Natural and Applied Sciences** _____

Prof. Dr. Tolga Çiloğlu
Head of Department, **Electrical and Electronics Engineering** _____

Prof. Dr. Haluk Külah
Supervisor, **Electrical and Electronics Engineering, METU** _____

**Examining Committee Members:**

Prof. Dr. Tayfun Akın
Electrical and Electronics Engineering, METU _____

Prof. Dr. Haluk Külah
Electrical and Electronics Engineering, METU _____

Assist. Prof. Dr. Serdar Kocaman
Electrical and Electronics Engineering, METU _____

Prof. Dr. Rengül Çetin Atalay
Graduate School of Informatics, METU _____

Prof. Dr. Uğur Tamer
Analytical Chemistry, Gazi University _____

Date: 27.12.2018

**I hereby declare that all information in this document has been obtained and presented in accordance with academic rules and ethical conduct. I also declare that, as required by these rules and conduct, I have fully cited and referenced all material and results that are not original to this work.**

Name, Surname: Zeynep Çağlayan

Signature :

# ABSTRACT

## ENRICHMENT OF MCF7 BREAST CANCER CELLS FROM LEUKOCYTES THROUGH CONTINUOUS FLOW DIELECTROPHORESIS

Çağlayan, Zeynep
Master of Science, Electrical and Electronics Engineering
Supervisor: Prof. Dr. Haluk Külah

December 2018, 124 pages

Circulating tumor cells (CTCs) are cancerous cells detached from a primary tumor site and enter the bloodstream, causing the development of new tumors in a secondary site. Therefore, their detection in blood is critical to assess the metastatic progression and to guide the line of the therapy. However, the rarity of CTCs in the bloodstream and the lack of suitable detection tool hinders their use as a biomarker in malignancies. Recent advances in microfluidic technologies enabled development of point-of-care (POC) medical diagnostic tools, which offers low cost, rapid, and sensitive analysis of variety of clinical disorders, especially in resource-limited settings. Integration of microfluidic systems with on-chip mechanical and electronic parts have been enabled by Micro-Electro-Mechanical Systems (MEMS) technology, allowing low-cost fabrication of fully integrated microfluidic detection tools. Dielectrophoresis (DEP) is a technique used for separating particles with different sizes and/or dielectric properties. Fabrication of microelectrodes thanks to MEMS technology, allows DEP to be applied in biomedical applications such as manipulation, separation and enrichment of targeted cells from untargeted ones without any labeling. Among numerous applications, rare cell detection from blood occupies an important place in diagnostics of fatal diseases such as cancer. Because of the difficulties in detecting only a few rare cells inside of billions of blood cells in 1 ml blood, rare cell enrichment

from blood becomes essential. Starting from this point of view, enrichment of CTCs from blood by using DEP is decided as the main objective of the thesis.

One of the most critical issue related to successful design of a DEP-based enrichment device is that DEP spectra of the targeted particles should accurately be known. In this content, DEP spectrum analysis method was developed. This study presents an approach for analyzing the dielectrophoretic (DEP) spectra of biological cells without ascertaining their membrane and cytoplasmic properties. For the proof of DEP spectrum investigation of the biological cells with the proposed analysis method, MEMS-based DEP spectrum device was designed. In this design, reciprocal V-shaped planar electrodes were utilized to generate non-uniform electric field in the chamber that holds the cell solution. Fabrication flow for this design was developed and fabrication of these devices was performed. Testing of the proof of concept DEP spectrum devices was carried out with polymoprhonuclear leukocytes and mononuclear leukocytes obtained from 2 different healthy donors and MCF7 cells (human breast adenocarcinoma cell line) for 15 different frequencies in the range from 100 kHz to 50 MHz at 10 $V_{pp}$. The results reveal that at 1 MHz, a significant velocity difference occurs between MCF7 cells (33.99 μm/s) and leukocytes, mononuclear leukocytes (7.9 μm/s) and polymorphonuclear leukocytes (13.82 μm/s), which can be utilized as the working frequency for DEP-based enrichment of MCF7 cancer cells from WBCs as a future work.

Considering the problems associated with the experimental setup, testing and post-processing of the proof of concept devices, the proposed DEP spectrum study was improved. The design of the device used in the improved DEP spectrum study was the same as the proof of concept device, except the gap between the electrodes was increased from 20 μm to 30 μm in order to generate more proper electric field gradient distribution on the surface. Testing of the improved analysis was carried out with leukocytes obtained from single donor and MCF7 cells at 10 $V_{pp}$ for 9 different frequencies in the range from 500 kHz to 10 MHz, by considering the results presented for the proof of concept analysis. The results reveal that there are significant velocity

differences occur between MCF7 cells and leukocytes at 500 kHz, 850 kHz and 1 MHz with the ratios 3.58, 3.37 and 3.12, respectively. With the improved DEP spectrum study, the examination method was automated and approximately 130 MCF7 cells were examined for each frequency value.

By considering the results obtained from DEP spectrum analysis, DEP-based enrichment microfluidic device was designed. In this design, rectangular and evenly spaced planar electrodes rotated with a certain degree relative to the main flow (13º) were utilized at the bottom of parylene microchannel with 1000 μm in wide. The proposed structure performs the separation of the cells focused on the microchannel wall (with the help of hydrodynamic focusing principle) by using the positive dielectrophoresis (pDEP) method in the active DEP area. Fabrication flow for this design was developed and fabrication of these devices was performed. Testing of the fabricated devices was started with the selection of experimental parameters to examine hydrodynamic focusing and expected cell movements. Later, CTC enrichment experiments of the DEP-based enrichment devices were conducted with MCF7 and leukocyte mixture. Recovery rate result for MCF7 cells were calculated as 83.3% at 10 $V_{pp.}$ Cell enrichment factor for these rare cells were calculated as 3, which means the desired rare cell ratio was increased to 3 fold at the output relative to the input.

Keywords: Dielectrophoresis (DEP), Dielectrophoretic Spectrum, MCF7, Leukocyte, Rare Cell Enrichment

# ÖZ

## DİELEKTROFOREZ YÖNTEMİ İLE SÜREKLİ AKIŞ ALTINDA MCF7 MEME KANSERİ HÜCRELERİNİN AKYUVAR HÜCRELERİNDEN ZENGİNLEŞTİRİLMESİ

Çağlayan, Zeynep
Yüksek Lisans, Elektrik ve Elektronik Mühendisliği
Tez Danışmanı: Prof. Dr. Haluk Külah

Aralık 2018, 124 sayfa

CTC'ler birincil tümör bölgesinden koparak kan dolaşımına karışan ve başka bir dokuya yerleşerek ikincil tümörlerin oluşumuna yola açan metastatik kanser hücreleridir. Bu nedenle, CTC'lerin erken tespiti ve tedavi süresince takibi, hastalık seyrini ve uygun tedavi yöntemini belirlemede kritik öneme sahiptir. Ancak CTC sayısının metastazın ilk aşamalarında oldukça az olması ve tespitinin zor olması, bunun biyolojik bir işaret (biomarker) olarak kullanılmasını kısıtlamaktadır. Son yıllarda mikroakışkan teknolojisindeki gelişmeler, özellikle laboratuvar olanaklarının kısıtlı olduğu bölgelerde çeşitli hastalıkların hızlı, hassas ve düşük maliyetli teşhisi için "hasta başı test" (Point-of-Care, POC) cihazlarının geliştirilmesine olanak sağlamıştır. Diğer taraftan, Mikro-Elektro-Mekanik Sistemler (MEMS) teknolojisi mikroakışkan sistemlerin çip-üstü mekanik ve elektronik sistemlerle entegre edilmesine olanak sağlamakta ve kendi başına çalışabilen, düşük maliyetli tam-entegre biyomedikal analiz platformlarının geliştirilebilmesinin önünü açmaktadır. Dielektroforez (DEF), boyutları ve/veya dielektrik özellikleri farklı parçacıkları ayrıştırmakta kullanılan bir tekniktir. MEMS teknolojisi sayesinde üretilebilen mikroelektrotlar, hedeflenen hücrelerin etiketleme olmaksızın yönlendirilmesi, hedeflenmeyen hücrelerden ayrıştırılması ve zenginleştirilmesi gibi biyomedikal

uygulamalarda dielektroforezin uygulanmasına olanak sağlar. Sayısız uygulamalar arasında, kanser gibi ölümcül hastalıkların tanısında kandan ender hücre tespiti önemli bir yere sahiptir. 1 ml kandaki milyarlarca kan hücresi arasından sadece bir kaç adet ender hücrenin tespit edilmesindeki zorluklar nedeniyle, kandan ender hücre zenginleştirmesi vazgeçilmez hale gelmektedir. Bu bakış açısı ile DEF yöntemi kullanılarak kandaki CTC'lerin zenginleştirilmesi tezin amacı olarak belirlenmiştir.

DEF bazlı zenginleştirme cihazının başarılı bir şekilde tasarlanmasıyla ilgili en kritik konulardan biri, hedeflenen parçacıkların dielektroforetik (DEF) spektrumlarının doğru olarak bilinmesidir. Bu kapsamda, DEF spektrum analiz yöntemi geliştirilmiştir. Bu çalışma, biyolojik hücrelerin membran ve sitoplazmik özelliklerini tespit etmeden DEF)spektrumlarını analiz etmek için bir yaklaşım sunmaktadır. Önerilen analiz yöntemiyle biyolojik hücrelerin DEF spektrumlarının araştırılmasının yapılabileceğinin kanıtlanması için MEMS tabanlı DEF spektrum cihazı tasarlanmıştır. Bu tasarımda, hücre çözeltisini tutan haznede düzgün olmayan elektrik alan oluşturmak için karşılıklı V-şekilli düzlemsel elektrotlar kullanılmıştır. Bu dizayn için üretim akışı geliştirilerek, bu çiplerin üretimi yapılmıştır. Bu cihazların tesleri 2 farklı sağlıklı donörden elde edilen polimorfonükleer ve mononükleer lökositler ve MCF7 meme kanseri hücreleri ile 10 $V_{pp}$'te 100 kHz'den 50 MHz'e kadar 15 farklı frekansta gerçekleştirilmiştir. Sonuçlar 1 MHz'de MCF7 hücreleri (33.99 μm/s) ve lökositler, mononükleer lökositler (7.9 μm/s) ve polimorfonükleer lökositler (13.82 μm/s) arasında önemli bir hız farkı olduğunu ortaya çıkarmıştır. Bu frekans değeri, gelecek çalışma olan MCF7 hücrelerinin akyuvar hücrelerinden DEF-tabanlı zenginleştirilmesi için çalışma frekansı olarak kullanılabilir.

Önerilen DEF spektrum çalışması , ilk tasarım için oluşturulan deney düzeneği, test ve test sonrası incelemelerde karşılaşılan sorunlar göz önüne alınarak geliştirilmiştir. Geliştirilmiş DEF spektrum çalışmasında kullanılan cihazın tasarımı, yüzey üzerinde daha uygun elektrik alan gradyan dağılımı oluşturmak için elektrotlar arasındaki boşluğun 20 μm'den 30 μm'ye yükseltilmesi haricinde, konsept cihazın tasarımı ile aynıdır. İyileştirilmiş analizin test edilmesi, ilk aşamada sunulan sonuçlar göz önünde

bulundurularak, tek donörden elde edilmiş lökosit ve MCF7 hücreleri ile 10 $V_{pp}$'te 500 kHz'den 10 MHz'e kadar 9 farklı frekans için gerçekleştirilmiştir. Sonuçlar, MCF7 hücreleri ile akyuvarlar arasında 500 kHz'de, 850 kHz'de ve 1 MHz'de, sırasıyla 3.58, 3.37 ve 3.12 oranlarında önemli hız farklılıkları olduğunu ortaya koymaktadır. Geliştirilen DEF spektrum çalışması ile inceleme yöntemi otomatize edilmiş olup, her frekans değeri için yaklaşık 130 MCF7 hücresi incelenmiştir.

DEF spektrum analizinden elde edilen sonuçlar göz önüne alınarak DEF-bazlı mikroakışkan zenginleştirme cihazı tasarlanmıştır. Bu tasarımda, ana akışa göre belirli bir derece (13º) ile döndürülen dikdörtgen ve eşit aralıklı düzlemsel elektrotlar, 1000 µm genişliğindeki parilen mikrokanalın tabanında kullanılmıştır. Önerilen yapı, aktif DEF bölgesinde pozitif dielektroforez (pDEF) yöntemini kullanarak mikrokanal duvarına (hidrodinamik odaklama prensibini yardımıyla) odaklanan hücrelerin ayrıştırılmasını gerçekleştirmektedir. Bu dizayn için üretim akışı geliştirilerek, bu çiplerin üretimi yapılmıştır. Hidrodinamik odaklamayı ve beklenen hücre hareketlerini incelemek için, fabrikasyonu tamamlanan cihazların test edilmesi deneysel parametrelerin belirlenmesine dair testler ile başlatılmıştır. Daha sonra DEF-bazlı zenginleştirme cihazlarının CTC zenginleştirme deneyleri, MCF7 ve lökosit karışımı ile gerçekleştirilmiştir. MCF7 hücreleri için geri kazanım oranı, 10 $V_{pp}$'te %83.3 olarak hesaplanmıştır. Bu nadir hücreler için zenginleştirme faktörü 3 olarak hesaplanmıştır. Bu değer, nadir hücre oranının kanal girişine göre çıkışta 3 misline yükseltildiği anlamına gelmektedir.

Anahtar Kelimeler: Dielektroforez (DEF), Dielektroforetik Spektrum, MCF7, Lökosit, Ender Hücre Zenginleştirilmesi

To my family

## ACKNOWLEDGMENTS

I always want to be a part of developing innovative technologies as an electronics engineer for the intersection of electronics and biology. For this reason, being a part of the BioMEMS family was a very important step for me. Because of giving me this chance, I would like to express my special thanks to Prof. Dr. Haluk Külah. I would also like to convey my gratefulness to my thesis advisor, Prof. Dr. Haluk Külah for his endless support, trust and guidance during my undergraduate and graduate studies.

I would like to thank to my jury members, Prof. Dr. Tayfun Akın, Prof. Dr. Rengül Çetin Atalay, Prof. Dr. Uğur Tamer and Assist. Prof. Serdar Kocaman. Moreover, I am grateful to Prof. Dr. Tayfun Akın for his efforts for METU MEMS Research and Applications Center and making it possible to study MEMS in Turkey. I would also like to thank Prof. Dr. Rengül Çetin Atalay and Postdoc Deniz Cansen Kahraman of her research group, CanSyL (Cancer System Biology) Laboratory, for collaborating with us and providing liver cancer cell lines.

I would like to thank The Scientific and Technological Research Council of Turkey (TUBITAK) for the scholarship support for me.

I am grateful to Dr. Yağmur Demircan Yalçın for sharing her knowledge and experience with me whenever I need and Taylan Töral for guiding me through the MEMS fabrication stages. I am grateful to all METU-MEMS Center staff for their kind helps in cleanroom, especially many special thanks to Orhan Akar for sharing his deep knowledge and experience on microfabrication. I am thankful to all my friends in BioMEMS and PowerMEMS groups.

I would like to express my deepest thankfulness to my mother, Ayşe Çağlayan, and my father, Süreyya Çağlayan for their support, trust and care for my whole life. Finally, a debt of gratitude is also owed to my dearest, Atabey Arslan for his endless love.

## TABLE OF CONTENTS

## LIST OF TABLES

TABLES

## LIST OF FIGURES

FIGURES

## LIST OF ABBREVIATIONS

| | |
|---|---|
| **DEP** | Dielectrophoresis |
| **pDEP** | Positive Dielectrophoresis |
| **nDEP** | Negative Dielectrophoresis |
| **CTC** | Circulating Tumor Cell |
| **RBC** | Red Blood Cell |
| **WBC** | White Blood Cell |
| **PWBC** | Polymorphonuclear White Blood Cell |
| **MWBC** | Mononuclear White Blood Cell |

# CHAPTER 1

# INTRODUCTION

Cancer is one of the most fundamental health problems in the world and has been the second cause of death in the United States. In 2012, 8.2 million people died from cancer with approximately 14.1 million new cases [1]. The number of deaths from cancer in 2030 is estimated to reach 13.2 million [2].

Systemic disease is the cause of 90% of deaths due to cancer [3]. Systemic spread of cancer refers to the development of metastasis by arising secondary tumors from the cells originating from the initial tumor side. For this reason, numerous studies have investigated metastatic cancer cells in detail. These cells consist of tumor cells located in the bone marrow and circulating tumor cells (CTCs) available in the bloodstream. The examination of disseminated tumor cells that are located in bone marrow is quite difficult because it requires aspiration of the bone marrow, which is an invasive and a highly painful process for patients [3]. Therefore, it is much easier to analyze CTCs in determining the level of metastasis. CTCs in bloodstream, originated from primary or metastatic tumor regions, are the cells that have acquired the properties that provide migration to the blood circulation. These cells can settle into another tissue in the body and cause the formation of secondary tumors and the spread of cancer to different tissues in the body. The illustration of CTCs forming metastasis is shown in Figure 1.1.

The rate of tumor cell release, the rate of separation and moving away of individual tumor cells or clusters from the primary tumor region, is still unknown. Experimental models for determining the rate of tumor cell release have shown that millions of cancer cells are continuously distributed to the body, but only a portion of these tumor cells can reach a distant organ, escape from the immune system and systemic therapy,

and eventually form a metastasis [4]. Therefore, early diagnosis and specification of circulating tumor cells (CTC) is of great importance to monitor and prevent the development of metastasis. In other words, early detection of CTCs in blood provides the reduction of cancer-related mortality and shortening the treatment process. Therefore, it is important to conduct regular, real-time and quantitative CTC analyzes of cancer patients in order to make cancer treatment effective. The number of critical CTC showing that metastasis occurred varies according to the type of cancer. For example, in patients that have metastatic breast cancer and prostate cancer with a CTC of 5 in 7.5 ml and more than 3 CTCs in metastatic colon cancer, the patient's chance of survival is reduced [5].

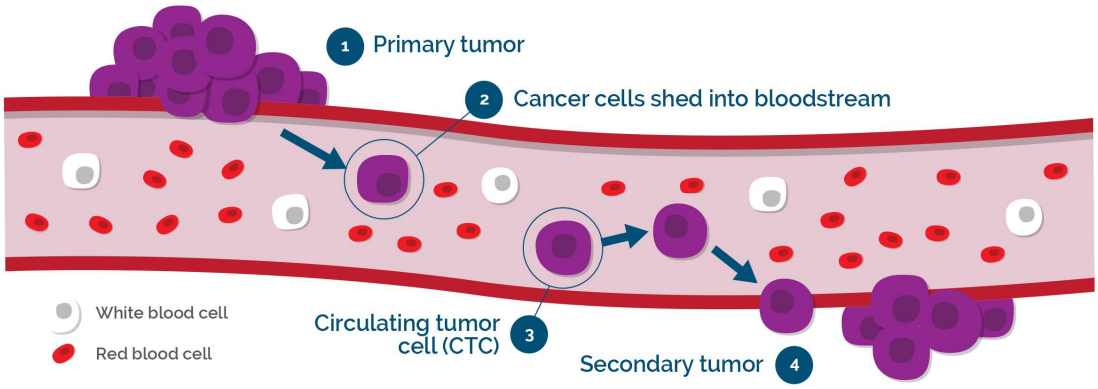


*Figure 1.1.* The illustration of CTCs forming metastasis [6]

## 1.1. CTC Enrichment

Nowadays, CTC counting is performed using a variety of high cost methods based on continuous flow cytometer principle. In these methods, called FACS (fluorescent activated cell sorting) and MACS (magnetic activated cell sorting), the cells must be marked as fluorescent or magnetic [7]. Although these techniques provide high-throughput screening, the cells do not remain viable, require biological marking, are

not portable, and cannot be applied in areas with limited resources due to equipment costs and specialist personnel requirements.

The greatest difficulty in isolating CTCs is that they are in very low concentrations (1-100 cells/ml) compared to other cell types that are available in blood [8]. Therefore, it is necessary to selectively enrich tumor cells and/or remove peripheral blood cells systematically to detect CTCs in the bloodstream of a cancer patient. To date, more than 40 methods have been developed for CTC detection and new methods are continuously being published [9]. CTC enrichment and detection methods are classified into two main groups according to whether they use the biological properties (viability, cell surface protein expression, invasive capacity) or physical properties (size, density, deformability, electric charges) of the cells (Figure 1.2).

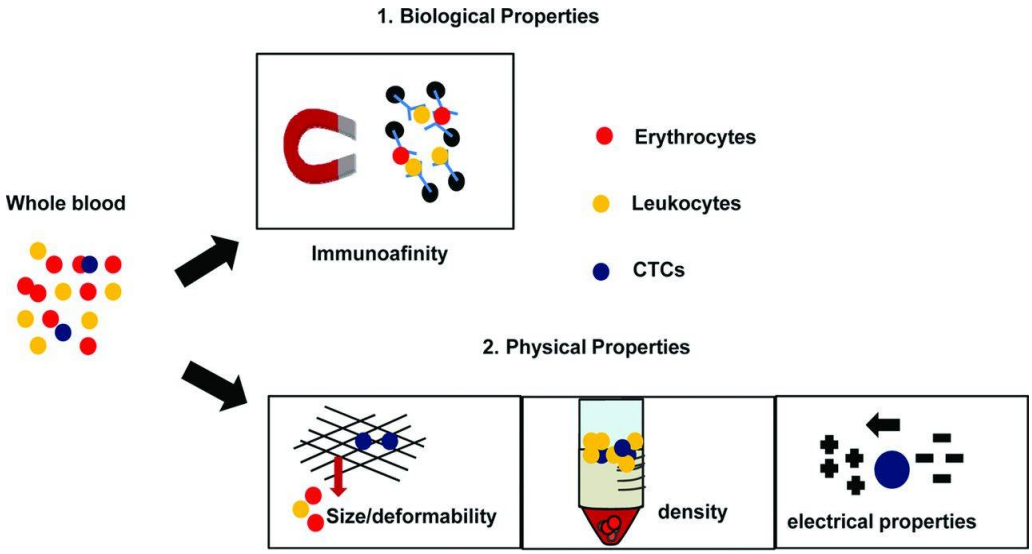


*Figure 1.2.* Methods used in CTC isolation form whole blood [10]

### 1.1.1. Methods Based on Biological Properties

Biological properties of the cells are utilized in immunological procedures with antibodies against either tumor-associated antigens, which is referred as positive

selection, or common leukocytes antigen CD45, which is referred as negative selection [11]. For example, epithelial tissue-derived CTCs have epithelial cell adhesion protein (EpCAM) in the cell membrane. EpCAM is used as a biomarker in the detection of CTCs with epithelial tissue origin. However, as there is no EpCAM in non-epithelial tissue-derived CTCs (such as melanoma, brain cancer, sarcoma), it cannot be used alone in the detection of CTCs. In addition, EpCAM expression can be completely lost during epithelial to mesenchymal transition (EMT), which occurs during the first stage of metastasis and enables the cells to be separated from the tumor and mixed into the bloodstream. Therefore, in the detection of CTC cytokeratin (CK) expression, the presence of cell nucleus and CD45 (leukocyte specific antigen) as well as different markers that discriminate CTCs from other peripheral blood cells are also looked at [12]. These four criteria (EpCAM (+), CK (+), CD45 (-) and the presence of cell nucleus) are recognized as gold standards approved by the FDA for the detection of CTC with current technology.

In recent years, the FDA-cleared CellSearch™ system has gained significant attention among the existing EpCAM-based CTC detection strategies [13]. In this system, CTCs are labeled with anti-EpCAM labeled magnetic particles to provide immuno-magnetic separation. Subsequently, cells are stained for detection of cytokeratin and CD45 by immuno-fluorescent staining, for cell nucleus detection by fluorescent staining. Cells with EpCAM (+), CK (+), CD45 (-) and cell nuclei are visually determined and counted by an operator under a fluorescence microscope. The workflow of the CTC enumeration by CellSearch is given in Figure 1.3. Although CellSearch can be seen as an effective method for the detection of metastases from various types of cancer, differences arising from the operator may occur. Furthermore, the method can only be used for the detection of EpCAM (+) cells because the first step of the magnetic separation method depends on the presence of EpCAM. Furthermore, the method requires a lot of fluorescent staining, which increases the cost and removes the method from practicality. Cells separated by CellSearch do not allow for advanced molecular analysis of cancer cells as they lose their vitality. Other

popular EpCAM targeting assays include MagSweeper, AdnaTest, and IsoFlux [14], [15], [16].

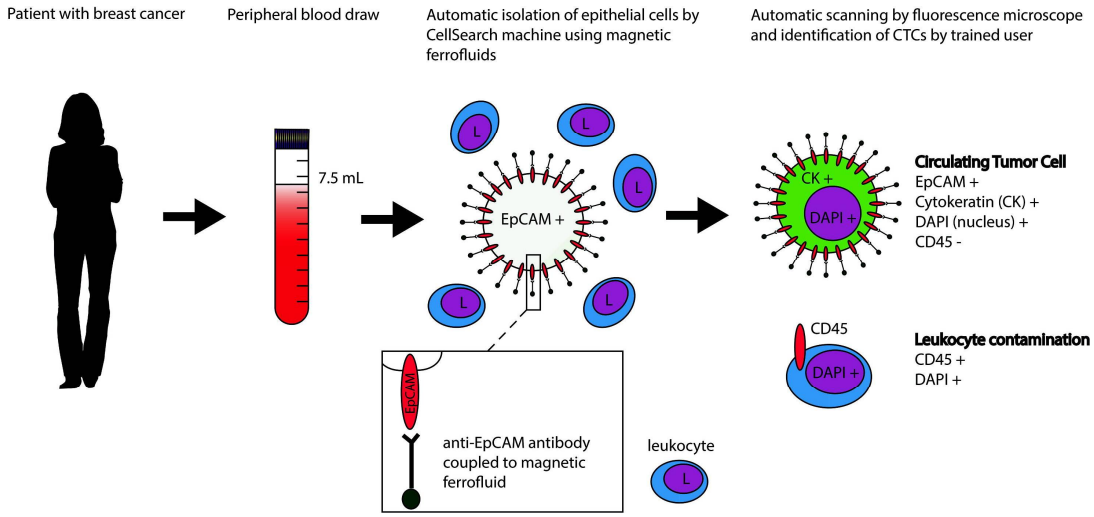


*Figure 1.3.* Workflow of CTC enumeration by CellSearch [17]

### 1.1.2. Methods Based on Physical Properties

Density gradient centrifugation is a standard method used to separate components of blood based on differences in the sedimentation coefficients of cells. With the application of a liquid medium to the whole blood and then centrifugation, cells will be collected at different levels according to their density. While red blood cells and polymorphonuclear white blood cells migrate to the bottom, CTCs and mononuclear white blood cells stay at the top and form the buffy coat. For density-based isolation OncoQuick® (Greiner Bio-One) and Percoll, Ficoll-Hypaque® (GE Healthcare Life Sciences) are commonly used density gradient media [18][18], [19], [20]. Although this technique has been used for a long time in laboratories and provides a conventional approach for isolating blood components, it has some drawbacks. For example, due to aggregate formation as a natural consequence of the method, some tumor cells may be lost in plasma section or at the bottom part of the gradient. In

general, methods based on density centrifugation technique are reliable and inexpensive. On the other hand, the loss of large CTCs and the migration of CTCs at the bottom because of aggregation are the major problems of this technique. In addition to them, elimination of white blood cells is not easy. Due to all these reasons, another enrichment strategy should be combined with centrifugation [10].

Another method for CTC isolation based on physical properties of the cells is microfiltration. Microfiltration techniques aim to capture targeted tumor cells by utilizing an array of microscale barriers. In order to achieve this goal, the size and/or deformability differences between the targeted and non-targeted cells are used. For CTC enrichment, many microfiltration devices have been proposed. While some of them are on the market, some of them are still in prototype and pre-clinical research steps. Membrane microfilters, developed in the content of microfiltration based CTC enrichment technique, are consist of a semi-permeable membrane with a 2D micropore array. It has been demonstrated that in order to successfully retain CTCs, optimum pore size of a membrane should be 8 μm [21]. Dead flow fractionation, isolation by size of epithelial tumor cells (ISET), Metacell filtration device and ScreenCell Cyto all benefit from the size information of the cells to provide selection of CTCs [22]–[26]. These size-based methods provide the separation of CTCs in a short time. However, successful results are obtained for the CTCs that are larger in size than other peripheral blood cells. These methods fail to isolate CTCs that are similar in size and/or deformability to other blood cells and especially to leukocytes. Another important disadvantage related with the microfiltration techniques is that releasing the collected CTCs from the membranes for further analyses is difficult and problematic [8]. Although the recovery rates are high around 90%, further operation is compulsory since the final purity is usually 10% or less which is absolutely not enough for downstream applications. The main drawbacks of the filtration-based enrichment methods are differences between the CTC dimensions, formation of clusters, the clogging of the membrane microfilters and problems associated with the collecting the cells on the membrane for the further analysis [10].

### 1.1.3. Microfluidic Platforms

Microfluidic platforms have transformed the whole healthcare system and found remarkable applications. Some of these applications can be listed as point-of-care diagnosis, chemical and biological analysis, DNA sequencing, fertility analysis, infectious disease diagnostics, cell sorting, and tissue engineering. One of the most important features of the microfluidic platforms is that they enable enrichment of live targeted rare cells which implies further downstream analysis can easily be done with either microscopic, molecular or cellular techniques. Moreover, combination of isolation and detection strategies in one device and formation of a point-of-care CTC device are now possible thanks to microfluidic platforms. The biggest challenge encountered with the microfluidic platforms is the examination of the large volumes of blood samples in order to enrich CTCs. The combination of the device with micro-level fluidic channels and fluid dynamics allow for efficient capturing of CTCs if the design and format of the microfluidic platform arranged properly [27].

The isolation strategy utilized in microfluidic platforms can be based on differences in physical properties between the targeted CTCs and non-targeted blood cells. Size-based filtration, size-based streamline sorting and dielectrophoresis (DEP) separation are some examples of available strategies. A number of proposed microfluidic devices to enrich CTCs have been developed using the principle that CTCs are larger in size than other peripheral blood cells [28]. As explained earlier, this principle brings the inadequate results when heterogeneity in CTC size is considered. Moreover, if the operating conditions used in the device are not carefully adjusted, problems such as damage or loss of CTCs may be encountered due to the shear stress created during the cell passage from small openings. Another size-based filtration technique used in CTC enrichment is streamline sorting. In this method, cells with different sizes go through different streamlines in the microfluidic platform thanks to generated fluidic forces. With the formation of different streamlines, the bulk-flow can be separated to collect each streamline from different output. The main advantage of this technique is that by eliminating the physical constrictions, the reduction in the shear forces that the cells

are exposed to minimizes the cell damage and loss. Furthermore, these devices provide high throughput since they typically work at high flow rates. On the other hand, the fluidic forces forming the basis of the enrichment should be precisely controlled in these kind of devices. This feature often requires dilution of the patient's blood sample with a carrier fluid with well-known properties. As a natural consequence of this situation, the volume of the sample that can be examined at once is small. Although this system makes generic use possible and works equally for blood samples from different patients, the enrichment efficiency is limited.

*Dielectrophoresis (DEP) Separation*

Similar to the physical properties like deformability and cell size differences between CTCs and blood cells, differences in electrical properties between them can also be used to enrich CTCs from other blood cells. Electrical properties of the cells are also intrinsic properties of them and depend on the cell membrane, cell size and cellular composition. Enrichment of CTCs can be easily accomplished by applying non-uniform electric field around the separation region thanks to formation of different polarization induced dielectric forces. Dielectrophoresis (DEP) is technique that is utilized to separate CTCs from blood cells with the generation of different dielectrophoretic forces exerted on the cells with dissimilar dielectric properties in a non-uniform electric field [29]. As explained, DEP-based separation techniques directly depends on the intrinsic dielectric properties of the cell types and the differences between them; therefore, they enable conducting the separation in a label-free manner. In order to utilize a DEP-based enrichment system dielectric properties of the cells that are going to be separated must be known. In the literature, plasma membrane capacitance and conductance values are measured in alternating electric field gradients and reported as cell dielectric measurements. These dielectric properties are then utilized to enrich CTCs from peripheral blood cells.

DEP technique has motivated developing new approaches for the enrichment of cancer cells from blood cells by utilizing electrical properties. As an example, the use of

interdigitated gold electrodes in the separation of cancer cells from blood cells can be given [30]. ApoStream™ system (ApoCell) was the first commercial tool that is based on DEP field flow fractionation technique (Figure 1.4). In this system, in order to reduce the levitation of the cells and to guarantee the cells will remain in the active DEP region the sample is provided from the bottom of the chamber at a low flow rate. With the introduction of cells into the active DEP region, while the cancer cells are pulled towards to the bottom of the chamber the other cells are repelled by the effect of DEP force along the electrodes [31]. This method needs an initial enrichment process prior to the above explained step. For this system, recovery rate and viability results are more than 70% and over 97%, respectively. On the other hand, the purity is smaller than 1%, even though this value can be increased with the addition of extra enrichment stages.

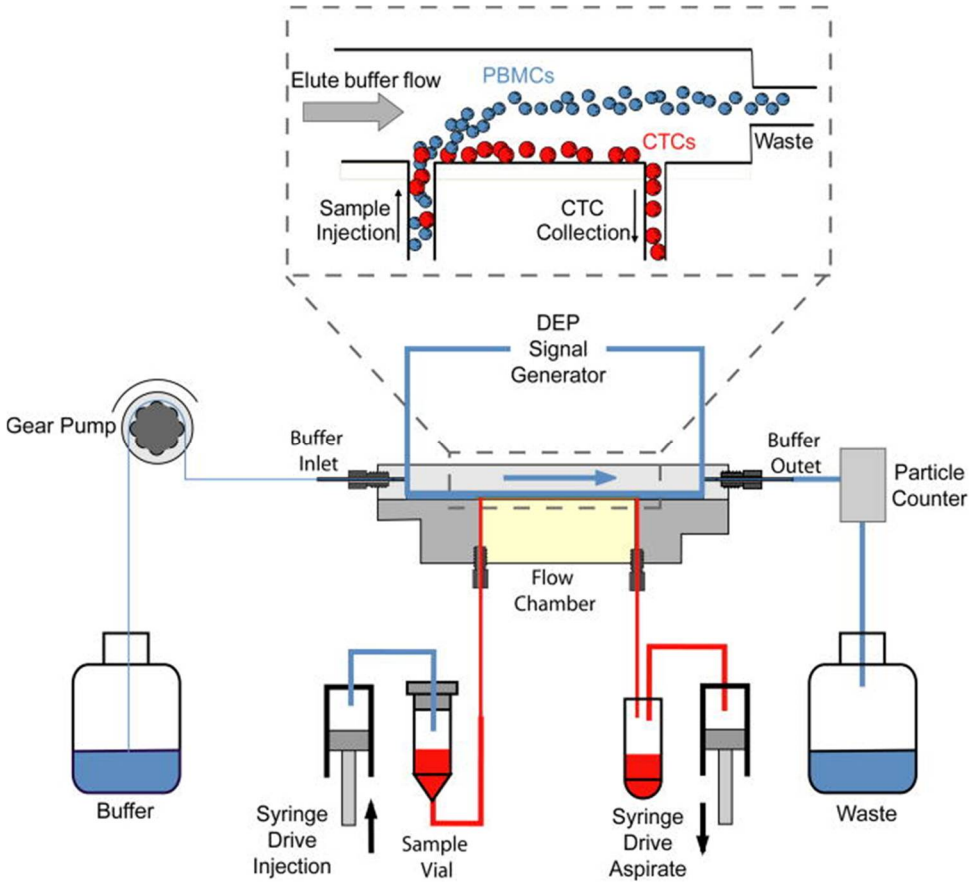


*Figure 1.4.* Schematic view of the ApoStream™ device [31]

Another use of DEP-based microfluidic device brings DEP forces with the light application in order to separate CTCs from blood cells. With the application of this method, cancer cells are isolated from leukocytes with a purity of up to 82% [32]. Contactless DEP (cDEP) is another available DEP-based enrichment technology. In this method, conventional metallic electrodes to generate non-uniform electric field gradients were replaced by fluidic electrode channels. This design was used to isolate cervical carcinoma cells from the concentrated red blood cells. According to the experimental results, recovery rate of the system was 64.5% [33]. Another application was developed by utilizing DEP-Field Flow Fractionation (DEP-FFF) to run continuously. Separation of spiked cancer cells (MDA-MB-435 (human melanoma), MDA-MB-231) from other blood cells was performed with this system and approximately 75% recovery rate was achieved. In addition, results for the separation of cancer cells obtained from cancer patients was also submitted. According to the results, the proposed system can examine 10 ml patient sample in less than an hour [34].

As a label-free technique, DEP exploits the intrinsic dielectric property differences between the targeted and non-targeted cell types. Therefore, in order to develop a successful DEP-based CTC enrichment device, dielectric properties of the cells intended to be separated should be known. According to different dielectrophoretic responses of the cells, formation of the optimum electric field-induced devices is crucial for DEP-based CTC enrichment [29].

DEP-based isolation methods provides high purity of collected CTCs. Since these methods are based on the manipulation and isolation of the cancer cells as a label-free manner in an electrical way, their translations to the clinical applications are easy. The most advantageous properties of DEP-based methods are that they provide single cell resolution with high cell viability and recovery ratios. The main pitfall related to these techniques is the changes in membrane and cytoplasmic permittivity and conductivity values during the enrichment process. However, to eliminate this problem enrichment process can be adjusted to reduce these alterations and cell to cell interactions. In brief,

the disadvantages associated with DEP-based enrichment methods can be largely eliminated by means of microfluidic technology.

### 1.2. Research Objectives and Thesis Organization

CTCs are rare and appear at an estimated level of one against the background of millions ($10^6$–$10^7$) of other blood cells [4]. An ideal CTC detection method should be able to distinguish heterogeneous CTC populations at high sensitivity and selectivity, give results in a short time, and have a quantitative result without requiring labeling. In addition, the cells should remain viable for further molecular analysis at the end of separation, and the proposed system should be able to be operated at low cost, attainable and portable, without the need for qualified personnel.

The main goal of this thesis is to generate a DEP-based MEMS device to enrich rare cells from peripheral blood cells with high sensitivity, selectivity and throughput. In order to develop a successful DEP-based CTC enrichment device, cell response to the applied non-uniform electric field should be characterized. This step is critical because it provides an accurate determination of the separation strategy to be used in the DEP-based enrichment device.

To achieve this main goal, following studies are conducted:

- Designing a DEP spectrum device to obtain DEP spectra of different cell types within the specified frequency range
- Electrical analysis of the proposed DEP spectrum device with COMSOL Multiphysics® 5.3 software by using finite element model (FEM) simulations
- Development of the MEMS fabrication flow and the MEMS fabrication of the DEP spectrum device
- Testing the fabricated DEP spectrum devices with the MCF7 (human breast adenocarcinoma cell line) and leukocytes
- Analyzing the DEP spectra of MCF7 cells and leukocytes

- Designing a DEP-based enrichment microchannel according to the DEP spectra results of the MCF7 cells and leukocytes
- Electrical analysis of the proposed DEP-based enrichment microchannel with COMSOL Multiphysics® 5.3 software by using finite element model (FEM) simulations
- Development of the MEMS fabrication flow and the MEMS fabrication of the DEP-based enrichment microchannel
- Testing of the DEP-based enrichment microchannel with MCF7 and leukocyte mixture
- Cell counting and computing recovery rate and enrichment factor results of the DEP-based enrichment microchannel

Thesis is divided into 5 chapters as follows:

Chapter 2 explains the theory behind the DEP briefly. Chapter 3 explains dielectrophoretic (DEP) spectrum analysis. The chapter starts with the device generated for the proof of concept. In this content, design, simulation, fabrication and experimental steps of the corresponding device are explained in detail. Then, same steps will be explained for the final DEP spectrum devices. Chapter 4 presents the generated DEP-based enrichment device. According to the results obtained in Chapter 3, design of the DEP enrichment unit is explained. Then, simulation, fabrication and testing of this device are given. Chapter 5, the last chapter, summarizes the overall work and highlights the key points of the thesis. The chapter is concluded with the governing idea, future works, and suggestions on the related research topic.

# CHAPTER 2

# THEORY OF DIELECTROPHORESIS

## 2.1. Dielectrophoretic (DEP) Force

A particle experiences a net force named as dielectrophoretic (DEP) force in a non-uniform electric field. In the case of a uniform electric field created by AC-current there is no net force. The dielectrophoretic force (DEP) force exerted on a spherical particle is defined by the equation:

$$F_{DEP} = 2\pi r^3 \varepsilon_0 \varepsilon_m Re(F_{CM}) \nabla |E|^2 \tag{2.1}$$

where $r$ is the radius of the particle, $\varepsilon_0$ is the permittivity of the vacuum, $\varepsilon_m$ is the relative permittivity of the suspending medium and $E$ is the amplitude of the electric field. $\nabla |E|^2$ is the gradient of electric field squared term. The non-uniformity of the electric field is given with $\nabla |E|^2$ term. $Re(F_{CM})$ is the real part of the Clausius-Mosotti factor of the particle. The Clausius Mosotti factor, $F_{CM}$, is given as:

$$F_{CM} = \frac{\varepsilon_p^* - \varepsilon_m^*}{\varepsilon_p^* + 2\varepsilon_m^*} \tag{2.2}$$

where $\varepsilon_p^*$ and $\varepsilon_m^*$ are the complex permittivities of the particle and the suspending medium, respectively. $\varepsilon_p^*$ and $\varepsilon_m^*$ are formulized as:

$$\varepsilon_p^* = \varepsilon_0 \, \varepsilon_P - j \frac{\sigma_P}{w}, \tag{2.3}$$

$$\varepsilon_m^* = \varepsilon_0 \, \varepsilon_m - j \frac{\sigma_m}{w}. \tag{2.4}$$

In Equation 2.3, $\varepsilon_0$ is the permittivity of the vacuum, $\varepsilon_p$ is the relative permittivity of the particle and $\sigma_P$ is the electrical conductivity of the particle. In Equation 2.4, $\sigma_m$ corresponds to the electrical conductivity of the suspending medium. In both equations

(Equation 2.3 and Equation 2.4), $w$ represents the angular frequency ($w = 2\pi f$) and is $j$ the imaginary number ($\sqrt{-1}$). Particles, for example cells and bacteria, have a conductivity from the mobile ions in their structure. The medium that these particles are suspended is generally a conducting electrolyte. In the case of AC field application, these conduction losses are placed in the complex permittivity expression.

Given equations reveal the following consequences:

- If the created electric field is uniform, the DEP force equals to zero ($\nabla E = 0$).
- DEP force can be created by using AC or DC field because it depends on the square of the generated electric field magnitude.
- The DEP force is directly proportional to particle volume. In other words, while other factors that have effects on the created DEP force remaining constant, the DEP force exerted on the particle would be greater as the particle volume increases.
- The DEP force is controlled by the sign and the magnitude of the $Re(F_{CM})$, Clausius-Mosotti factor of the particle.
- The DEP force is proportional to $\varepsilon_m$, the dielectric permittivity of the suspending medium.
- Generally, the DEP force vector is not parallel to the electric field vector, instead it is aligned with the gradient of the electric field intensity [35].
- In the control of gradient of electric field squared term ($V^2/m^3$), utilized electrode geometry is a key experimental parameter. Acquiring $10^{12}$ $V^2/m^3$ for this term with suitable microelectrode configuration, indicates that an adequate DEP force generated on the biological cells [36].

The charges on the particle surface and the charges in the suspending medium at the particle-medium surface are redistributed with the application of non-uniform electric

field. Complex permittivity of the medium and particle ($\varepsilon_m^*$ and $\varepsilon_p^*$) indicates the effect of polarizability and they should be evaluated in order to examine the DEP force exerted on the particle. If the particle is more polarizable than its suspending medium, more charges are collected at particle surface, near the particle-medium interface. This situation implies that complex permittivity of the particle is larger than the complex permittivity of the medium ($\varepsilon_p^* > \varepsilon_m^*$). For this case, $Re(F_{CM})$ will be positive as can be seen from Equation 2.2. Positive $Re(F_{CM})$ indicates that the cell is attracted toward high electric field gradient under the positive-DEP (pDEP) force (Figure 2.1(a)-(c)).

If particle is less polarizable than the medium, more charges are collected in the medium, near the particle-medium interface. In this case, complex permittivity of the particle is smaller than the complex permittivity of the medium ($\varepsilon_p^* < \varepsilon_m^*$). Therefore, $Re(F_{CM})$ is negative indicating that the particle is attracted toward low electric field gradient and repelled from high electric field gradient under the negative-DEP (nDEP) force (Figure 2.1(b)-(d)).

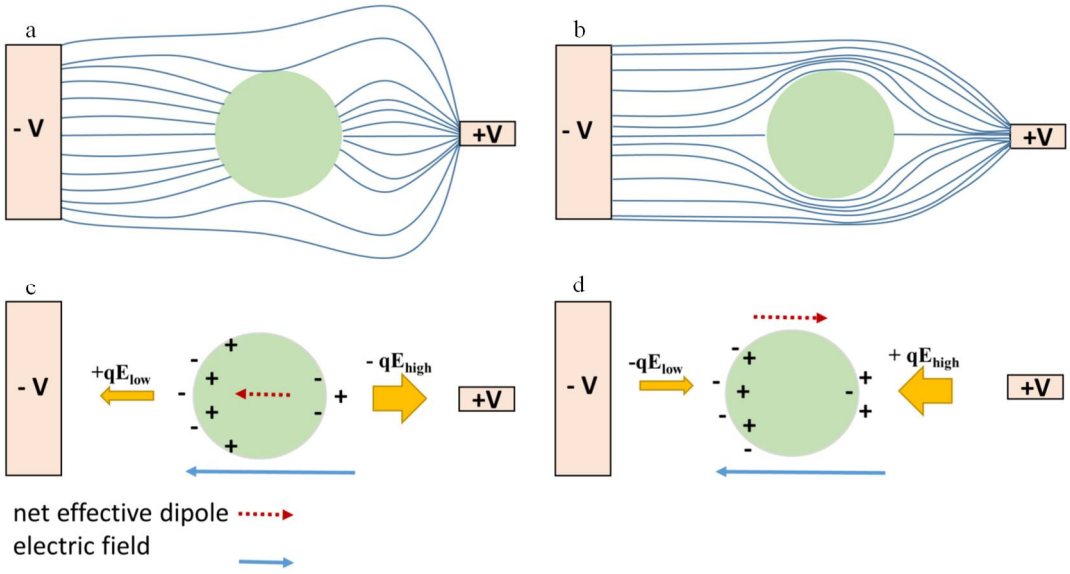


*Figure 2.1.* Schematic diagram that shows the cell and its suspending medium under the effect of positive-DEP (a),(c) and negative-DEP (b), (d) [37]

The created DEP force is equal to zero at a certain frequency called as *crossover frequency* or *zero force frequency* [38]. At crossover frequency particles do not move since there is no DEP force present. This situation occurs when $Re(F_{CM})$ becomes zero ($Re(F_{CM}) = 0$). Zero $Re(F_{CM})$ indicates that the real parts of the complex permittivity values of the medium and the particle are equal to each other.

The direction of the created DEP force does not depend on the voltage applied. In other words, altering the voltage does not affect the direction of the generated DEP force. On the other hand, frequency of the applied non-uniform electric field can be utilized in changing the direction of the DEP force acting on the particles. Frequency alters relative polarizability of the particle and suspending medium and by using this DEP force direction can be reversed. As explained above, positive dielectrophoresis and negative dielectrophoresis depend on Clausius-Mossotti (CM) factor. When this factor is examined carefully, at frequencies below ~50 kHz,

$$Re(F_{CM}) \approx \varepsilon_m \left( \frac{\sigma_p - \sigma_m}{\sigma_p + 2\sigma_m} \right), \tag{2.5}$$

and for frequencies above ~50 MHz,

$$Re(F_{CM}) \approx \varepsilon_m \left( \frac{\varepsilon_p - \varepsilon_m}{\varepsilon_p + 2\varepsilon_m} \right). \tag{2.6}$$

At low frequencies, DEP behavior of the particle is controlled by the conductive properties of the particle and the suspending medium (Equation 2.5). At high frequencies, permittivity values of the particle and medium controls the DEP behavior of the particle (Equation 2.6) [36]. At the intermediate frequencies, the polarity (nDEP or pDEP) and the magnitude of the DEP force are established by both the dielectric and conductive properties of the particle and the suspending medium. The relationship between $Re(F_{CM})$ and signal frequency is govern by two main cases. In the first case, $\varepsilon_p > \varepsilon_m$ and $\sigma_p < \sigma_m$ conditions make $Re(F_{CM})$ positive at high frequencies and negative at low frequencies. In the second case, $\varepsilon_p < \varepsilon_m$ and $\sigma_p > \sigma_m$ conditions

make $Re(F_{CM})$ negative at high frequencies and positive at low frequencies. For these two main conditions, the change of $Re(F_{CM})$ with signal frequency is shown in Figure 2.2.

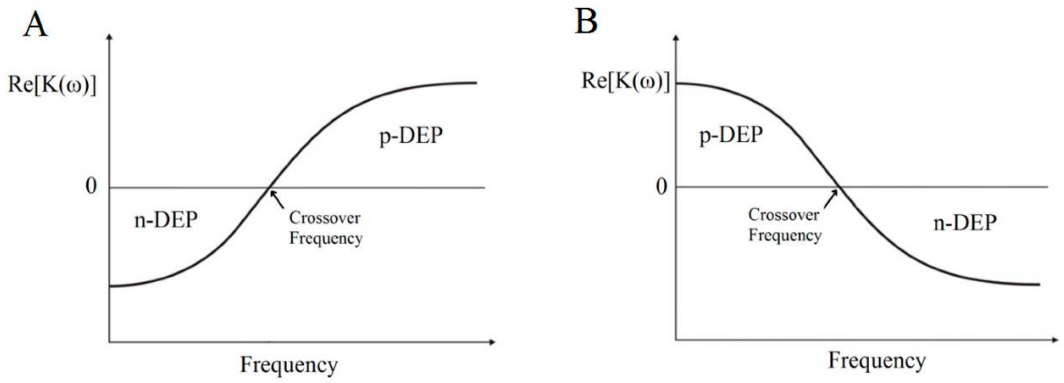


*Figure 2.2.* DEP spectrum (Re($F_{CM}$) vs. frequency) for a polarizable particle. (A) for $\varepsilon_p > \varepsilon_m$ and $\sigma_p < \sigma_m$ ; (B) for $\varepsilon_p < \varepsilon_m$ and $\sigma_p > \sigma_m$ [38]

## 2.2. Dielectrophoretic Modelling of Single-Shell Spherical Biological Cells

Single-shell model is utilized to model a spherical cell that has a cytoplasm and a cell membrane surrounding it, in a simplest manner. Most of the eukaryotic cells such as mammalian cells are examples of spherical cells. With the help of this model, the Clausius-Mossotti factor for a particle is found by examining the effective value for the relative complex permittivity ($\varepsilon_p^*$) of the particle. Most of the particles, especially the biological ones, are in heterogeneous structure. The effective value for the relative complex permittivity ($\varepsilon_p^*$) of the particle, mentioned above, corresponds to the calculated complex permittivity ($\varepsilon_p^*$) for the simplified model. This implies that, conceptually there is no difference between the heterogeneous (real) particle and the model homogeneous particle and replacement of one particle with the other one in electric field would create no difference in the surrounding medium. Modeling of a nucleated cell to a homogenous and simple spherical particle can be seen from Figure 2.3.

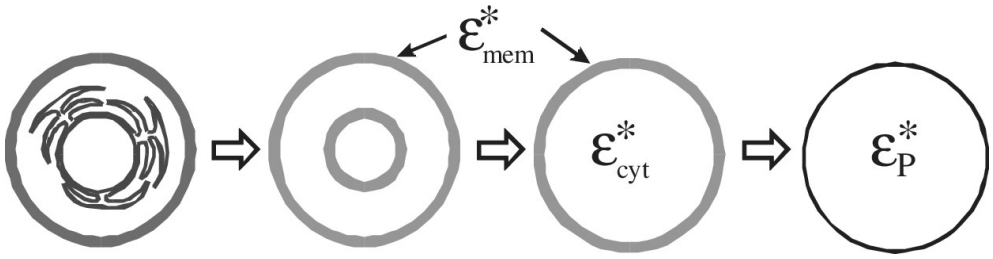


*Figure 2.3.* Schematic representation of conversion from a nucleated cell to a simplified homogenous spherical particle with effective complex permittivity [36]

According to the single-shell model, the effective complex permittivity is given by the equation:

$$\varepsilon_p^* = \varepsilon_{mem}^* \left[ \frac{(R/[R-d])^3 + 2\left(\frac{\varepsilon_{cyt}^* - \varepsilon_{mem}^*}{\varepsilon_{cyt}^* + 2\varepsilon_{mem}^*}\right)}{(R/[R-d])^3 - \left(\frac{\varepsilon_{cyt}^* - \varepsilon_{mem}^*}{\varepsilon_{cyt}^* + 2\varepsilon_{mem}^*}\right)} \right] \tag{2.7}$$

where $R$ corresponds to the outer radius of the cell, $d$ is the thickness of the cell membrane, $\varepsilon_{cyt}^*$ and $\varepsilon_{mem}^*$ and are the complex permittivities of the cytoplasm and membrane, respectively. The Clausius-Mosotti (CM) function can be obtained by inserting this calculated value for $\varepsilon_p^*$ in Equation (2.2). An example of DEP spectrum for a single-shell particle at different medium conductivities is given in Figure 2.4.

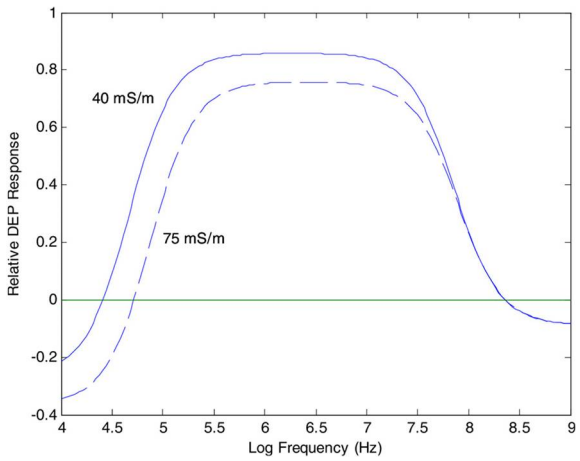


*Figure 2.4.* DEP spectrum (Re($F_{CM}$) vs. frequency) for a single-shell spherical particle at different medium conductivities [36]

For some bacteria and cells, such as E. coli or leukocytes, single-shell model is not applicable. E.coli and some other bacterial cells are in rod shape that creates different dipole moments along each semi axis. Moreover, these cells have another layer named as cell wall, in addition to cell membrane and cytoplasm. Therefore, to accurately model these types of cells single-shell model must be replaced with double-shell ellipsoidal model. In the case of leukocytes, three-shell model must be utilized to compensate three different layers (cell membrane, cytoplasm and the membrane surrounds the nucleoplasm) present in them. In other words, in order to model nonspherical cells and the cells have additional layer single-shell model must be improved to the multi-shell model.

# CHAPTER 3

## DEP SPECTRUM ANALYSIS OF BIOLOGICAL CELLS

One of the crucial steps in the design of a successful DEP-based separation/enrichment platform is knowing correctly the dielectric properties of the particles. If the dielectric properties of the particles to be separated are known well, the DEP-based separation/enrichment device will be designed more accurate and target-oriented, which will make the separation/enrichment more successful. Impedance measurement, electrorotation and dielectric crossover frequency determination are some of the methods used to determine the dielectric properties of cells [39]. These techniques involve a comprehensive analysis of the membrane and cytoplasmic properties of the particles for cell modeling to obtain DEP spectrum.

Several studies have been conducted on dielectric characterization on MCF7 cells and leukocytes. The main limitation related with the available literature data is that performed measurements for the crossover frequencies were obtained for different medium conductivities which has impact on the cell response. Therefore, there are certain discrepancies in these submitted reports for MCF7 [40]–[45]. In general, the first crossover frequency was found between 20 kHz and 100 kHz, however one of these reports states that the first crossover frequency above 150 kHz [40]. For the second crossover frequency, the range increases and results are available from 20 MHz to 55 MHz. Additionally, because of the inadequate data about MCF7 human breast adenocarcinoma cell line, some important values such as cytoplasmic permittivity is even unavailable [46]. Similar situation was also occurs for leukocytes.

In most cases, only a comparison between the DEP spectra of the relevant particles is sufficient, rather than a detailed cell modeling for the isolation of subpopulations from a heterogeneous group. As an alternative to these methods, a DEP spectrum device

that creates a non-uniform electric field required for particle manipulation makes it possible to observe the effect of the dielectrophoretic force exerted on the particles [47]. This method allows to investigate the relative strength and polarity of the DEP force over the applied frequency range without concerning the specific particle properties [48]. By applying this method to the particles that are planned to be separated, the DEP spectra of them can be determined and compared over the frequency range scanned. With the proposed DEP spectrum analysis method in this thesis, DEP spectra of the particles that are going to be separated are investigated differentially without considering the specific particle properties. In other words, the generated DEP spectrum device is one-to-one modeling of the DEP-based enrichment microchannel without flow parameters, which allows the direct comparison of the DEP force acting on the cells. Subsequently, according to the DEP spectra information of the corresponding particles, it is possible to determine and design the most accurate DEP-based enrichment device.

In this chapter, studies on DEP spectrum analysis of biological cells are presented. Firstly, the design, simulation and fabrication of the proof of concept device for DEP spectrum analysis, the experiments performed with these devices and the spectrum results obtained are submitted. Secondly, the improved DEP spectrum analysis is explained. Similar to the proof of concept device section, the design, simulation and fabrication of the final DEP spectrum device and the characterization studies performed with these devices and the obtained spectrum results are presented. The simulations of the designed DEP spectrum devices are done by using COMSOL Multiphysics® 5.3 software. At the end, obtained results related to DEP spectra of biological cells are discussed and evaluated for the DEP-based enrichment system.

## 3.1. Proof of Concept DEP Spectrum Devices

### 3.1.1. Design

The aim of the DEP spectrum device is to determine dielectrophoretic (DEP) spectra of biological cells. In this context, non-uniform electric field which is required to

provide cell movement is created by planar electrodes, in an easiest manner. Planar electrodes can easily be placed on the base of DEP-based devices. In addition, when compared to the side wall electrodes, by utilizing planar electrodes the necessary non-uniform electric field gradient distribution is created without losing any DEP force [49]. Therefore, electrode structure is selected as planar for the proposed DEP spectrum device. To ease the experiments and not to deal with hydrodynamic flow conditions, DEP spectrum devices are designed as a chamber directly open to the air instead of a microchannel. This chamber creates a reservoir for cell solution.

Different electrode geometries are employed to create necessary non-uniform electric field distribution in DEP-based systems. The electrode geometry used is a decisive factor in the dispersion of the non-uniform electric field created and therefore the cell movements to be observed. Another design parameter that has a role in determining the DEP force exerted on the particles is the gap between the opposing electrodes. The non-uniform electric field gradient distribution created on the DEP spectrum device, and therefore the DEP force exerted on the particles, depends on the shape of the electrodes and the gap between them. The choice of material to be used for the electrodes is also an important consideration. The electrodes should be resistant to chemicals used during the experiments and should be formed in a permanent structure [49].

According to above explained decisions, the basic design considerations, namely, the electrodes shape, the gap between them; chamber height and diameter; and magnitude and frequency range of the applied voltage were decided.

Electrode shape was selected as reciprocal V-shaped planar electrodes to easily generate DEP force acting on the particles. V-shaped planar electrodes placed in the bottom of the chamber creates the required non-uniform electric field. The gap between the opposing electrodes was selected as 20 μm by considering the diameter of the cells that are going to be examined. Above the electrodes, for cell containing solution placement a parylene chamber (20 μm in height) is formed. These electrodes

are isolated from the chamber by means of very thin parylene layer, which decreases the Joule heating, and eliminating electrolysis and cell damaging without remarkable loss in DEP force. This chamber holds the cell solution together and prevents it from spreading to the contact pads. For this reason, the chamber diameter was determined to be 5600 μm in order to provide a large area for releasing the cell solution. The chamber height was chosen to be 20 μm, the limit for the resist wall height used in METU-MEMS fabrication facilities without encountering any wall collapse problem. Figure 3.1 shows the physical structure of the designed DEP spectrum device.

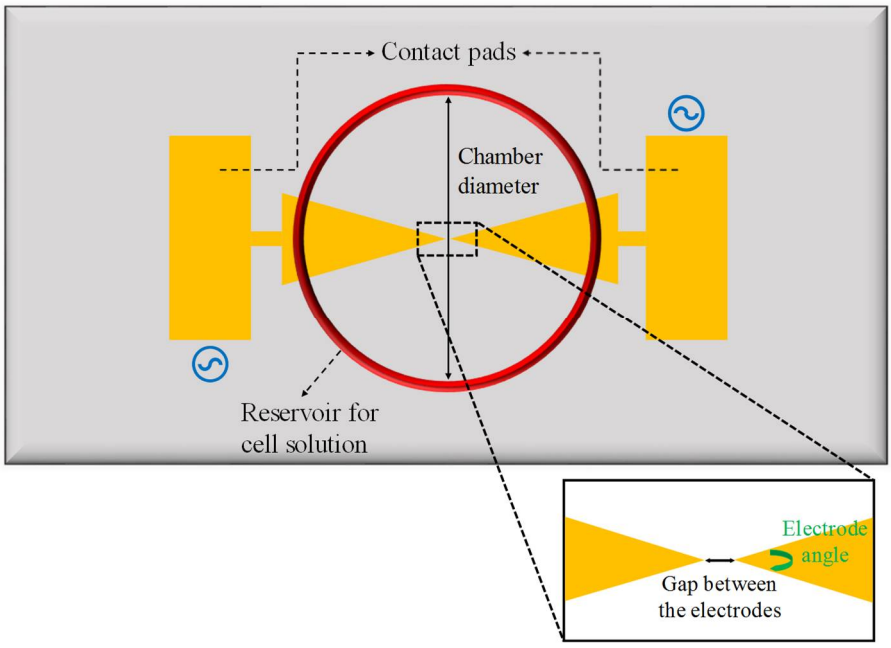


*Figure 3.1.* The illustration of the DEP spectrum device, with enlarged view of the electrode tips

The magnitude of the voltage was determined as 10 $V_{pp}$. It was decided to obtain the DEP spectra information for the cells for 15 different frequencies ranging from 100 kHz to 30 MHz. The frequencies to be tested are 100 kHz, 300 kHz, 500 kHz, 700 kHz, 850 kHz, 1 MHz, 3 MHz, 5 MHz, 7 MHz, 8.5 MHz, 10 MHz, 15 MHz, 20 MHz, 25 MHz and 30 MHz.

Table 3.1 presents the parameters used in the design of DEP spectrum devices.

Table 3.1. *Design parameters used for the DEP spectrum device*

| Design Criteria | DEP Spectrum Device |
|---|---|
| **Electrode type** | Planar |
| **Electrode shape** | Reciprocal V-shaped |
| **Electrode height** | 0.3 µm |
| **Electrode material** | Gold |
| **Angle between the arms of electrodes** | 30° |
| **Gap between electrode tips** | 30 µm |
| **Parylene thickness** | 0.5 µm |
| **Chamber diameter** | 5600 µm |
| **Chamber height** | 20 µm |
| **Voltage magnitude** | 10 $V_{pp}$ |
| **Voltage frequencies** | 100 kHz, 300 kHz, 500 kHz, 700 kHz, 850 kHz, 1 MHz, 3 MHz, 5 MHz, 7 MHz, 10 MHz, 15 MHz, 20 MHz, 25 MHz, 30 MHz |

### 3.1.2. Simulation Method

The necessary simulations are made by using COMSOL Multiphysics® 5.3 software after design parameters of the device were determined. The purpose of the simulations is to examine the magnitude and the distribution of the created DEP force on the chamber by the proposed electrode structure before the fabrication stage.

In order to simulate the DEP force generated by the proposed planar electrodes "Time Dependent" study in "Electric Currents (ec)" in "AC/DC" module was chosen COMSOL Multiphysics® 5.3 software. Then, designed device structure was imported from CADENCE, the software utilized for generating masks for MEMS fabrication, to COMSOL. Therefore, simulated electrode geometries and device structures are exactly the same of the fabricated devices. After importing the device structure, required arrangements in geometry section was done to reflect the actual device and

experiment conditions. In this content, the insulation parylene layer was modeled as being 0.5 µm thick below a suspending DEP medium of 50 µm height. Relative permittivity and electrical conductivity values of the parylene were utilized as 2.95 and $1 \times 10^{-15}$ S/m, respectively [50]. Relative permittivity and electrical conductivity and of the suspending DEP buffer were utilized 78 and 2.5 mS/m, respectively. In order to create DEP force, sinusoidal voltage with 180° phase difference at frequency of 1 MHz was applied to opposing electrodes by using $\pm|V|sin(wt)$ formula. To decide the maximum mesh size between the electrode tips, different mesh sizes were tried and the simulations were completed according to these values. In the simulation results, the convergence of the gradient of the electric field square term ($\nabla E^2$) was examined and the maximum mesh size was determined accordingly. As a result, the maximum mesh size between the electrode tips was 0.6 µm which allows accurate detection of changes in $\nabla E^2$ distribution. These simulations were performed time dependently for one period of the applied sinusoidal signal. Start and stop times and the time step between these two time points were determined according to the frequency and the required resolution, respectively.

In DEP force equation, except $\nabla E^2$ term all parameters are constant. Therefore, the distribution of $\nabla E^2$ term on the proposed device was simulated in order to examine the DEP force exerted on the particles. The following equation was used to accomplish this simulation, where V stands for the voltage.

$$\nabla E^2 = \left| \begin{matrix} \left(\frac{\partial^3}{\partial x^3} + \frac{\partial^3}{\partial y^2 \partial x} + \frac{\partial^3}{\partial z^2 \partial x}\right)\hat{x} \\ \left(\frac{\partial^3}{\partial y^3} + \frac{\partial^3}{\partial x^2 \partial y} + \frac{\partial^3}{\partial z^2 \partial y}\right)\hat{y} \\ \left(\frac{\partial^3}{\partial z^3} + \frac{\partial^3}{\partial x^2 \partial z} + \frac{\partial^3}{\partial y^2 \partial z}\right)\hat{z} \end{matrix} \right| V^2 \qquad (3.1)$$

The equation given above was transferred to the COMSOL language and with the application of it in the results section, 3D $\nabla E^2$ simulations were obtained. In the

simulations generated, it should be presented that the $\nabla E^2$ term is greater than $10^{12}$ $kg^2m/s^6A^2$ , which is minimum required value for the manipulation of the cells.

Assuming the diameter of 10-12 μm for the cells and taking into account the levitation forces inside the suspending DEP medium, a plane that is 10 μm above the parylene surface was chosen for examining the $\nabla E^2$ term distribution on the x-y plane. In addition, a circular area having a radius of 500 μm from the device center, which is the midpoint of the electrode tips, was defined to correspond to the area that can be examined by microscope during the experiments. It should be noted that, all DEP spectrum simulation results were submitted for this circular area. In other words, the $\nabla E^2$ distribution was examined for the circular area having a radius of 500 μm from the center, located 10 μm above the parylene surface. Moreover, the obtained COMSOL simulation results for this case were examined by exporting the $\nabla E^2$ values through a line defined from the midpoint between the electrode tips to 500 μm away from that point in y direction. To be able to perform further numerical analyses on FEM results (COMSOL), exported FEM data were transferred to EXCEL.

#### 3.1.2.1. Simulation Results

Applying the explained simulation method, $\nabla E^2$ simulations of the proof of concept DEP spectrum devices were made. Initially, it was aimed to determine the optimum mesh size between the electrode tips to accurately detect the changes in $\nabla E^2$ distribution. For this purpose, simulations were completed by providing different mesh sizes (6 μm, 3 μm, 1.5 μm, 1 μm, 0.75 μm and 0.6 μm) between the electrode tips and the distributions of $\nabla E^2$ derived from these simulations are presented in Figure 3.2. As shown in Figure 3.2, the results of the changes in $\nabla E^2$ for the mesh dimensions of 1 μm, 0.75 μm and 0.6 μm are significantly close. In particular, the curves obtained for 0.6 μm and 0.75 μm are almost the same indicating convergent results. As a result, in order to get the change of $\nabla E^2$ accurately, the maximum mesh size between the electrodes was determined as 0.6 μm according to these results. Table 3.2 shows the

complete mesh number and the number of degrees of freedom solved for each mesh size tested during FEM modeling and simulations.

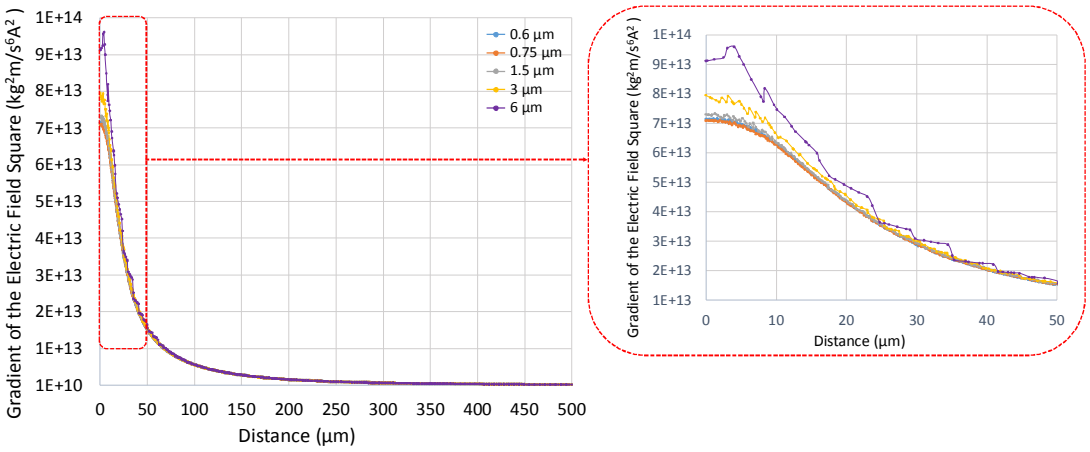


*Figure 3.2.* $\nabla E^2$ distribution for six different mesh sizes between the electrode tips

Table 3.2. *Complete mesh number and the number of degrees of freedom solved for each mesh size tested during FEM modeling and simulations*

| Mesh size between the electrode tips | Complete mesh number | Number of degrees of freedom solved |
|---|---|---|
| 0.6 | 6700428 | 27465003 |
| 0.75 | 5586504 | 22902703 |
| 1.5 | 2913351 | 11952538 |
| 3 | 1330434 | 5465773 |
| 6 | 575022 | 2368483 |

Figure 3.3 shows where $\nabla E^2$ is greater than $10^{12}$ $kg^2m/s^6A^2$ at 10 $V_{pp}$ for 0.6 µm mesh size between the electrode tips. As explained in the simulation methodology, it shows the changes of $\nabla E^2$ for the circular area having a radius of 500 µm from the center of the device located 10 µm above the parylene surface. Exported data for this simulation result is presented in Figure 3.4.

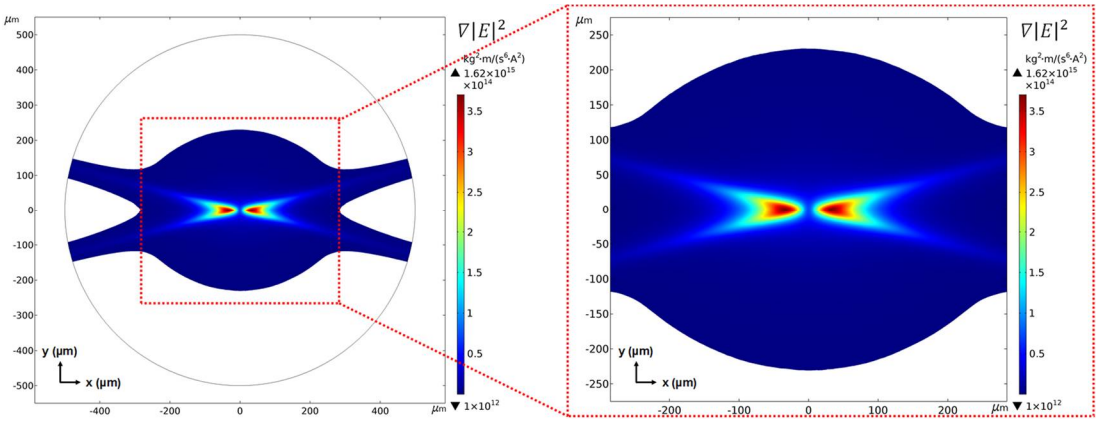


*Figure 3.3.* The change of $\nabla E^2$ for proof of concept device

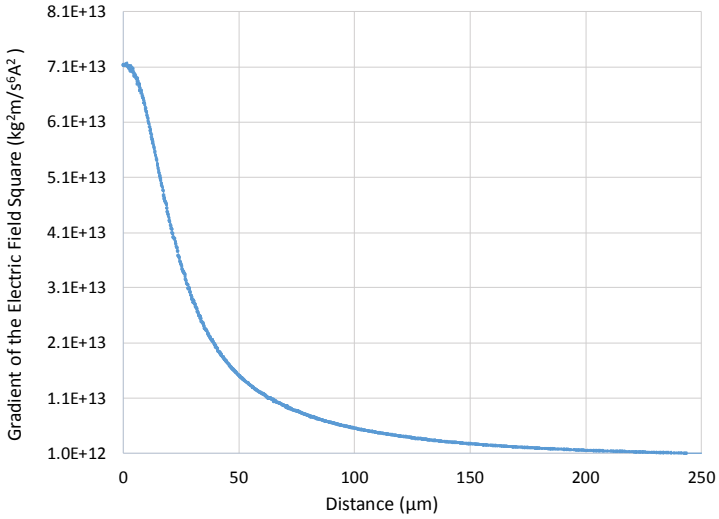


*Figure 3.4.* The graph of $\nabla E^2$ distribution for proof of concept device

According to the simulation results, the proposed electrode design creates the required $\nabla E^2$ distribution and the DEP force to manipulate the cells within the area from the midpoint between the electrode tips to a distance of approximately 245 µm. The results of all simulation studies were examined and it was decided to include the cells remaining in the 245 µm (the limit where $\nabla E^2$ is greater than $10^{12}$ $kg^2m/s^6A^2$, which

is necessary for the manipulation of the cells) from the center of the device for DEP spectrum calculations.

### 3.1.3. Fabrication

In this section, microfabrication techniques used in the fabrication of the proof of concept DEP spectrum chips are presented. Surface micromachining techniques have been used to produce DEP spectrum devices. Fabrication flows with the photos showing important stages of fabrication, screenshots of mask drawings generated through Cadence Layout Editor software, and images of the fabricated device will be presented in the following sections.

DEP spectrum device fabrication is a two-mask process. It involves photolithography, metal sputtering, lift-off, photolithography and polymer (Parylene-C) coating. The fabrication flow and all related parameters are given in the Appendix A. Figure 3.5 shows the entire fabrication process followed for DEP spectrum device.

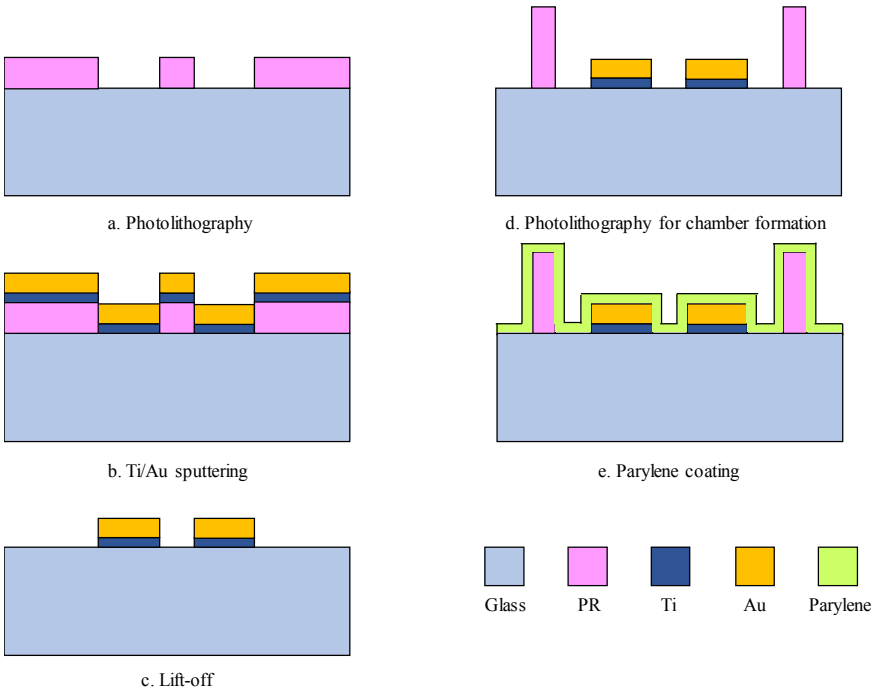


*Figure 3.5.* The fabrication flow of DEP spectrum device

Fabrication started with the preparation of 6" glass wafers. In this content, pre-cleaning processes were applied to the wafers. Initially, the wafers were cleaned for organic residues with piranha solution. Then, the wafers were etched with BHF (1:7) (HF:NH4F) solution. Afterwards, the lift-off lithography for the electrodes and contact pads were done with SPR 220-3 positive photoresist utilizing 1st mask (clear field) shown in Figure 3.6. The intended use of SPR 220-3 positive photoresist is to protect sharpness of the electrode tips and edges during lift-off.

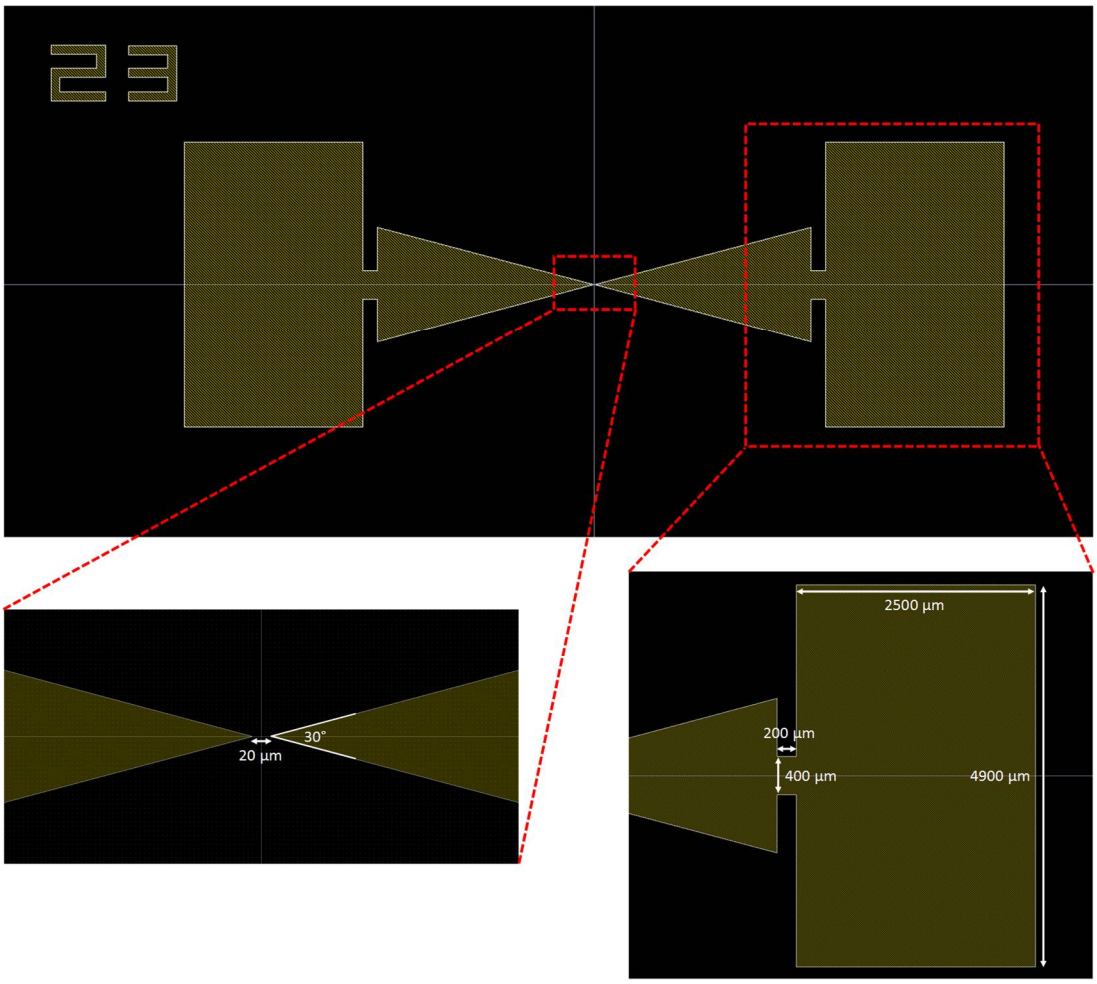


*Figure 3.6.* 1st mask layer of the DEP spectrum device

After patterning the photoresist layer in the lift-off lithography step, Ti (30 nm) and Au (400 nm) were coated on the wafers. Ti is an adhesive layer for Au. Afterwards, these metal layers (Ti and Au) were patterned with lift-off procedure with acetone lift-off. Figure 3.7 presents the planar electrode structure after lift-off.

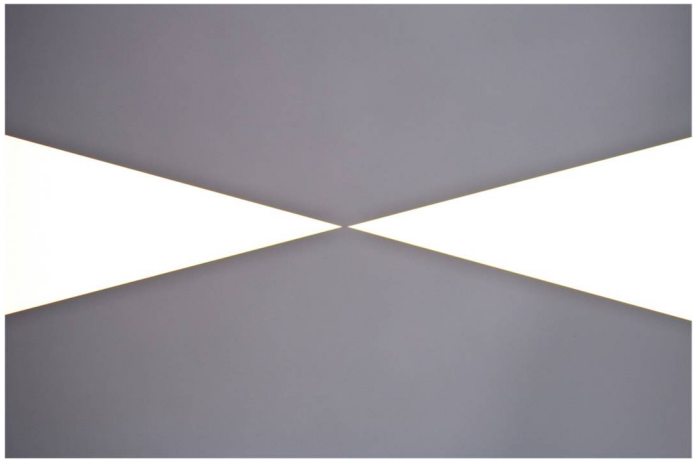

*Figure 3.7.* The image of the planar electrodes after lift-off

The chamber was patterned with 2nd mask (clear field) utilizing AZ 40XT photoresist. View of the 2nd mask is shown in Figure 3.8. The chamber was designed as a circular resist wall aligned to the center of the electrode tips.

The resist walls hold the cell solution together by preventing it from spreading to the contact pads. In other words, it will be an obstacle for cell drops. For this reason, a thick resist (~20 µm) was needed in this lithography to ensure that the chamber to be formed was high. Therefore, AZ 40XT photoresist was used by performing single spin. The appearance of the chamber walls formed at the end of this lithography is given in Figure 3.9.

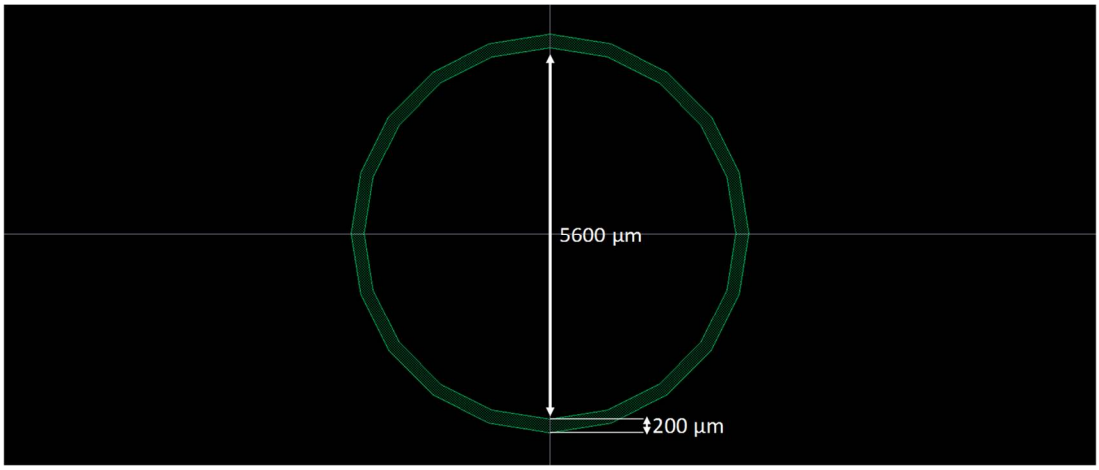


*Figure 3.8.* 2nd mask layer of the DEP spectrum devices

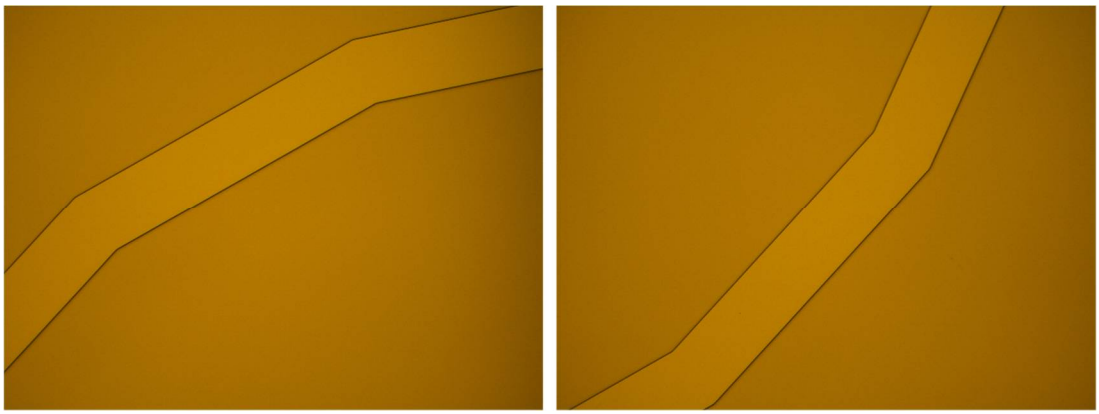

*Figure 3.9.* The AZ 40XT photoresist walls are formed as an obstacle for drops of cell solution

To provide isolation of electrodes, a thin layer of Parylene-C coating (0.5 µm) was performed with silane. This coating method, parylene coating with silane, allows parylene to stick to the surface. This method can be used when there is no photoresist on the wafer surface. On the other hand, if photoresist is present on the surface before the parylene coating, the parylene coating method with silane cannot be used because silane damages the structure of the photoresist. In this given fabrication flow, AZ 40XT photoresist walls are present to form chamber prior to the Parylene coating with silane. Despite the photoresist present on the wafer surface, parylene coating with

silane method was preferred to increase the adhesion of the parylene to the wafer surface. In addition to this, by being well aware of the fact that used silane will damage the present photoresist on the wafer surface AZ 40XT photoresist walls will not be used as sacrificial layer instead they will support the chamber by creating hard walls. Therefore, damages formed in the photoresist due to silane were neglected. According optimizations performed for parylene coater, all parylene coatings were made at a ratio of 1:2, the thickness of the coated parylene layer in micrometers to parylene weight in grams [51]. At the end of fabrication, each wafer was diced and 92 devices were acquired per one 6" wafer. The image of the fabricated DEP spectrum device is presented in Figure 3.10.

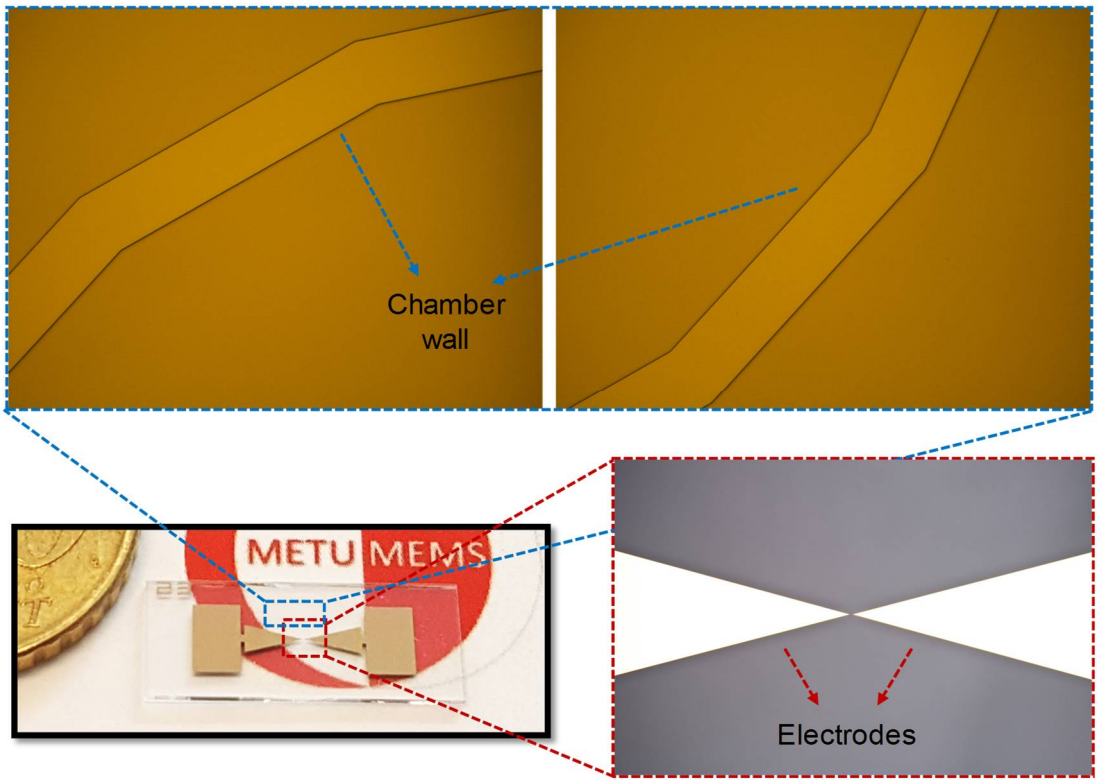


*Figure 3.10.* Fabricated DEP spectrum device

### 3.1.4. Materials & Method

In this section, the preparation steps of the cells used in the DEP spectrum experiments, experimental set-up and the examination method of the DEP spectrum records obtained during the experiments are explained in detail.

#### 3.1.4.1. Preparation of the Cells

Studies of cell characterization in DEP spectrum experiments were performed for MCF7 breast cancer cells as CTC and leukocytes as blood cells. Since several different preparation steps are used for these two different cell groups examined, the steps followed during preparations are described in detail in two separate sub-parts.

*Preparation of MCF7 breast cancer cells*

The MCF7 breast cancer cells tested in this study were obtained from METU Biology Department of METU, in collaboration with research group of Prof. Dr. Ufuk Gündüz. MCF7 cancer cells were cultured and raised in RPMI 1640 medium containing 0.2% gentamicin and 10% (w/v) fetal bovine serum (FBS) in humidified incubator with 5% $CO_2$ at 37 ˚C. MCF7 cancer cells are known as adherent cells and their adhesion to the flask surface is important during their growth. For this reason, trypsin is used to facilitate removal of adherent cells from the growth surface. In this content, trypsin is applied to the flask after the removal of the RPMI 1640 medium. Approximately 7 minutes is waited for the removal of the MCF7 cells from the surface of the flask for our experiments. Obtained cells after this step were then washed by centrifugation. Cell pellet at the end of this centrifugation was re-suspended in its own growth medium [49]. Cells obtained from the Biology Department before each experiment in their own media were washed twice by centrifuging for 7 minutes at 210 g at room temperature. Obtained pellets at the end of centrifuge steps were re-suspended in the prepared DEP medium. This prepared DEP medium contains 8.5% (w/v) sucrose and 0.3% (w/v) dextrose in order to adjust osmotic pressure inside the cell. The conductivity of the DEP medium is arranged to 2.5 mS/m by applying phosphate buffered saline (PBS, Gibco, 10X).

*Preparation of White Blood Cells (WBCs)*

For the testing of DEP spectrum devices, mononuclear white blood cells (MWBCs) and polymorphonuclear white blood cells (PWBCs) were prepared.

To extract mononuclear and polymorphonuclear WBCs separately density gradient centrifugation technique was used. Density gradient centrifugation is a powerful technique used to separate substances according to their molecular mass. In this method, the separation interval can be specified when the density range is selected [52]. In other words, cells can be isolated with this method according to the density differences.

The PWBCs obtained from human peripheral blood sample is composed of primarily neutrophils and relatively much less basophils and eosinophils. These cells have densities above 1.077 g/ml except for a part of the basophil population. Mononuclear white blood cells are composed of lymphocytes and monocytes, with densities less than 1.077 g/ml (Figure 3.11). This information indicates that extraction of mononuclear and polymorphonuclear WBCs separately is only possible by using a discontinuous gradient media. However, as can be seen from Figure 3.11, density of neutrophils significantly overlaps that of erythrocytes. Therefore, extraction of these cells, especially the PWBCs, should be done from a leukocyte rich plasma in order to eliminate red blood cell contamination.

In order to carry out the tests, whole blood samples taken from healthy volunteers were obtained at the METU Medical Center with the ethics committee approval certificate. Whole blood samples taken from peripheral blood vessels of healthy volunteers were collected in tubes containing $K_3$EDTA. Collected blood samples were first treated with Ficoll® Paque Plus (GE Healthcare) solution to remove red blood cells, the most common cell group in blood. Ficoll® Paque Plus (GE Healthcare) is a solution that adheres to red blood cell; therefore, red blood cells are aggregated and settled down. After precipitation of the red blood cells, the OptiPrep™ (Sigma-Aldrich) protocol was used to separate different WBCs (mononuclear and

polymorphonuclear WBCs). OptiPrep™ is a sterile density gradient medium used for isolation of blood cells. The details of the protocol used in the preparation of WBCs cells are given below.

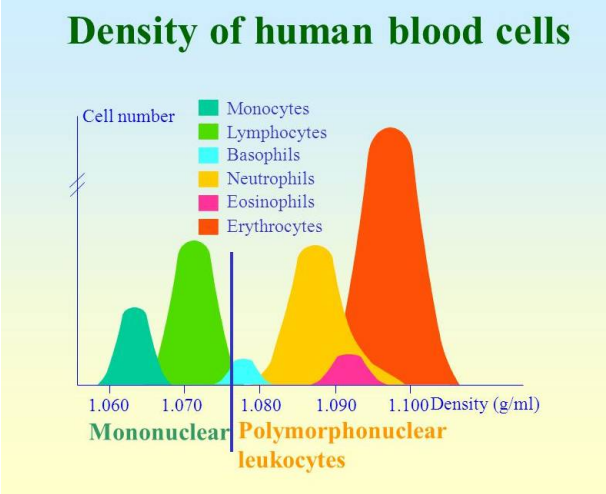


*Figure 3.11.* Density of human blood cells [52]

5 ml whole blood sample was mixed with Ficoll® Paque Plus (GE Healthcare) and allowed to stand for 1 hour. At the end of this step red blood cells are aggregated and settled down. As a result, approximately 3 ml leukocyte rich plasma (LRP) which is free from red blood cells was obtained from 5 ml whole blood sample. Two solutions with a density of 1.077 g/ml and 1.095 g/ml were prepared using OptiPrep and another solution containing NaCl, HEPES and EDTA. 1.095 g/ml solution was slowly introduced into a 15 ml tube. A solution of 1.077 g/ml was then added to the tube without mixing with the initially placed solution. 2 ml of white blood-rich plasma obtained from whole blood was placed at the top of them without mixing with the two remaining solutions and centrifuged at 800 g for 25 minutes at 18-22 ° C. As a results of this process 5 layers are be obtained. While mononuclear WBCs were harvested from upper interface, polymorphonuclear WBCs were harvested from lower interface. Extracting mononuclear WBCs from whole blood was completed with this step. To

complete extraction of PWBCs a few more steps were followed. Harvested PWBC suspension was diluted with an equal volume of another solution prepared with NaCl, HEPES and EDTA. Obtained solution was centrifuged at 350 g for 10 min. Obtained cell pellet at the end of this centrifugation was mixed with another solution containing $NH_4Cl$ and HEPES and incubated for 7 minutes. This step removes the residual red blood cell contamination. Then, PWBCs were harvested by another centrifugation [53].

After MWBCs and PWBCs were extracted from the whole blood sample separately, the harvested cells were washed twice with the prepared DEP medium as in the preparation stage of the MCF7 cells. This prepared DEP medium contains 8.5% (w/v) sucrose and 0.3% (w/v) dextrose in order to adjust osmotic pressure inside the cell. The conductivity of the DEP medium is arranged to 2.5 mS/m by applying phosphate buffered saline (PBS, Gibco, 10X).

#### 3.1.4.2. Experimental Setup and Test Procedure

This section presents the developed and used experimental setup for conducting DEP spectrum experiments with the proof of concept devices. The experimental setup is demonstrated in Figure 3.12. Probe station provides to take contacts from micro DEP spectrum devices. Before energizing the electrodes for each test, the reservoir was filled with a 1 µl cell solution. In order to get rid of the drag force generated in the DEP medium, which is against of the motion of the cells at the creeping-flow limit, sufficient time (approximately 30 seconds) was allowed to lapse for the solution become stationary. In this condition, DEP force becomes the major factor that regulates the acceleration of the cells [48]. At the end of this waiting period, in addition to stopping the initial cell movements, it was provided that the cells were brought to the same plane as the electrodes. In addition, at the beginning of the experiment, the focus was adjusted to the electrode plane and the not changed throughout the entire experiment. Thus, cells in the same plane (in the electrode plane) were examined during the entire experiment. DEP force required to provide cell

movement was created by applying voltage to the electrodes with a signal generator (Agilent, 81150A). Two of its four outputs were connected to the two V-shaped planar electrodes via probe station. 10 $V_{pp}$ with a 180° phase difference sinusoidal signals were applied to each electrode at 15 different frequencies, in the range from 100 kHz to 50 MHz. During the experiment, the cells inside the chamber were replaced with the fresh cells at each frequency in order to eliminate the possibility of change in cells' dielectric properties due to application of an external electric field. The cell motion was recorded with a CCD camera (SONY/DXC-107AP) for approximately 1.5 minutes for each frequency.

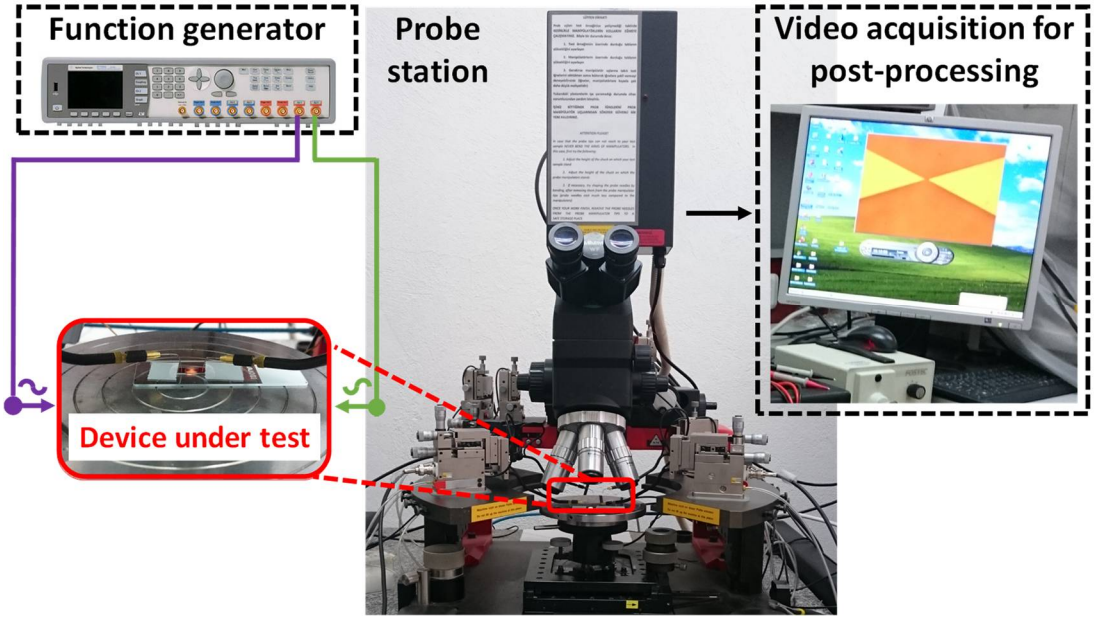


*Figure 3.12.* Experimental setup used for testing proof of concept DEP spectrum devices

### 3.1.4.3. DEP Spectra Examination Method

Proof of concept devices were tested after through the determined frequency range after the fabrication. During the experiments, the immobilized cells in the chamber are attracted towards the electrodes under the effect of DEP with the application of

voltage. The cell movement generated by the pDEP effect observed during the experiment is presented in Figure 3.13.

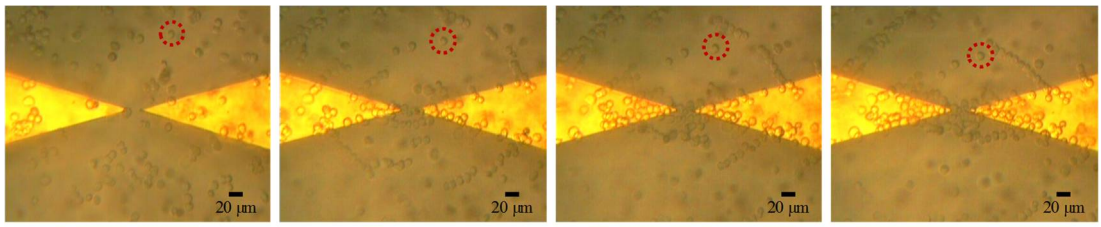


*Figure 3.13.* Movement of MCF7 cells under pDEP (voltage = 10 $V_{pp}$, frequency = 1 MHz)

The main goal of the proposed DEP spectrum study was to find a frequency value that provides the enrichment/isolation of MCF7 cells from blood cells without ascertaining their cytoplasmic and membrane properties. As explained in Section 3.1.4.2, the test of each frequency during the experiments was not initiated until the flow of the cell solution left in the parylene chamber stopped. In this way, the cells became stable and the cell movement observed with the application of voltage was generated by the force of DEP. Thus, the observed cell movement after voltage application was directly associated with the DEP force (Equation 2.1), specifically with the $Re(F_{CM})\nabla|E^2|$ term. All DEP spectrum experiments were performed using DEP media with the same characteristics at 10 $V_{pp}$, regardless of the type of cell being tested. This implies that the $\nabla|E^2|$ term was constant for all experiments. As a result, the cell movement generated by DEP force was directly associated with the $Re(F_{CM})$ parameter, which represents the intrinsic property of the cell. From this point of view, the proposed DEP spectrum analysis was performed in the exactly same experimental conditions for different cell types and comparison of the DEP forces that the cells were exposed to was examined. The average velocity of the cells remaining in the measurement area determined according to the COMSOL simulation results was decided as the comparison parameter. The average velocity of the cells was calculated from the time

of voltage application to the time the cells adhered to the electrodes with the effect of pDEP. As a result, DEP force-frequency variations from the average velocity information of the cells at the tested frequencies were obtained for different cell types.

Recorded cell movements for each frequency during the experiments were analyzed and utilized to obtain DEP spectra of the corresponding cells. Examinations on the recorded videos were performed by using VirtualDub, video capture/processing utility, and Meazure™, display measurement software. The moment when the voltage was applied and the moment when the cells traced were attached to the electrodes were found by employing VirtualDub program for experiment records. The distance taken between these two time points by the monitored cell was determined by using pixel measurement software, Meazure™. The gap between the electrode tips, 20 μm for the proof of concept DEP spectrum devices, was taken as a reference to convert distance measurements in to μm. The average velocity of the cell monitored was calculated after these steps. This value was calculated for all cells, and the average velocity at the frequency applied for the cell type being examined was determined. With this way, the predetermined frequency values were tested and the determined frequency spectrum was scanned.

### 3.1.5. DEP Spectra Results

*MCF7 Breast Cancer Cells:*

Figure 3.14 shows images of MCF7 cells during the DEP spectrum experiments with the proof of concept devices. The immobilized cells, which were randomly distributed in the chamber, were observed to move towards the electrodes under the effect of pDEP with the application of voltage. The live cells must be lined up on the electric field lines after waiting for sufficient time to complete their movement with the application of voltage. Collected cells around the electrode periphery with the formed pearl chain structures at the end of the experiment record are shown in Figure 3.14.

DEP spectrum of MCF7 cells was obtained with the repetition of experiments on 3 different days with freshly supplied cells. Obtained spectrum result is presented in

Figure 3.15. The data points shown in Figure 3.15, indicate the average cell velocity calculated for each frequency with the corresponding standard error of the mean. To calculate the average cell velocity, the number of cells examined for each frequency is given in Table 3.3.

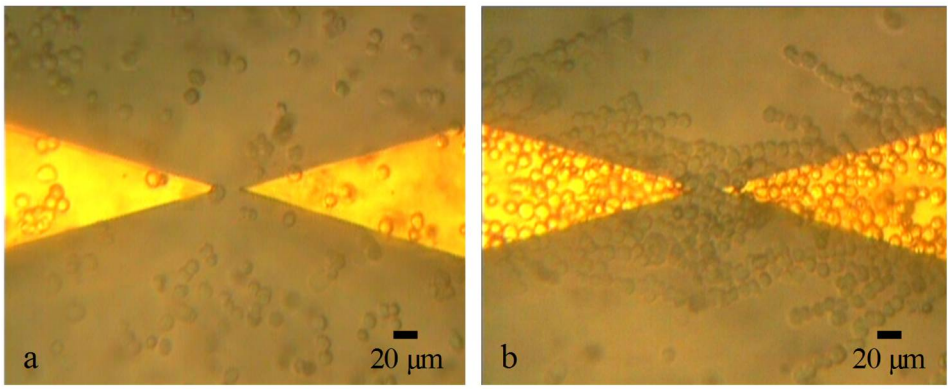


*Figure 3.14.* MCF7 cells under DEP spectrum experiments with proof of concept device (a) Distribution of cells on the device before voltage is applied (b) Collection of cells at the electrode periphery as a result of voltage application and formation of pearl chain structures on electric field lines

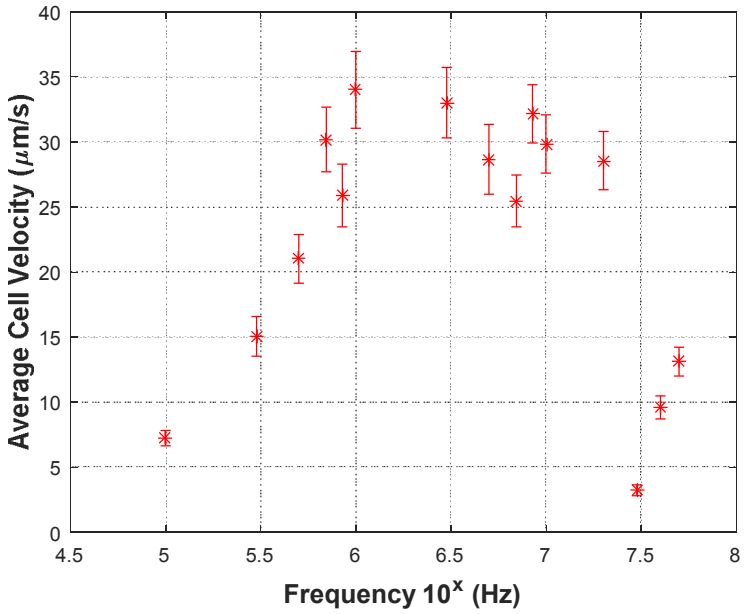


*Figure 3.15.* DEP spectrum of MCF7 breast cancer cells

Table 3.3. *The number of cells examined at each frequency in determining the DEP spectrum of MCF7 breast cancer cells*

| Frequency | Number of cells examined | Frequency | Number of cells examined | Frequency | Number of cells examined |
|---|---|---|---|---|---|
| **100 kHz** | 30 | **1 MHz** | 19 | **10 MHz** | 17 |
| **300 kHz** | 23 | **3 MHz** | 19 | **20 MHz** | 15 |
| **500 kHz** | 23 | **5 MHz** | 16 | **30 MHz** | 18 |
| **700 kHz** | 14 | **7 MHz** | 16 | **40 MHz** | 20 |
| **850 kHz** | 14 | **8.5 MHz** | 17 | **50 MHz** | 18 |

*Mononuclear WBCs:*

Figure 3.16 shows images of MWBCs during the DEP spectrum experiments with the proof of concept devices. The immobilized cells, which were randomly distributed in the chamber, were observed to move towards the electrodes under the effect of pDEP with the application of voltage. At the end of the test record the cells collected at the electrode periphery are shown in Figure 3.16.

MWBCs were extracted from 2 healthy donors as described in Section 3.1.4.1. Obtained spectrum result is presented in Figure 3.17. The data points shown in Figure 3.17, indicate the average cell velocity calculated for each frequency with the corresponding standard error of the mean.

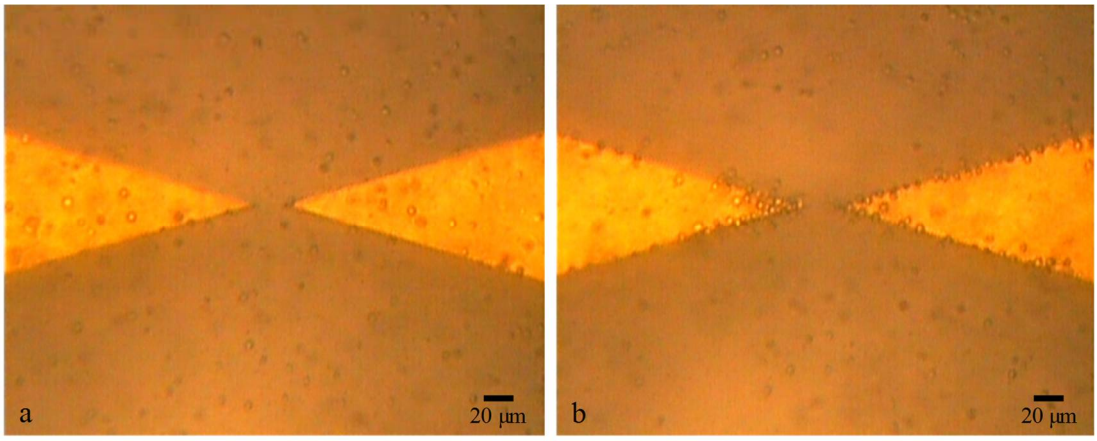


*Figure 3.16.* MWBCs under DEP spectrum experiments with proof of concpet device (a) Distribution of cells on the device before voltage is applied (b) Collection of cells at the electrode periphery as a result of voltage application

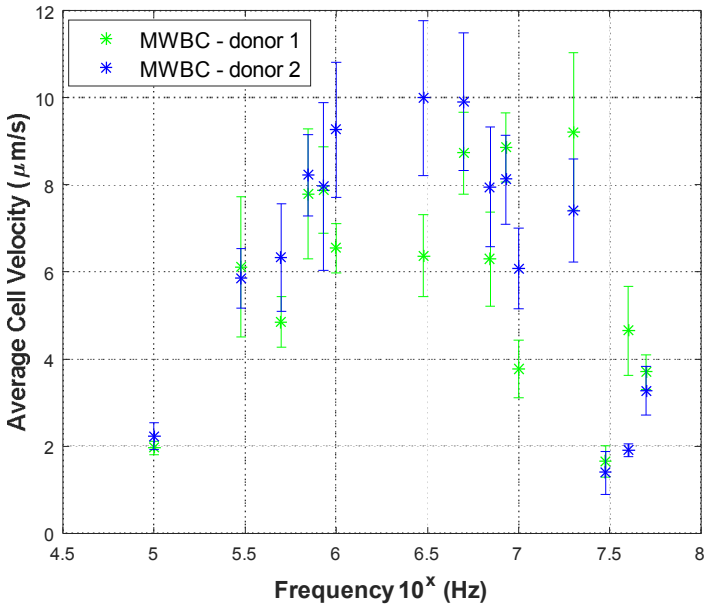


*Figure 3.17.* DEP spectra of MWBCs for 2 donors

To calculate the average cell velocity, the number of cells examined for each frequency is given in Table 3.4.

Table 3.4. *The number of cells examined at each frequency in determining the DEP spectra of MWBCs*

| Frequency | Number of cells examined (Donor 1) | Number of cells examined (Donor 2) | Frequency | Number of cells examined (Donor 1) | Number of cells examined (Donor 2) |
|---|---|---|---|---|---|
| **100 kHz** | 6 | 9 | **7 MHz** | 8 | 8 |
| **300 kHz** | 4 | 5 | **8.5 MHz** | 8 | 13 |
| **500 kHz** | 7 | 5 | **10 MHz** | 7 | 10 |
| **700 kHz** | 6 | 7 | **20 MHz** | 4 | 9 |
| **850 kHz** | 6 | 4 | **30 MHz** | 8 | 4 |
| **1 MHz** | 7 | 10 | **40 MHz** | 4 | 4 |
| **3 MHz** | 8 | 8 | **50 MHz** | 7 | 8 |
| **5 MHz** | 5 | 11 | | | |

*Polymorphonuclear WBCs:*

Figure 3.18 shows images of PWBCs during the DEP spectrum experiments with the proof of concept devices. The immobilized cells, which were randomly distributed in the chamber, were observed to move towards the electrodes under the effect of pDEP with the application of voltage. At the end of the test record the cells collected at the electrode periphery are shown in Figure 3.18.

PWBCs were extracted from 2 healthy donors, the same individuals used in MWBC experiments, as described in Section 3.1.4.1. Obtained spectrum result is presented in Figure 3.19. The data points shown in Figure 3.19 indicate the average cell velocity calculated for each frequency with the corresponding standard error of the mean.

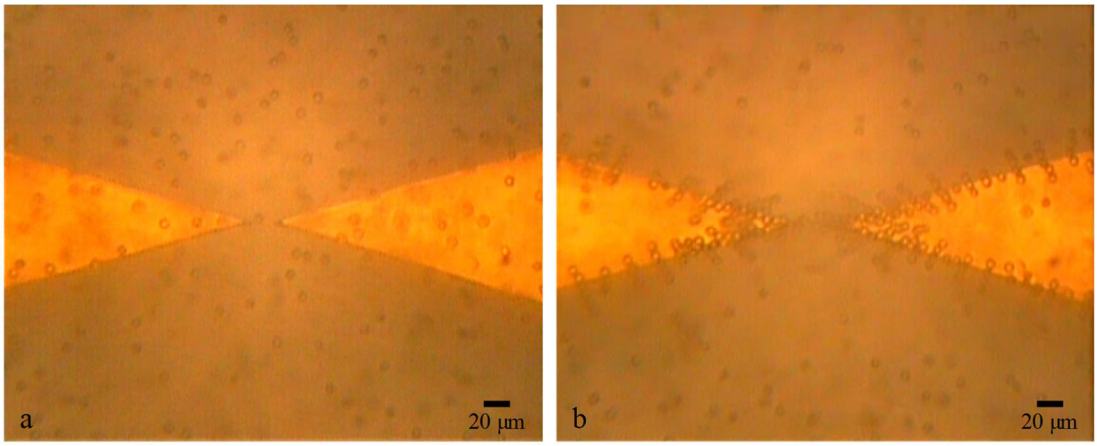


*Figure 3.18.* PWBCs under DEP spectrum experiments with proof of concept devices. (a) Distribution of cells on the device before voltage is applied. (b) Collection of cells at the electrode periphery as a result of voltage application.

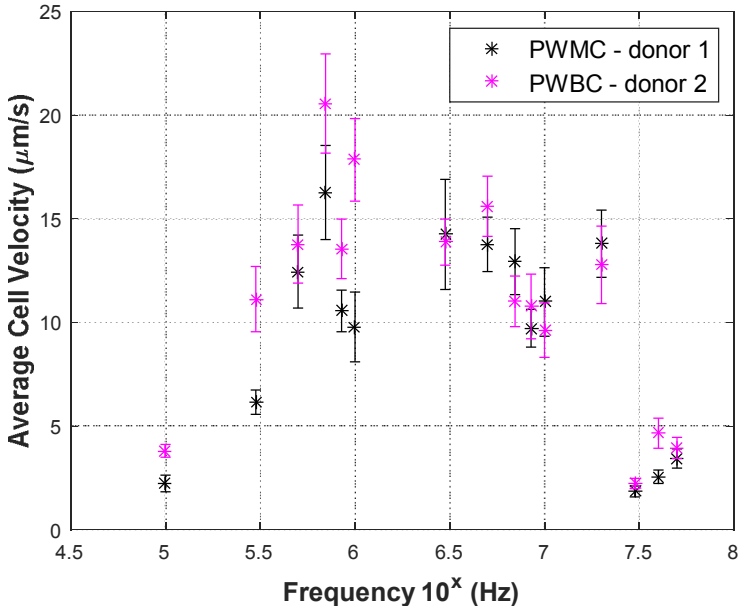


*Figure 3.19.* DEP spectra of PWBCs for two donors

To calculate the average cell velocity, the number of cells examined for each frequency is given in Table 3.5.

Table 3.5. *The number of cells examined at each frequency in determining the DEP spectra of PWBCs*

| Frequency | Number of cells examined (Donor 1) | Number of cells examined (Donor 2) | Frequency | Number of cells examined (Donor 1) | Number of cells examined (Donor 2) |
|---|---|---|---|---|---|
| **100 kHz** | 14 | 16 | **7 MHz** | 11 | 15 |
| **300 kHz** | 16 | 14 | **8.5 MHz** | 19 | 17 |
| **500 kHz** | 17 | 11 | **10 MHz** | 16 | 14 |
| **700 kHz** | 15 | 12 | **20 MHz** | 10 | 17 |
| **850 kHz** | 19 | 9 | **30 MHz** | 9 | 11 |
| **1 MHz** | 12 | 13 | **40 MHz** | 10 | 15 |
| **3 MHz** | 12 | 16 | **50 MHz** | 9 | 17 |
| **5 MHz** | 12 | 17 | | | |

### 3.1.6. Discussions

The main goal targeted by the proposed DEP spectrum study is to investigate the frequency that will enable MCF7 cells to be isolated/enrichment from the blood cells to be applied in the DEP-based separation enrichment system to be developed. For this purpose, experiments with MWBCs and PWBCs obtained from two different healthy individuals and MCF7 breast cancer cells were completed for 15 different frequencies in the determined range at constant voltage (10 $V_{pp}$). All experiment records were examined as explained in Section 3.1.4.3, and at the end DEP spectra of the corresponding cells were found. In Figure 3.20, the results presented in Section 3.1.5 for each cell type are shown together.

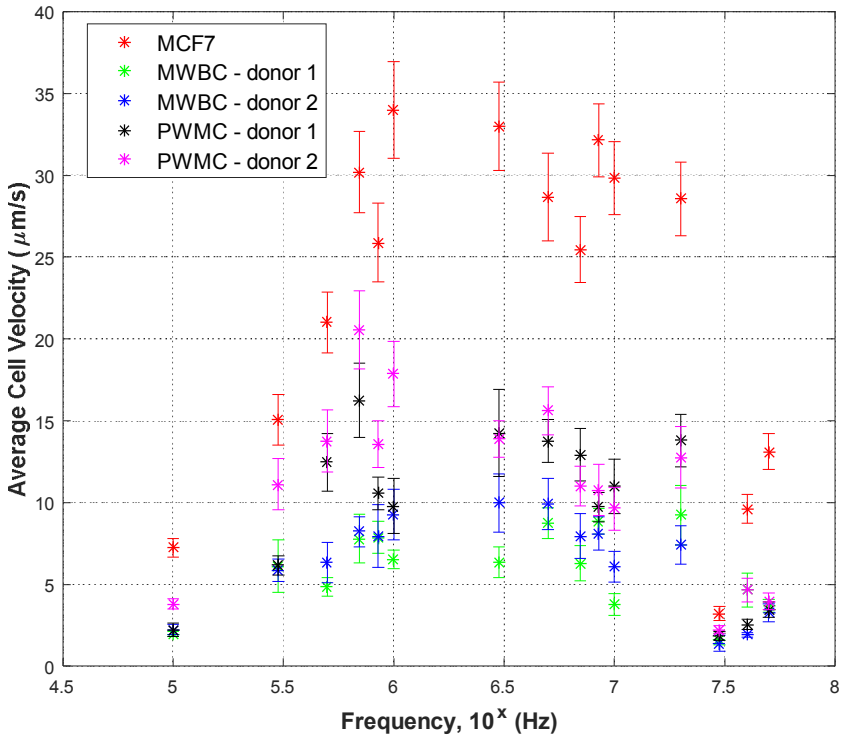


*Figure 3.20.* DEP spectra of MCF7 cells, mononuclear and polymorphonuclear WBCs (voltage = 10 $V_{pp}$)

The results reveal that at 1 MHz, a significant velocity difference occurs between MCF7 cells (33.99 µm/s) and WBCs, MWBCs (7.9 µm/s) and PWBCs (13.82 µm/s), which can be utilized as the working frequency for DEP-based enrichment of MCF7 cancer cells from leukocytes as a future work. When the average velocity and standard error of the mean data obtained for MWBCs and PWBCs are evaluated, it is determined that the DEP spectra of the corresponding cells are not same. In other words, the average velocity of MWBCs are lower than the PWBCs in both donors. This indicates that, the elimination of the MWBCs from MCF7 cells will be easier than the elimination of PWBCs from MCF7 cells in DEP-based enrichment unit.

As can be seen in Figure 3.14, Figure 3.16 and Figure 3.18 submitted in Section 3.1.5, in the DEP spectrum experiments with WBCs, it was observed that the cells collected around the electrode did not form pearl chain structure as strong as the MCF7 cells.

This is due to the fact that the WBCs are exposed to considerably lower DEP force than the MCF7 cells. Therefore, at the end of the determined recording period, WBCs could not be collected around the electrodes as much as the MCF7 cells during the experiments.

These results proved the proposed DEP spectrum study for examining the DEP spectra of biological cells without directly analyzing their cytoplasmic and membrane properties. The proposed method is tested with PWBCs, MWBCs, extracted from 2 healthy donors, and MCF7 breast cancer cells. DEP spectra of the corresponding cells are obtained for 15 different frequencies in the range from 100 kHz to 50 MHz at 10 $V_{pp}$.

### 3.2. DEP Spectrum Devices

Studies conducted with the proof of concept devices have been useful in the detection of problems related to the experimental setup, testing and post-processing and led to the improvements of the DEP spectrum analysis. From this section, the finalized DEP spectrum study with the improvements has been described.

#### 3.2.1. Design

The design of the device used in the improved DEP spectrum study was the same as the proof of concept device, except the gap between the electrodes was increased to 30 μm in order to generate more proper electric field gradient distribution on the surface.

#### 3.2.2. Simulation Method

The simulation method used for the final design is identical to the method described for the initial devices in Section 3.1.2. The method described in this section was applied one by one and only an additional simulation step was added. This additional simulation step for the final devices was included due to the modification of the experimental setup. In the new experimental setup, with the replacement of bright-field microscope to fluorescence microscope for observing cell movements during

experiment, it was consider that the cells to be examined may not be exactly in the electrode plane. For this reason, the distribution of the $\nabla E^2$ and the generated DEP force at the elevation at which the cells can be suspended was included as an additional step to the simulations of the final devices. In order to see the effect of elevation on the generated DEP force, variations in the $\nabla E^2$ along the z-axis was also examined in the 3D analyses. To achieve this examination, obtained $\nabla E^2$ distributions were studied for 6 different z planes, defined from $z = 0.5$ µm plane to $z = 50.5$ µm plane with 10 µm increment between the planes. The changes in $\nabla E^2$ distribution on these z planes were exported through a line, defined from the midpoint between the electrode tips to 500 µm away from that point in y direction. To be able to perform further numerical analyses on FEM results (COMSOL), exported FEM data were transferred to EXCEL.

#### 3.2.2.1. Simulation Results

Following the explained simulation method, the $\nabla E^2$ simulations of the proof of concept DEP spectrum devices were made. As in the initial devices, in this case the optimum mesh size between the electrodes was determined first. For this purpose, simulations were completed by providing different mesh sizes (6 µm, 3 µm, 1.5 µm, 1 µm, 0.75 µm and 0.6 µm) between the electrode tips and the distributions of $\nabla E^2$ derived from these simulations are presented in Figure 3.21. As shown in Figure 3.21, the results of the changes in $\nabla E^2$ for the mesh dimensions of 1 µm, 0.75 µm and 0.6 µm are significantly close. In particular, the curves obtained for 0.6 µm and 0.75 µm are almost the same indicating the convergent results. As a result, in order to get the change of $\nabla E^2$ accurately, the maximum mesh size between the electrodes was determined as 0.6 µm. Table 3.6 shows the complete mesh number and the number of degrees of freedom solved for each mesh size tested during FEM modeling and simulations.

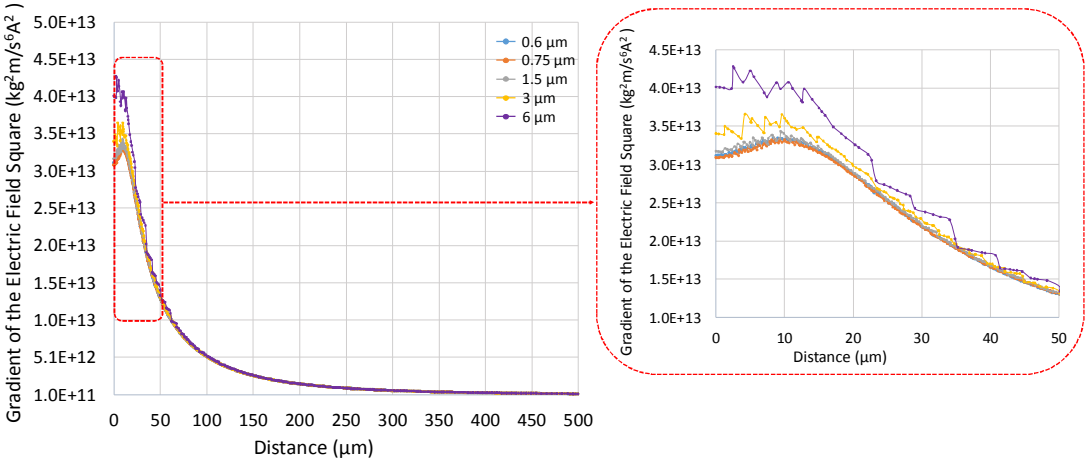


*Figure 3.21.* The change of $\nabla E^2$ term for six different mesh sizes between the electrode tips

Table 3.6. *Complete mesh number and the number of degrees of freedom solved for each mesh size tested during FEM modeling and simulations*

| Mesh size between the electrode tips | Number of degrees of freedom solved | Complete mesh number |
|---|---|---|
| 0.6 | 27304011 | 6661116 |
| 0.75 | 23019921 | 5615148 |
| 1.5 | 11999107 | 2924712 |
| 3 | 5641858 | 1373379 |
| 6 | 2382071 | 578340 |

Figure 3.22 shows where $\nabla E^2$ is greater than $10^{12}$ $kg^2m/s^6A^2$ at 10 $V_{pp}$ for 0.6 µm mesh size between the electrode tips. As explained in the simulation methodology, it shows the changes of $\nabla E^2$ for the circular area having a radius of 500 µm from the center of the device located 10 µm above the parylene surface. Exported data for this simulation result is presented in Figure 3.23.

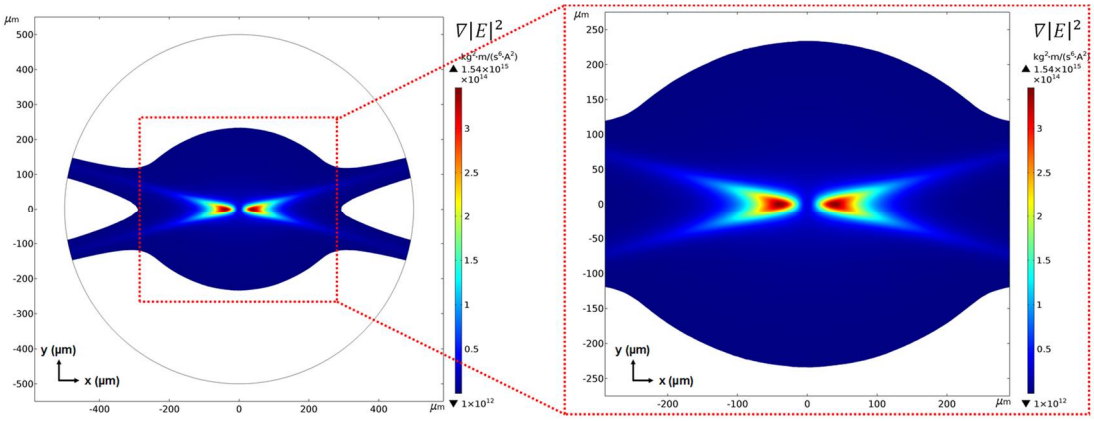


*Figure 3.22.* The change of $\nabla E^2$ for final DEP spectrum design

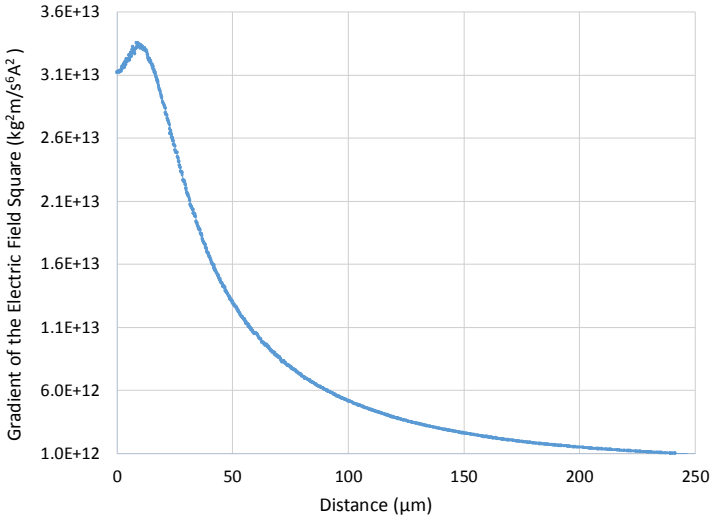


*Figure 3.23.* The graph of $\nabla E^2$ distribution for final DEP spectrum device

According to the simulation results, the proposed electrode design creates the required electric field gradient within the area from the midpoint between the electrode tips to a distance of approximately 240 µm. As described in Section 3.2.2, the final analysis with simulations was performed to see the effect of elevation on the generated DEP force. In this content, variations in the $\nabla E^2$ along the z-axis was examined in the 3D analyses for 6 different z planes, defined from $z = 0.5$ µm plane to $z = 50.5$ µm plane

with 10 µm increment between the planes. The changes in $\nabla E^2$ distribution on these z planes are shown in Figure 3.24. As a result, it is seen that the height difference around the device center has an effect on the generated DEP force and the force gradually decreases with the height. However, when moving away from the center of the device, the distributions of the $\nabla E^2$ term converge and give the same results for different z planes. The distance of 80 µm from the center was accepted as a limit to eliminate the variations in the magnitude of the DEP force exerted on the cells due to possible height differences. At this point (80 µm away from the center), the change of $\nabla E^2$ between the lowest ($z = 0.5$ µm) and highest planes ($z = 50.5$) is about 7.5%. The results of all simulation studies were examined and it was decided to include the cells remaining in the 80 µm (the limit determined to eliminate the possible variations in the DEP force due to height differences) and 240 µm (the limit where $\nabla E^2$ is greater than $10^{12}$ $kg^2m/s^6A^2$, which is necessary for the manipulation of the cells) range from the center of the device for DEP spectrum calculations.

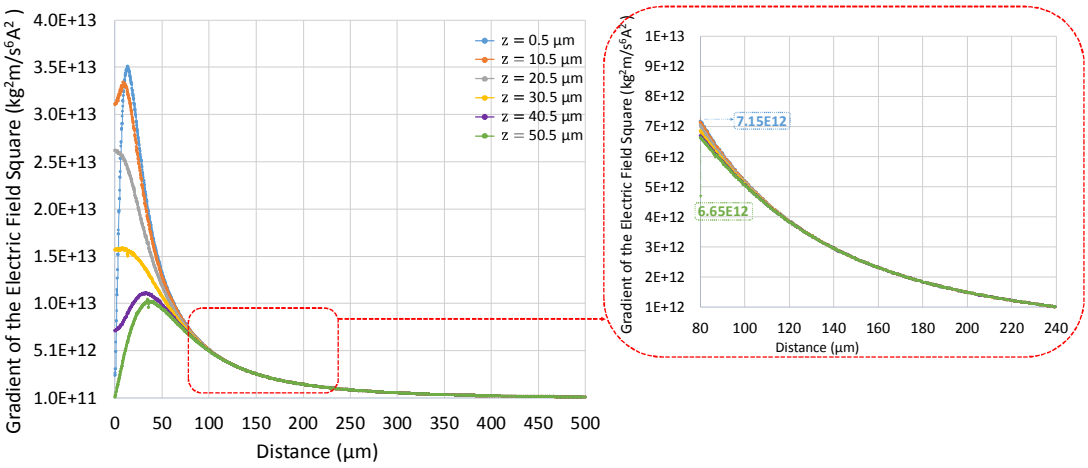


*Figure 3.24.* The graph of $\nabla E^2$ distribution on different z planes for final DEP spectrum device

### 3.2.3. Fabrication

DEP spectrum device fabrication is exactly the same of the initial proof of concept device fabrication. It has the same two masks and consists of photolithography, metal sputtering, lift-off, photolithography and polymer (Parylene-C) coating steps. Since the fabrication flow of the final DEP spectrum devices is the same as the fabrication flow used in the proof of concept, the fabrication flow and all related parameters are the same as those presented in the Appendix A. Utilized 1st mask (clear field) shown in Figure 3.25. The images of the planar electrodes after lift-off and the sharpness of the lift-off procedure with the narrow alignment marks are shown in Figure 3.26 and Figure 3.27, respectively.

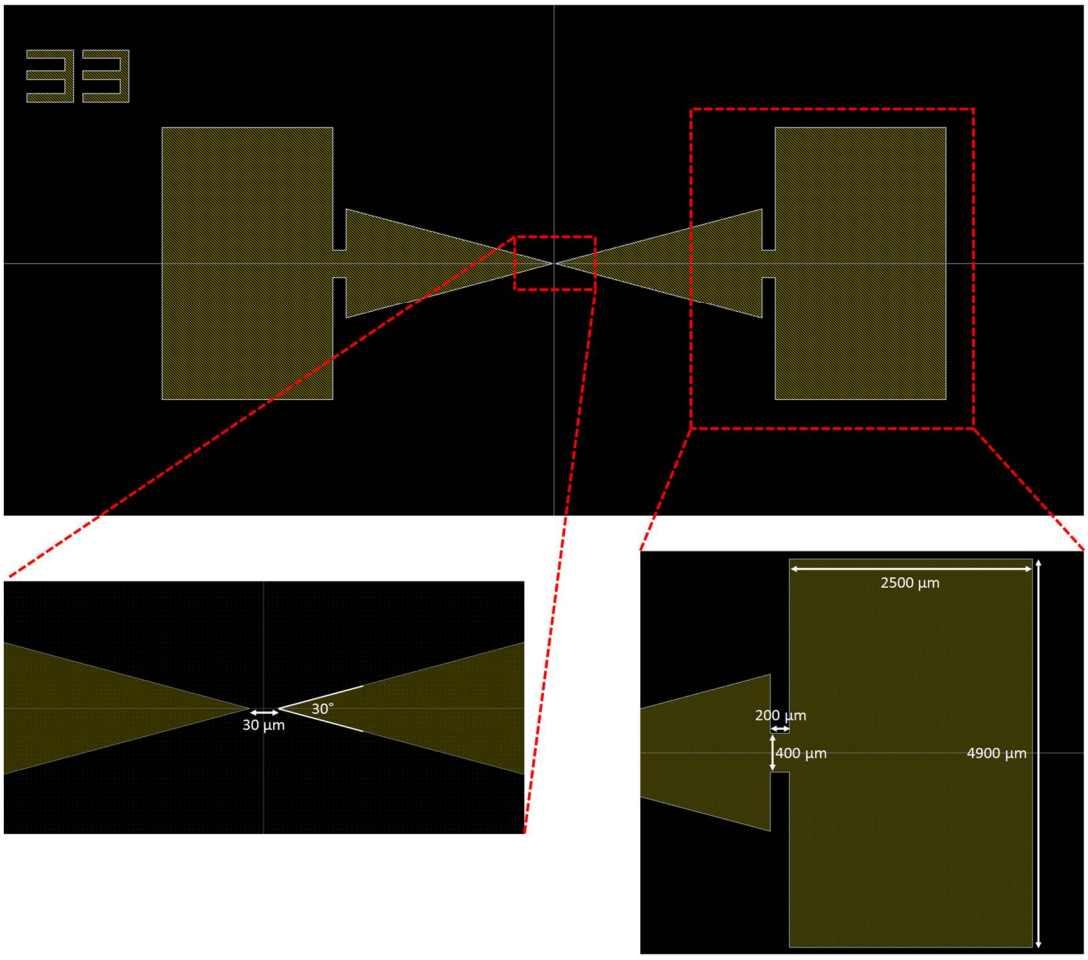


Figure 3.25. *1st mask layer of the DEP spectrum devices*

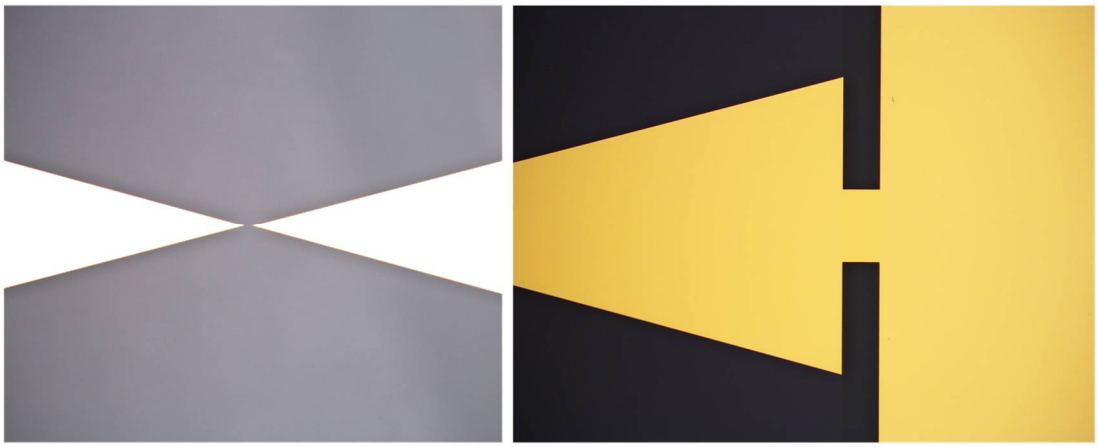

*Figure 3.26.* The images of the planar electrodes after lift-off

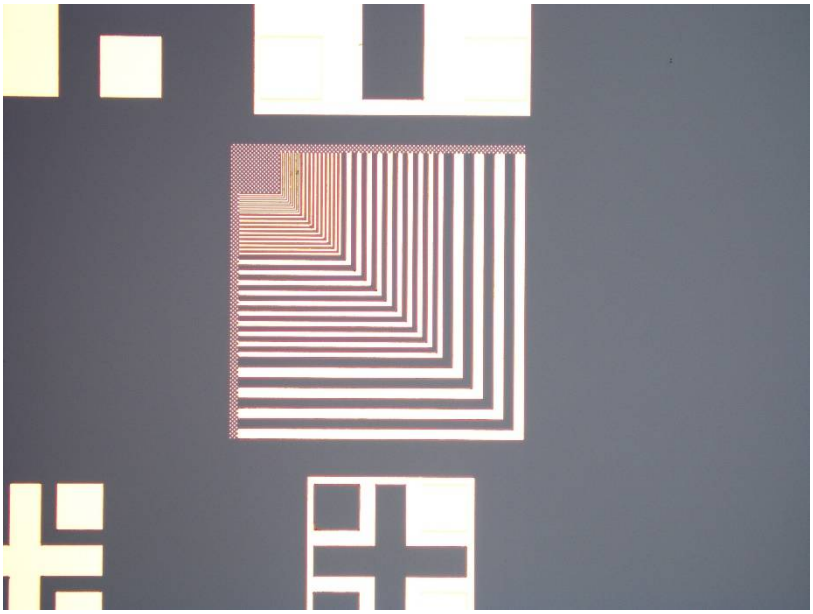

*Figure 3.27.* The lift-off performance is shown with the narrow line architecture

### 3.2.4. Materials & Method

In this section, the preparation steps of the cells used in the DEP spectrum experiments, the experimental set-up and the examination method of the DEP spectrum records obtained during the experiments are explained in detail.

### 3.2.4.1. Preparation of the Cells

*Preparation of MCF7 Breast Cancer Cells*

The preparation steps followed up to the fluorescein staining of MCF7 cancer cells are exactly the same as the preparation steps for MCF7 cells given in Section 3.1.4.1. The cells were stained with fluorescein diacetate (FDA), a fluorescent dye that stain live cells, in order to monitor the cells and to track the cell movements better. To prepare the FDA solution used for staining the cells, the FDA (in powder form) was dissolved in DMSO (10 μg/ml). For staining $10^6$ cells, approximately 1 μl of this solution was utilized. Cells were observed as green under fluorescent microscope with the FITC filter after staining procedure was completed. At the end of cell preparations, cell viability rates and cell concentration adjustments were made with automated cell counter (BIO RAD, TC20™ Automated Cell Counter).

*Preparation of the White Blood Cells (WBCs)*

For the testing of final DEP spectrum devices, leukocytes were prepared.

To extract leukocytes directly from whole blood sample without dealing with mononuclear and polymorphonuclear WBCs separately, Red Blood Cell (RBC) Lysis Solution (10×, MACS-Miltenyi Biotec) was used. RBC Lysis Solution (10×) has been developed for the lysis of red blood cells to provide optimal lysis of erythrocytes with minimal effect on all cell types obtained from blood or tissue samples [54].

In order to carry out the tests, whole blood samples taken from healthy volunteers were obtained at the METU Medical Center with the ethics committee approval certificate. Whole blood samples taken from peripheral blood vessels of healthy volunteers were collected in tubes containing $K_3$EDTA.

Initially, RBC Lysis Solution (10×) was diluted 1:10 ratio with double distillated water. For example, 1 ml of RBC Lysis Solution (10×) was diluted with 9 ml of double distillated water. With this way, 1× Red Blood Cell Lysis Solution was prepared. Then, 1 ml of blood sample was diluted with 10 ml of prepared 1× RBC Lysis Solution

and vortexed for 5 seconds. Obtained solution was incubated for 10 mins. At the end of this incubation time it became transparent red. Afterwards, it centrifuged at 300 g for 10 minutes at room temperature. The images obtained during the stages of this protocol are given in Figure 3.28. By aspirating supernatant completely obtained cell-pellet was re-suspended in the prepared DEP medium and washed twice with it. Obtained WBCs were stained with fluorescein diacetate (FDA) as described in the preparation of MCF7 cells.

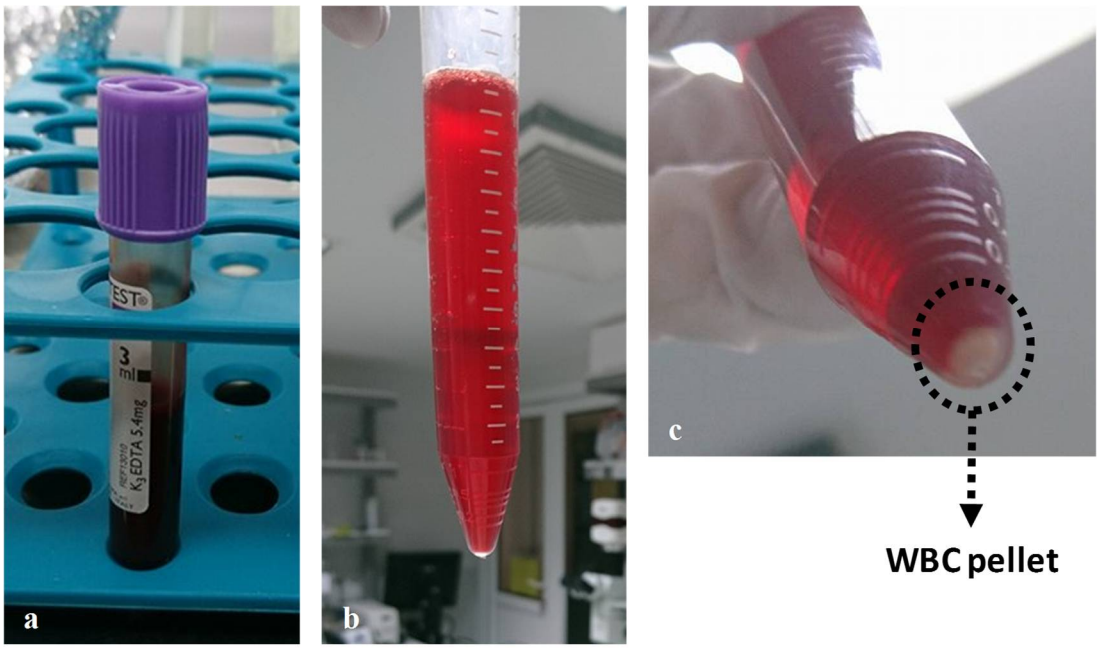


*Figure 3.28.* Images acquired during the protocol applied to remove red blood cells from whole blood sample (a) Untreated whole blood sample taken from donor (b) Transparent red appearance of blood and lysis solution mixture after 10 minutes incubation (c) Appearance of white blood cells precipitated after centrifugation (10 min at 300 g)

### 3.2.4.2. Experimental Setup and Test Procedure

This part presents the developed and used experimental setup for conducting improved DEP spectrum experiments with the final devices. The experimental setup is demonstrated in Figure 3.29. Before energizing the electrodes for each test, the

reservoir was filled with a 1 µl cell solution. As in the initial device experiments, sufficient time (approximately 30 second) was allowed to stabilize the cell solution and the cells to eliminate the initial cell movements resulting from the release of the cell solution into the reservoir. Cell movements observed and recorded in this way are directly generated by DEP force. At the end of this waiting period, in addition to stopping the initial cell movements, it was provided that the cells were brought to the same plane as the electrodes. In addition, at the beginning of the experiment, the focus was adjusted to the electrode plane and the not changed throughout the entire experiment. Thus, cells were examined in the same plane (in the electrode plane) during the entire experiment. DEP force required to provide cell movement was created by applying voltage to the the electrodes with a signal generator (Agilent, 81150A). Two of its four outputs were connected to the two V-shaped planar electrodes by 50Ω coaxial cables with BNC connections. 10 Vpp with a 180° phase difference sinusoidal signals were applied to each electrode at 9 different frequencies, in the range from 500 kHz to 10 MHz. Throughout the experiments, the cells placed in the chamber were changed with the fresh cell solution at each tested frequency in order to eliminate the possibility of change in cells' dielectric properties due to the presence of the electric field [11]. Movements of cells were recorded using an inverted microscope (Leica, DMi8) and camera (Leica, MC190) under FITC filter.

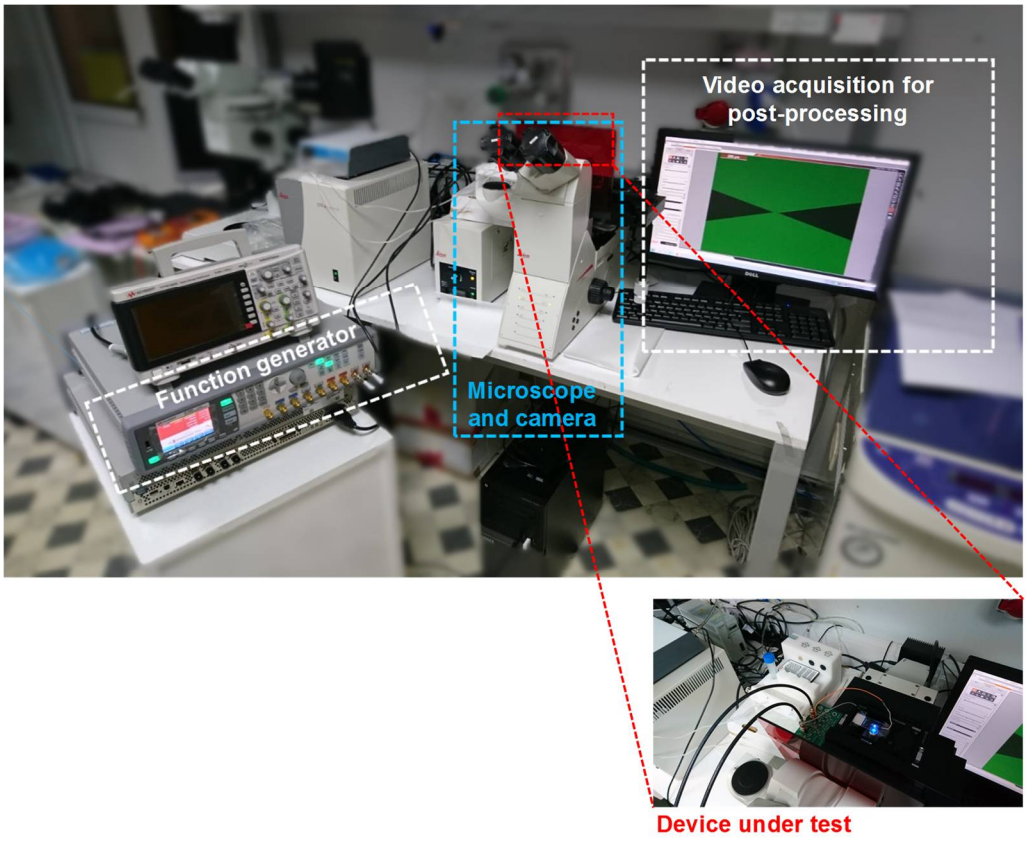


*Figure 3.29.* Experimental setup used for testing final DEP spectrum devices

### 3.2.4.3. DEP Spectra Examination Method

Final DEP spectrum devices were tested after fabrication with the improved experimental setup. As in the experiments of initial devices, the immobilized cells in the chamber are attracted towards the electrodes under pDEP with application of voltage. The examination method used to obtain DEP spectrum with the final devices is the same except for a single parameter from the method used in the proof of concept. In the initial examination, the average velocity of the cells, which indicates the strength of the DEP force acting on the cell, was calculated from the time of voltage application to the time the cells adhered to the electrodes with the effect of pDEP. However, in the examination of experiments with final devices, the average velocity of the first three-second movements after the voltage application, not all of the

movements of the cells until the electrode periphery, was taken as an indicator of the strength of the DEP force exerted on the cells. In this way, it is aimed to reduce the electric field gradient change that the cells are exposed to during the velocity studies included in the calculations.

The main purpose of the study carried out with the final devices is to automate the post-operations performed to obtain the DEP spectra of the cells. For this reason, the main improvements are provided in the tools that enable the implementation of this developed examination method. In the improved experimental setup, enhanced contrast was obtained between the cells stained with FDA and the background and the cell movements were recorded (Figure 3.30-a). Experiment records obtained with this way were examined by using TrackMate, a plugin which is available through Fiji software and used for tracking applications, and cell movements were easily monitored [55]. To automatically track cell movements through TrackMate, the experiment records are imported into the Fiji program and converted to 8-bit grayscale. After facilitating the detection of cells by adjusting brightness and contrast values optimally, the cell detection and tracking via TrackMate are initiated. TrackMate offers 3 different detection algorithms, Laplacian of Gaussian (LoG) detector, Difference of Gaussians (DoG) detector and Downsample LoG detector. All 3 detection algorithms are actually based on the Laplacian of Gaussian (LoG) segmentation, but are optimized with some additional methods to better detect different spot sizes. A plain LoG segmentation on the image is applied in the LoG detector. All calculations are performed in Fourier space, making the LoG detector ideal for medium spots with a diameter of between 5 and 20 pixels. DoG detector uses the difference of 2 Gaussians to approximate a LoG filter. Calculations are performed in the direct space, which makes it ideal for detection of small spots with a diameter below 5 pixels. The Downsample LoG detector utilizes LoG detector; however, it downsizes the image by an integer factor before filtering. This method makes it ideal for detection of large spots with a diameter larger than 20 pixels [56]. In view of the information given for these detector types, LoG detector was selected as the detection

algorithm by considering the diameter of the cells to be examined. Once LoG detector is selected, cell detection and tracking process is started by entering the diameter and threshold information of the cells to be detected. After detection process and initial spot filtering steps, HyperStack displayer is used as a visualization tool to display the tracking results. After arranging spot filtering and tracker selection-configuration steps, tracking results for the whole video were obtained. The images taken during the examination of the DEP spectrum video of MCF7 cells recorded at 850 kHz and 10 $V_{pp}$ with TrackMate are given in Figure 3.30. Cells detected by TrackMate before voltage application and at the end of the record are shown in Figure 3.30-b and Figure 3.30-c, respectively. The appearance of the paths followed by the cells during the corresponding record detected by the TrackMate is given in Figure 3.30-d.

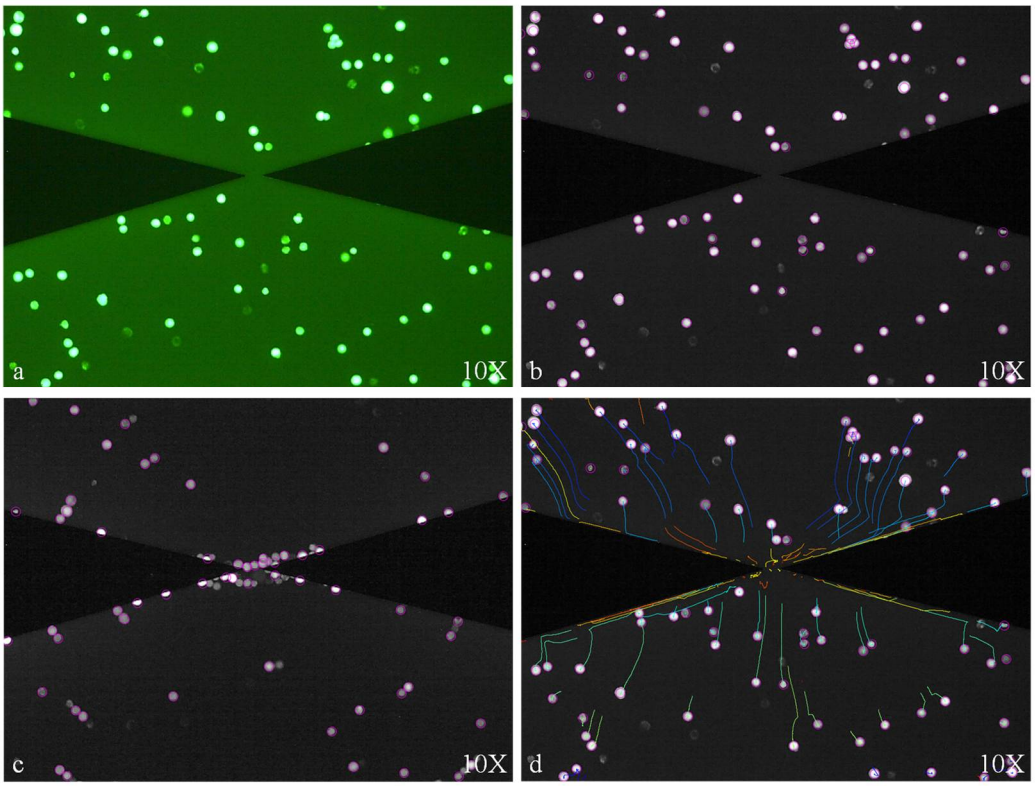


*Figure 3.30.* Images taken during the Fiji - TrackMate examination of the DEP spectrum video of MCF7 cells recorded for 850 kHz and 10 Vpp in the new experimental setup (a) The view of FDA-stained MCF7 cells under inverted microscope during DEP spectrum experiments with final devices (b) Cells detected before voltage application (c) Cells detected at the end of record (d) Tracks of the cells detected throughout the video

As a result, TrackMate detects the cells in each frame of the selected record according to the set characteristics and determines the respective track by following these cells throughout the video. It assigns a different ID number for every cell detected in each frame and creates the corresponding track number by linking them. By using the spots in track statistics display from the analysis feature of the TrackMate, assigned spot ID numbers, tracks and all related parameters are obtained. Assigned ID numbers for the cells detected and the corresponding spots in track statistics display are shown in Figure 3.31. In the spots in track statistics screen, there are calculated results such displacement in x and y positions and corresponding frame of the cells detected.

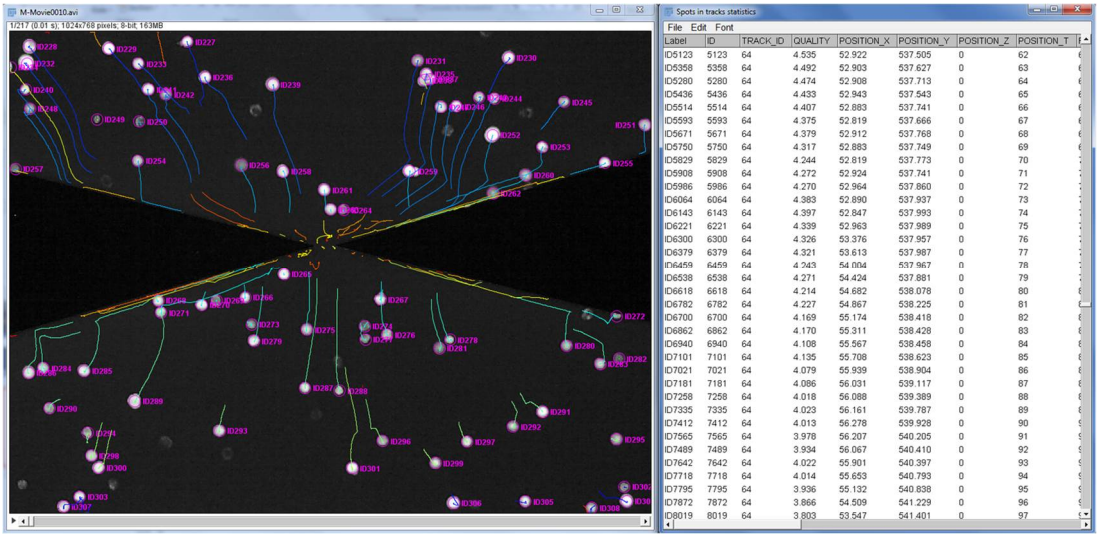


*Figure 3.31.* Assigned ID numbers for the cells detected and the corresponding spots in track statistics display

Recorded cell movements for each frequency during the experiments were analyzed and utilized to obtain DEP spectra of the corresponding cells. For this purpose, each recorded experiment video was examined using Fiji-TrackMate as described above and corresponding spots in track statistics results were exported to EXCEL and saved as a separate file. These steps were applied to all records obtained in the same set of

experiment. A code was generated by using C++ and complied/built with Borland Developer Studio 2006, to automatically measure the average velocity of the cells over these recorded files for their movements in the first three seconds after the voltage application for each frequency tested. Before the use of the developed code, all result files saved as EXCEL should be converted to .cmd file to be executable for this interface. The use of this code was initiated by uploading the created data file via the generated interface. This data file was composed of number of the experiment record, start and stop frames of the cell movement (the difference between them approximately 3 seconds), the exact time difference in these two frames and coordinates of the electrode tips in pixels. The generated code calculates the displacement of the cells in x and y directions between the given start and stop frames in the data file. The gap between the electrode tips, 30 μm for the final DEP spectrum devices, was taken as a reference to convert distance measurements from pixel to μm. According to the exact time difference between the start and stop frames, average cell velocity was found in μm/s for each cell. By using the code, the average velocity of all the cells detected and monitored by the Fiji program was calculated, and the selection of the cells to be included in the DEP spectrum averages which meet the specific criteria was performed. Criteria for the selection of cells included in the averages in determining the DEP spectra of cells:

- Cells moving towards to the electrodes (includes the cells that move towards higher electric field gradient region under the effect of pDEP),
- Cells with a mean velocity higher than 0 μm/s (eliminates stationary cells),
- Cells remaining between 80 μm and 240 μm distances from the midpoint of the electrode tips (indicates the area of examination determined as a result of COMSOL simulations),

- Cells remaining 5 µm away from periphery of the electrodes (eliminates sudden cell jumps observed for the cells located at the periphery of the electrodes with the voltage application),

- Cells that are continuously monitored between the start and stop frames (eliminates incomplete cells tracing and cell tracing with interruptions).

By applying these criteria, the data of the selected cells were saved in the result file.

### 3.2.5. DEP Spectra Results

*MCF7 Breast Cancer Cells:*

Figure 3.32 shows the MCF7 breast cancer cells during the DEP spectrum experiments with improved setup. As in the study of proof of the DEP spectrum concept, the live cells were lined up on the electric field lines after waiting for sufficient time to complete their movement with the application of voltage. Collected cells at the electrode periphery with the formed pearl chain structures at the end of the experiment record are shown in Figure 3.32.

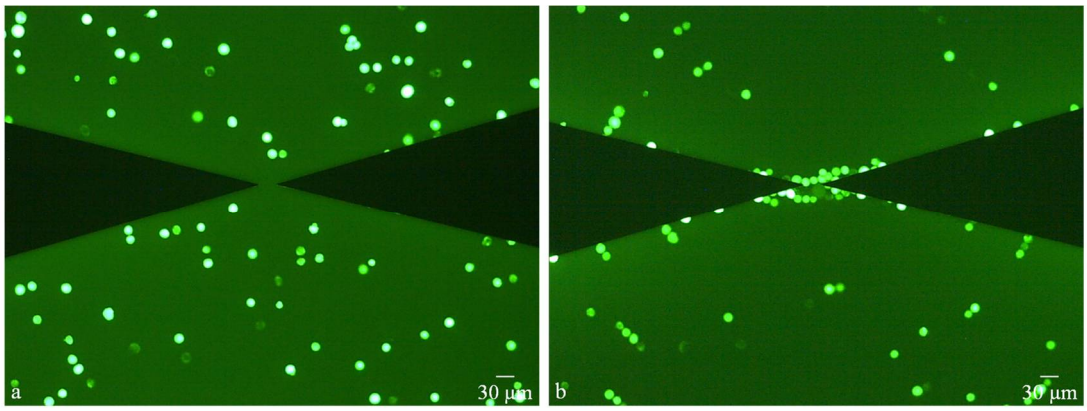


*Figure 3.32.* MCF7 cells under DEP spectrum experiments with improved setup (a) Distribution of cells on the device before voltage is applied (b) Collection of cells at the electrode periphery as a result of voltage application and formation of pearl chain structures on electric field lines

DEP spectrum of the MCF7 breast cancer cells with the improved setup and analyze method was obtained with the repetition of experiments on 4 different days with freshly supplied cells. Figure 3.33 shows the DEP spectrum result with the mean cell velocity calculated for each frequency and the corresponding standard error of the mean. The number of cells examined for each frequency to calculate average cell velocity is given in Table 3.7.

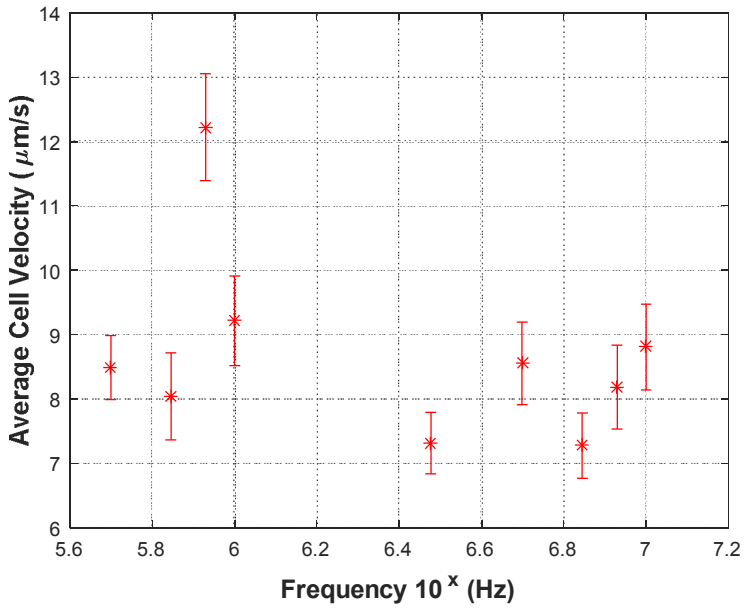


*Figure 3.33.* DEP spectrum of MCF7 breast cancer cells

Table 3.7. *The number of cells examined at each frequency in determining the DEP spectra of MCF7 cells*

| Frequency | Number of cells examined | Frequency | Number of cells examined |
|---|---|---|---|
| **500 kHz** | 161 | **5 MHz** | 122 |
| **700 kHz** | 86 | **7 MHz** | 137 |
| **850 kHz** | 143 | **8.5 MHz** | 133 |
| **1 MHz** | 150 | **10 MHz** | 161 |
| **3 MHz** | 131 | | |

*White Blood Cells:*

Views of WBCs during the DEP spectrum experiments with improved setup are shown in Figure 3.34.

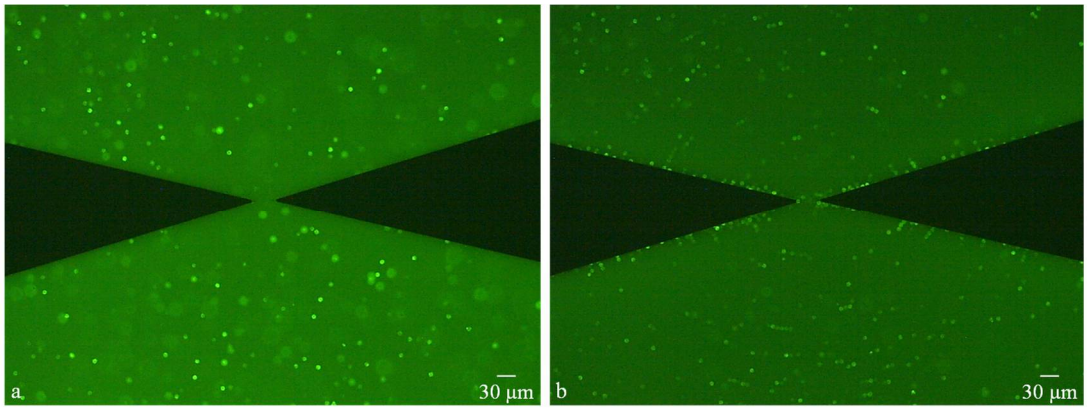


*Figure 3.34.* WBCs cells under DEP spectrum experiments with improved setup (a) Distribution of cells on the device before voltage is applied (b) Collection of cells at the electrode periphery as a result of voltage application and formation of pearl chain structures on electric field lines

DEP spectrum of the WBCs with the improved setup and analyze method was obtained with the repetition of experiments on 3 different days with freshly supplied WBCs from one healthy donor. Figure 3.35 shows the DEP spectrum result with the mean cell velocity calculated for each frequency and the corresponding standard error of the mean. The number of cells examined for each frequency to calculate average cell speed is given in Table 3.8.

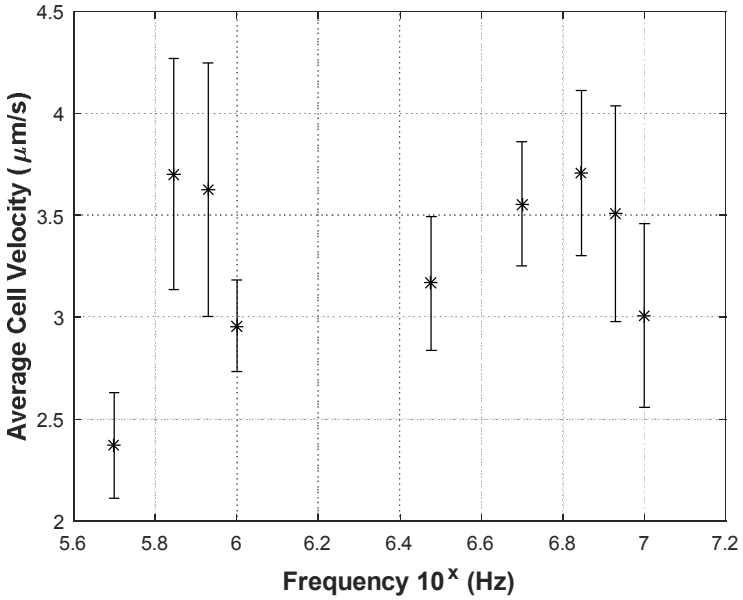


*Figure 3.35.* DEP spectra of WBCs

Table 3.8. *The number of cells examined at each frequency in determining the DEP spectra of MCF7 cells*

| Frequency | Number of cells examined | Frequency | Number of cells examined |
|---|---|---|---|
| **500 kHz** | 29 | **5 MHz** | 28 |
| **700 kHz** | 23 | **7 MHz** | 20 |
| **850 kHz** | 21 | **8.5 MHz** | 21 |
| **1 MHz** | 29 | **10 MHz** | 11 |
| **3 MHz** | 28 | | |

### 3.2.6. Discussions

The proposed DEP spectrum study was improved by the developed experimental setup and the automated cell examination method. With these improvements, experiments with MCF7 cells and leukocytes obtained from one healthy donor were repeated for 9 different frequencies at constant voltage (10 $V_{pp}$). Cell examinations were completed as described in Section 3.2.4.3 and DEP spectra of the corresponding cells were

determined. In Figure 3.36, the results presented in Section 3.2.5 for each cell type are shown together. The results reveal that there are significant velocity differences occurs between MCF7 cells and WBCs at 500 kHz, 850 kHz and 1 MHz. Table 3.9 shows the average velocity values measured for MCF7 and leukocytes at these frequencies, and the ratios of these velocities to each other. These results indicates that these 3 frequencies can be used to enrich MCF7 cancer cells from WBCs on a DEP-based separation system.

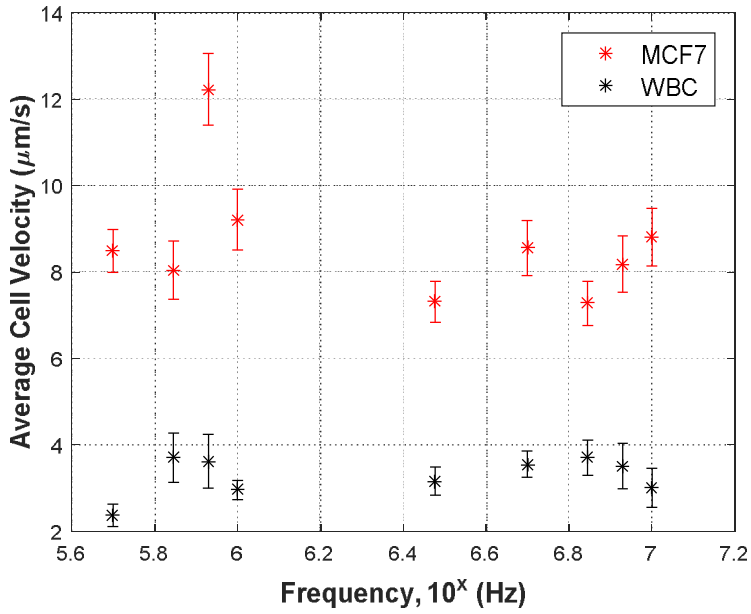


*Figure 3.36.* DEP spectra of MCF7 cells and WBCs (voltage = 10 $V_{pp}$)

Table 3.9. *The average velocities calculated for MCF7 and WBCs at the determined enrichment frequencies and the ratio of these velocities to each other*

| Frequency | Average Cell Velocity (μm/sec) | | Velocity Ratio (MCF7/WBC) |
|---|---|---|---|
| | **MCF7** | **WBC** | |
| **500 kHz** | 8.48 | 2.37 | 3.58 |
| **850 kHz** | 12.23 | 3.63 | 3.37 |
| **1 MHz** | 9.22 | 2.96 | 3.12 |

The main purpose of the change in the experimental setup is to facilitate and automate the cell tracking performed in the DEP spectrum determination. In this way, cell detection and tracking was performed easily by using Fiji-TrackMate and the required cell analysis was done successfully with generated C++ (Borland) code. Thus, the number of cells involved in dep spectrum data is greatly increased. The increase in cells included in the dep spectrum data was particularly significant in MCF7 cells. Although there was slight increase in leukocytes included in DEP spectrum data, it was not as remarkable as in MCF7 cells. The reason for this is that photobleaching problem is encountered in the DEP spectrum experiments of leukocytes (Figure 3.37). Photobleaching means the fading of the fluorescence signal during the imaging experiment due to the photochemical destruction of fluorophore. In the case of photobleaching, the fluorescence signal starts out bright but dims with illumination [57]. Although there was no change in fluorescence brightness of MCF7 cells during the experiment, photobleaching problem was encountered in WBCs. Therefore, detection and tracking of WBCs could not be performed even shortly after the beginning of the experiment due to lack of contrast. Due to this problem, investigations were limited to leukocytes obtained from a single healthy donor and the DEP spectrum of the leukocytes obtained from this donor were determined in 3 different experimental days. In addition to the Fiji-TrackMate program, Manual Tracking application, a plugin which is available through Fiji software, was also utilized in order to minimize the monitoring and detection problems encountered in leukocyte investigations. This application helps to obtain the data used in the calculation of the speed of the cells experiencing the problem of tracking automatically due to the problem of photobleaching.

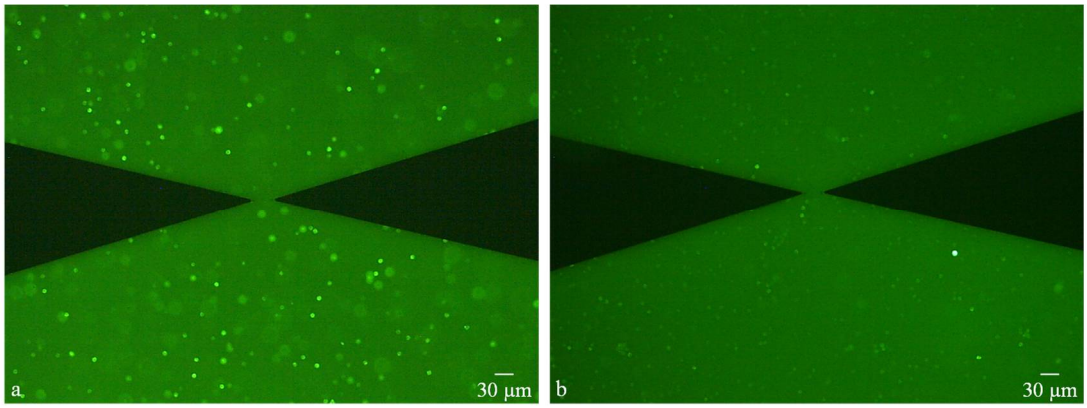


*Figure 3.37.* The photobleaching problem observed in leukocytes during the experiments with the improved experimental setup and procedure. (a) Initial intensity of leukocytes stained with FDA observed at the beginning of the experiment. (b) The view of FDA stained leukocytes with reduced fluorescence brightness due to photobleaching problem

### 3.3. Conclusion

The purpose of the proposed DEP spectrum study is to define the DEP spectra of the particles without considering the specific particle properties. Although there are methods for cell characterization in the literature such as impedance measurement, electrorotation and dielectric crossover frequency determination, these methods are highly comprehensive methods which include determining the specific dielectric properties of the cells. In addition to that, when the results of these studies were examined, some discrepancies were observed in the dielectric properties and crossover frequency information of the cells. Therefore, the proposed DEP spectrum study was conducted. The goal of this study is to define the DEP spectra of the particles differentially without considering the specific particle properties. This method allows direct observation of the effect of DEP force exerted on particles and hence eliminates the requirement of measuring membrane and cytoplasmic properties of particles to identify their DEP spectra. In other words, the generated DEP spectrum device is one-to-one modeling of the DEP-based enrichment microchannel without flow parameters, which allows the direct comparison of the DEP force acting on the cells.

For the proof of DEP spectra investigation of the biological cells with the proposed analysis method, MEMS-based DEP spectrum device was designed. In this design, reciprocal V-shaped planar electrodes were utilized to create non-uniform electric field in the chamber that holds the cell solution. Initial results obtained from the proof of concept DEP spectrum devices reveal that, at 1 MHz a significant velocity difference occurs between MCF7 cells (33.99 μm/s) and WBCs, mononuclear WBCs (7.9 μm/s) and polymorphonuclear WBCs (13.82 μm/s). Considering the problems associated with the experimental setup, testing and post-processing of the proof of concept devices, the proposed DEP spectrum study was improved. The results of the improved DEP spectrum study reveal that there are significant velocity differences occurs between MCF7 cells and WBCs at 500 kHz, 850 kHz and 1 MHz with the ratios 3.58, 3.37 and 3.12, respectively. When the whole obtained results are examined, it is seen that 1 MHz is determined as a possible enrichment frequency in both studies. In the improved DEP spectrum study, it is seen that in addition to this frequency, two new possible enrichment frequencies (500 kHz and 850 kHz) are determined. This situation is evaluated as a direct result of the improvement in the examination method. Since the cell examination method was limited by the movements of the cells in the first 3 seconds instead of all the movements of the cells, the mean DEP force exerted on the cells was decreased and the effect of the instantaneous DEP effect force was examined. In addition, the examination method was automated and approximately 130 MCF7 cells were examined for each frequency value with the developed DEP spectrum study. In the improved analysis, photobleaching problem was encountered during the DEP spectrum experiments of leukocytes. Therefore the number of examined leukocytes could not be increased as much as the MCF7 breast cancer cells, even if they are increased compared to the initial study.

The tests of the proposed and developed DEP spectrum study were also expanded with other cell types including Huh7 and Hep3B, liver cancer cells and cancer stem cells (CSCs). These cell lines are provided from METU CanSyL (Cancer Systems

Laboratory), in collaboration with research group of Prof. Dr. Rengül Çetin Atalay. Cancer stem cells are cancer cells with characteristics associated with normal stem cells, which can convert into diverse cell types due to their unlimited self-renewal and terminal differentiation capability. With this ability, CSCs have the capacity to develop into new tumors (tumorigenic), and are thought to have high metastatic potential, causing cancer relapse. Hence, therapies targeting CSCs may result in better prognosis. Therefore, their isolation from cancer cells is critical especially for drug development studies and cancer research. Conventionally, CSCs isolation is achieved using antibodies directed at cell-surface markers similar to current CTC detection methods. However, due to lack of a single biomarker to distinguish CSCs, immunologic methods cannot efficiently isolate CSCs. Therefore, to inspect the possibility of isolating corresponding CSCs from cancer cells via DEP-based methods, their DEP spectra were investigated also with the proposed method. For this purpose, DEP spectrum experiments of the respective cells were completed without any problem of photobleaching on large populations.

# CHAPTER 4

# DEP BASED RARE CELL ENRICHMENT

In this chapter, studies on DEP-based rare cell enrichment unit are presented. Firstly, the design and simulation of the DEP-based rare cell enrichment devices are explained. The finite element simulations of the designed DEP enrichment devices are done by using COMSOL Multiphysics® 5.3 software. Next, used microfabrication techniques in the MEMS fabrication of the DEP enrichment devices will be given. In the fabrication section, the parylene microchannel fabrication method, which is improved in the BioMEMS group, used in the fabrication of DEP enrichment units is described. Finally, experimental results on the DEP enrichment devices are presented. In this content, procedures related to the preparation steps of the MCF7 breast cancer cell and leukocyte mixture, designed and installed experimental setup are explained. Then, the obtained recovery rate results of the DEP enrichment units will be presented.

## 4.1. Design of the DEP Enrichment Devices

In the design of DEP-based enrichment devices, there are some criteria to be considered such as the purpose of the DEP device (e.g., enrichment, trapping, separation, focusing, etc.), the structure of electrodes (e.g., electrode type, electrode material, the gap between the opposing electrodes, etc.) and the design parameters (e.g., voltage and frequency of the generated electric filed, channel dimensions, etc.). The aim of the DEP-based enrichment unit is to remove blood cells, which are relatively much more present, from the system and thereby obtain a CTC-enriched sample.

In Chapter 3, by applying the proposed DEP spectrum analysis method to the MCF7 cells and leukocytes that are planned to be separated, the DEP spectra of the corresponding particles were determined and compared over the frequency range

scanned. Subsequently, according to the DEP spectra information of these particles, it is now possible to determine and design the most accurate DEP-based enrichment device. By considering the presented results in the Chapter 3, this design should achieve enrichment using the pDEP principle. In addition, enrichment should be conducted under continuous flow.

In the proposed enrichment strategy, enrichment will be made by using the positive DEP principle. The designed device structure has two inputs and two outputs. One of the inputs is the cell solution input while the other input is the DEP buffer medium input. The DEP buffer medium is pushed with more pressure than the cell solution, allowing the cells to focus on the channel wall on the cell inlet side before the active DEP region. In this way, at the beginning of the active DEP region, the cells will be exposed to positive DEP force from the microchannel wall at the cell inlet. Because the white blood cells and MCF7 cells are exposed to different values of positive DEP strength at the enrichment frequency as determined by the DEP spectrum study, these cell types will move at different rates along the channel width in the active DEP region. Because MCF7 cells are exposed to more positive DEP force, they will move to the other wall of the channel and move towards the cancer cell outlet. As the leukocytes are exposed to lower positive DEP force, they will move less in the channel width and will be collected at the WBC outlet.

While designing electrode geometries to be used in DEP-based microfluidic platforms with continuous flow, the two forces acting on the particles, DEP force and hydrodynamic forces should be considered together. The parameters required to define the electrode geometry, such as the tilt angle of the electrodes, the electrode width and the gap between the opposing electrodes, must be carefully determined to manipulate the particles under continuous hydrodynamic force. Iterations to determine electrode shapes, dimensions and angles have been studied with simulations. The planar electrodes can be inserted into the microchannel base during fabrication. Compared to the side-wall electrodes, the DEP force generated by this type of electrode can be sustained without any loss over the channel width. In this way, large

microchannels can be obtained. Therefore, electrode structure is selected as planar for the proposed DEP enrichment device. Additionally, as described in Chapter 3, the non-uniform electrical field required to provide cell movement in the DEP spectrum chips was also formed by planar electrodes. Selecting planar electrode structure for the DEP enrichment device provides a consistency between these two DEP devices.

According to the above explained choices, the design parameters, the electrodes type, shape and the gap between them; microchannel depth, length and width; parylene layer thickness; and magnitude of the applied voltage were determined. In this context, two different electrode structures which are supposed to provide enrichment by using pDEP were designed [58], [59]. In these designs, rectangular evenly spaced and trapezoidal electrodes were used. Different sub-designs were obtained by varying the parameters such as the position of the electrodes in the microchannel, number and dimension of the electrodes for each main electrode structure. For lateral evenly spaced electrode structure, 3 different sub-designs were generated by changing the gap between the electrodes (60 μm and 15 μm) and the angle of the electrodes relative to the main channel (13° and 25°). The width of the electrodes was constant and equal to 60 μm for all sub-designs. For trapezoidal electrode structure, 2 different sub-designs were generated by only changing the electrode dimensions (20 μm & 120 μm, 15 μm & 90 μm). In all these generated designs, to determine the optimum electrode number that provides the highest enrichment efficiency electrodes were expanded through the microchannel. Prepared mask layouts of the two sub-designs for each electrode structure are given in Figure 4.1 and Figure 4.2.

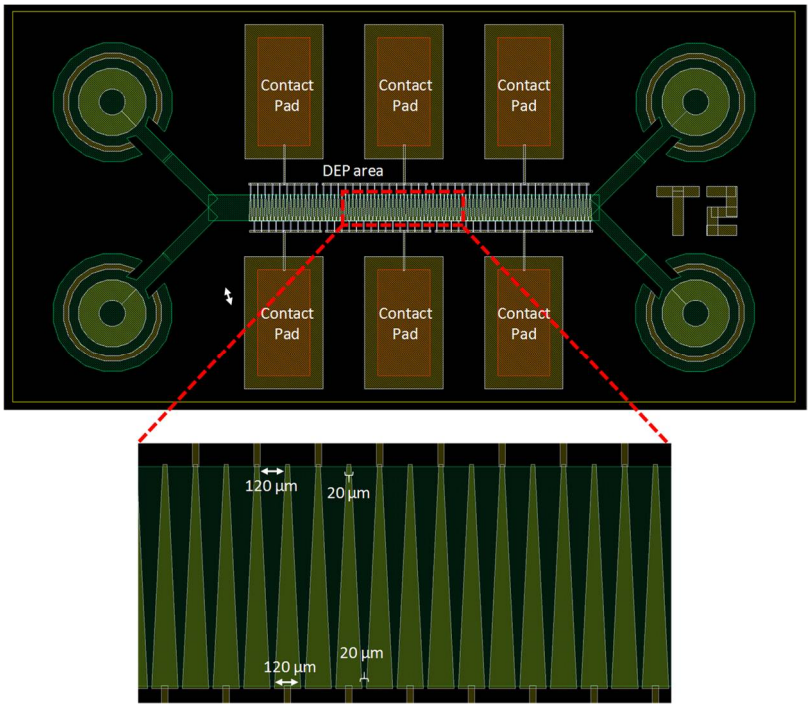


*Figure 4.1.* Mask layers of a sub-design for the trapezoidal electrode structure

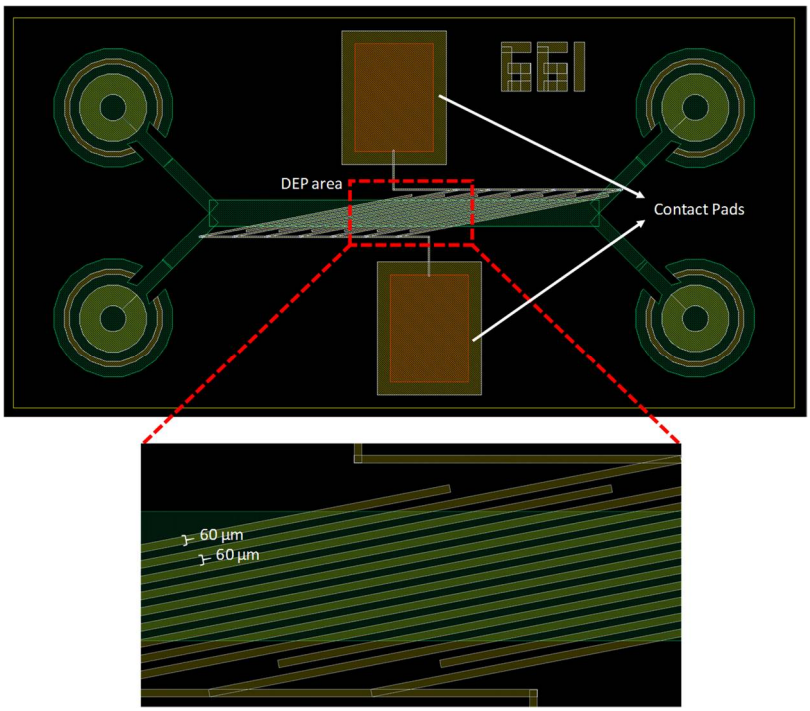


*Figure 4.2.* Mask layers of a sub-design for the rectangular evenly spaced electrode structure

Fabrication of these microchannels were done by using parylene microfabrication technique. Followed fabrication flow is same with the one used for the final DEP-based enrichment device which is explained in Section 4.3 in detail. Images of the electrode structures after the metal patterning with wet etching are given in Figure 4.3.

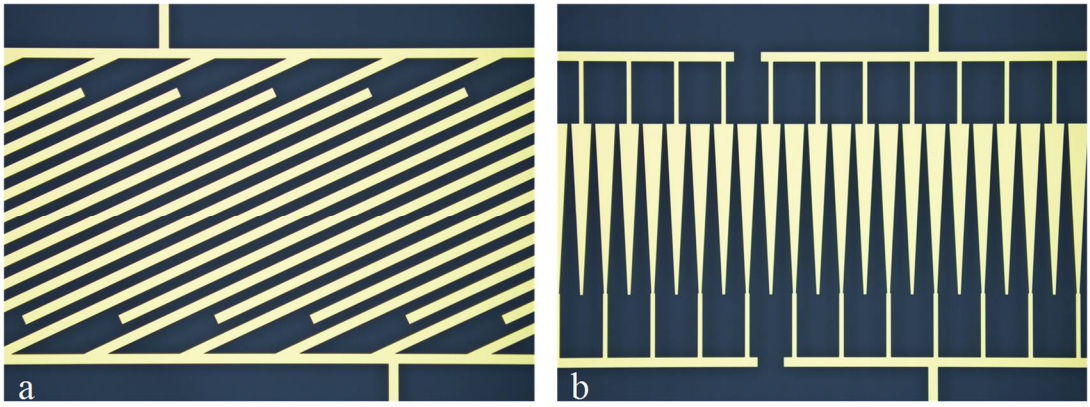


*Figure 4.3.* The images of (a) rectangular evenly spaced and (b) trapezoidal planar electrodes after wet metal etching

In order to realize the planned enrichment strategy through DEP-based enrichment devices, adjusting the design parameters of the electrodes is crucial. At this point, it should be noted that the aim of fabricated these initial enrichment devices was just to see whether proposed electrode structures will satisfy planned enrichment strategy or not. In addition, it was also aimed to improve the final enrichment device according to the feedback obtained from these trials.

After the fabrication of these devices, initial experiments were conducted with MCF7 cells. Experiments performed with the trapezoidal electrodes were unsuccessful to direct cells from focused region to cancer cell outlet under continuous flow. Instead of this, cells were trapped between the electrodes where the DEP force is higher (Figure 4.4). This situation was encountered in both designs involving the trapezoidal electrode structure. Although different flow rates and voltage values were applied

during the experiments cell trapping between the electrodes could not be eliminated. Due to all these reasons, the proposed trapezoidal electrode structure was leaved.

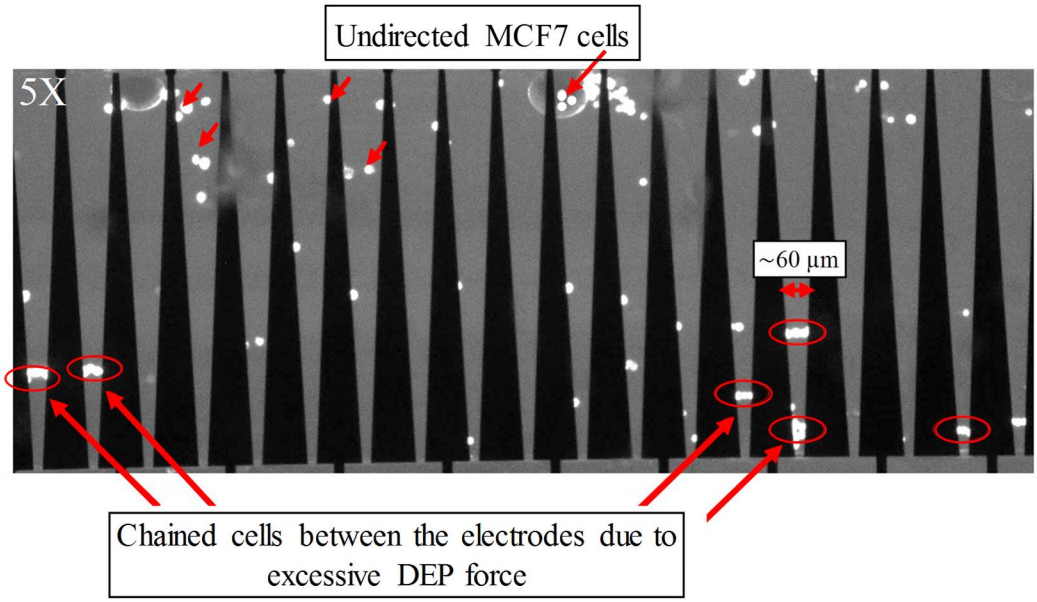


*Figure 4.4.* The appearance of the MCF7 cells forming the pearl chain structure between the trapezoidal electrodes (voltage = 20 $V_{pp}$, frequency = 3 MHz, cell inlet pressure = 300 mbar, DEP buffer inlet pressure= 100 mbar)

Experiments conducted with the rectangle and evenly spaced electrode structure with 60 µm gap between the electrodes and 13° tilt angel of the electrodes were promising. The appearance of the MCF7 cells in the active DEP region that are directed towards to bottom wall of the microchannel (to cancer cell outlet) under continuous flow is shown in Figure 4.5. In the given figure the cells in motion are not clearly seen. This is due to the inadequate speed of the camera (30 frames/second) for capturing cells in motion. The result obtained for this design indicates that by adjusting hydrodynamic flow conditions and dielectrophoretic forces exerted on the cells, aimed separation strategy can be implemented. Hence, the final DEP-based enrichment device was developed by utilizing rectangular evenly spaced electrodes and feedback gathered from this design.

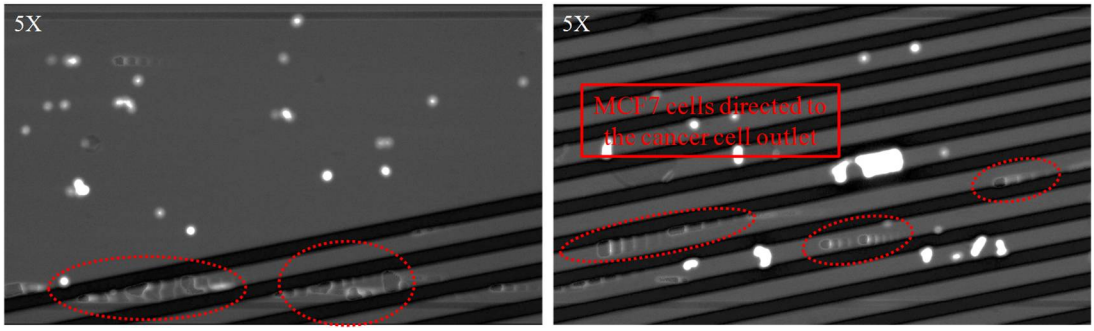


*Figure 4.5.* Sequential channel views showing that the MCF7 cells sliding along the rectangular electrodes and directed to the cancer cell outlet (voltage = 20 $V_{pp}$, frequency = 3 MHz, cell inlet pressure = 300 mbar, DEP buffer inlet pressure= 100 mbar)

*Final DEP-based Enrichment Device*

Schematics of the proposed finalized DEP-based enrichment device is shown in Figure 4.6. The finalized electrode structure consists of rectangular and evenly spaced electrodes which were rotated with a certain degree relative to the main flow. The width of the electrodes and the distance between them were 60 µm and a total of 4 electrodes were placed. The angle of the electrodes relative to the main channel was determined as 13°. To facilitate voltage application on the electrodes, the collateral electrodes were connected to each other and then to the electric pads.

The main channel width was chosen to be 1000 µm, the highest width limit for the parylene based microchannel used in METU-MEMS fabrication facilities without encountering any microchannel collapse problem. It was aimed to examine more sample volume by using the highest width limit for the main microchannel. The width of the side channels connecting the 2 inlets and 2 outlets to the main channel was 500 µm which is the half of the main channel width. Channel height (main channel and side channels) was limited to 20 µm considering the diameter of the cells that are going to be separated.

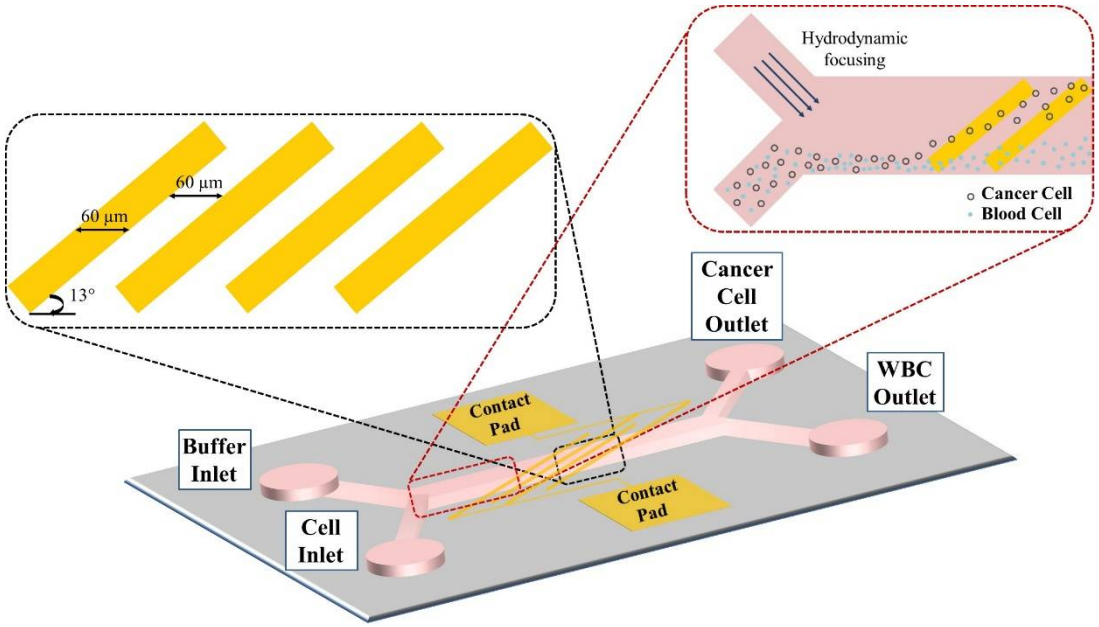


*Figure 4.6.* The schematic view of the DEP-based enrichment device with focused views of active DEP area and hydrodynamic focusing section

The magnitude and the frequency of the voltage was determined by taking into account of the obtained results in the Chapter 3. The separation frequency determined as a result of the DEP spectrum study was used directly in the DEP-based enrichment devices. The magnitude of the applied voltage for DEP-based enrichment devices was determined iteratively within 8-12 Vpp interval based on the voltage applied to the DEP spectrum examinations.

Table 4.1 presents all related design parameters, used in the DEP enrichment devices.

Table 4.1. *Design parameters used for the DEP-based enrichment device*

| Design Criteria | DEP Enrichment Device |
|---|---|
| **Electrode type** | Planar |
| **Electrode shape** | Rectangular |
| **# of electrodes** | 4 |
| **Electrode height** | 0.3 µm |
| **Electrode material** | Gold |
| **Tilt angel of the electrodes** | 13° |
| **Gap between the electrodes** | 60 µm |
| **Width of the electrodes** | 60 µm |
| **Parylene thickness** | 0.5 µm |
| **# of inlets & outlets** | 2 & 2 |
| **Main channel width** | 1000 µm |
| **Side channel width** | 500 µm |
| **Main channel length** | 8600 µm |
| **Channel depth (main & side)** | 20-21 µm |
| **Angels of side channels** | 45°, - 45° |
| **Voltage magnitude** | 8 - 12 $V_{pp}$ |
| **Voltage frequency** | 1 MHz |

## 4.2. Simulation Method

The necessary simulations are made by using COMSOL Multiphysics® 5.3 software after design parameters of the DEP enrichment devices were determined. The purpose of the simulations is to examine the strength and the distribution of the generated DEP force in the microchannel by the proposed electrode structure at the voltage and frequency values planned to be operated before the fabrication.

The simulation method followed is the same as the method followed for the DEP spectrum simulations except the defined geometry of the device. To reflect the actual device and experiment conditions, the microchannel filled with DEP medium was modeled as a height of 20 µm above an insulating parylene layer of 0.5 µm thick.

Modelled structure including parylene layer and microchannel is shown in Figure 4.7. Except the microchannel modelling of the device, all other simulation steps are the same with the simulation methodology explained for DEP spectrum devices. After completing required arrangements in the geometry and materials sections, sinusoidal voltage with 180° phase difference was applied to opposing electrodes by using $\pm|V|sin(wt)$ formula. Frequency and voltage magnitude were selected as 1 MHz and 10 $V_{pp}$ according to the results of enrichment operating data obtained in the DEP spectrum chapter. As in the DEP spectrum simulations, different mesh sizes between the electrodes were also tried to find optimum mesh size. In the simulation results obtained for different mesh sizes, the convergence of the $\nabla E^2$ term was examined and the maximum mesh size was determined accordingly. As a result, the maximum mesh size between the electrode tips was 2.5 µm which allows accurate detection of changes in the $\nabla E^2$ term distribution.

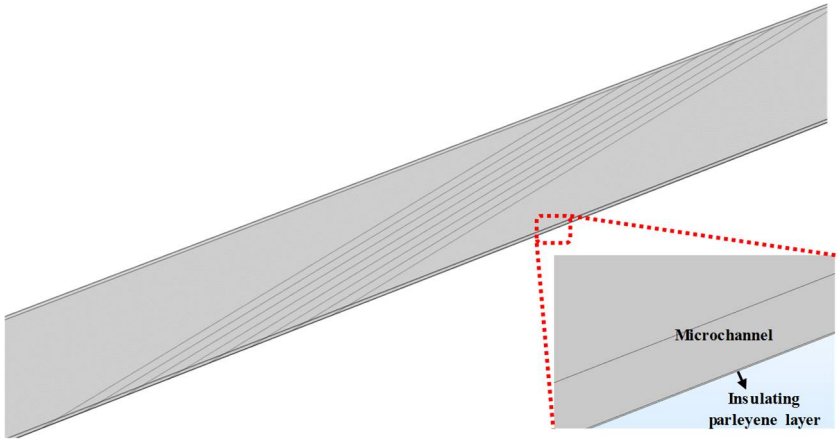


*Figure 4.7.* DEP enrichment device with parylene layer and microchannel modelled in COMSOL

In order to examine the created DEP force in the microchannel, the distribution of the $\nabla E^2$ is greater $10^{12}$ $kg^2m/s^6A^2$, which is minimum value for the manipulation of the cells, was studied. Assuming the diameter of 10-12 µm for the cells and the channel height 20 µm, a plane that is 10 µm above the parylene layer was chosen for examining $\nabla E^2$ on the x-y plane. For the analysis of changes in the $\nabla E^2$, a line was defined in the

x axis that divides the microchannel into two equal parts on this plane. Considering the size of the cells to be tested, the flow conditions and the height of the proposed microchannel limited to 20 µm, the change of the $\nabla E^2$ along the z axis was not examined. The obtained FEM (COMSOL) results were studied by exporting the $\nabla E^2$ values in order to perform further numerical analysis. Exported FEM data were transferred to EXCEL.

### 4.2.1. Simulations of the DEP Enrichment Devices

By applying the steps of the general simulation methodology, the distribution of $\nabla E^2$ term of the proposed DEP-based enrichment device was obtained. Initially, different mesh sizes between the electrodes were tried to obtain optimum mesh size. For this purpose, simulations were completed for 6 different mesh sizes (6 µm, 3 µm, 1.5 µm, 1 µm, 0.75 µm and 0.6 µm) and the distributions of $\nabla E^2$ derived from these simulations (Figure 4.8). Table 4.2 shows the complete mesh number and the number of degrees of freedom solved for each mesh size tested during FEM modeling and simulations. According to the results, maximum mesh size between the electrodes was determined as 2.5 µm in order to get the change of $\nabla E^2$ accurately.

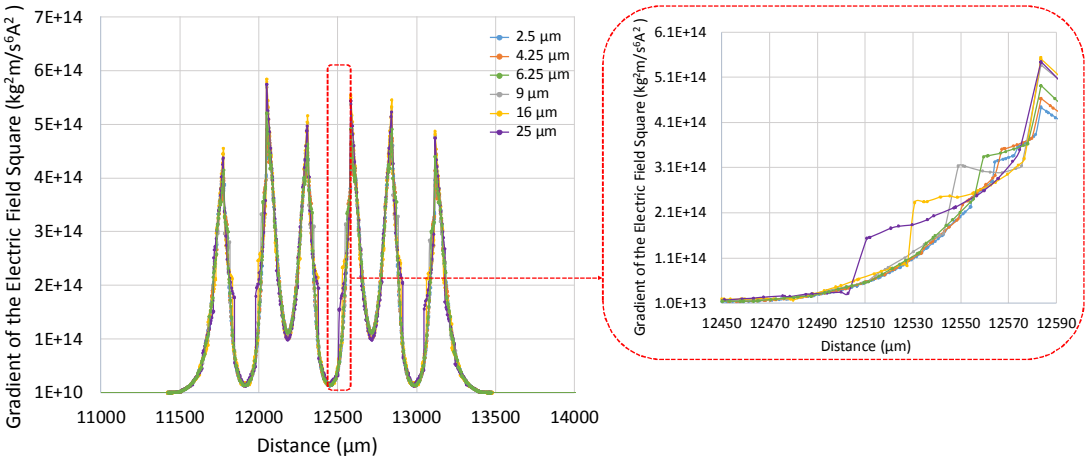


*Figure 4.8.* $\nabla E^2$ distribution for 6 different mesh sizes between the electrodes (25 µm, 16 µm, 9 µm, 6.25 µm, 4.25 µm and 2.5 µm)

Table 4.2. *Complete mesh number and the number of degrees of freedom solved for each mesh size tested during FEM modeling and simulations of DEP-based enrichment device*

| Mesh size between the electrodes | Number of degrees of freedom solved | Complete mesh number |
|---|---|---|
| 2.5 | 29031420 | 6589165 |
| 4.25 | 12983773 | 2944330 |
| 6.25 | 7605807 | 1723080 |
| 9 | 4360807 | 986740 |
| 16 | 1433025 | 323230 |
| 25 | 874313 | 196730 |

Figure 4.9 shows where $\nabla E^2$ is greater than $10^{12}$ $kg^2m/s^6A^2$ for 10 $V_{pp}$ at $z = 10.5$ µm. The $\nabla E^2$ distribution data for the line extending on the x axis that divides the microchannel into two equal parts on this z plane is presented in Figure 4.10.

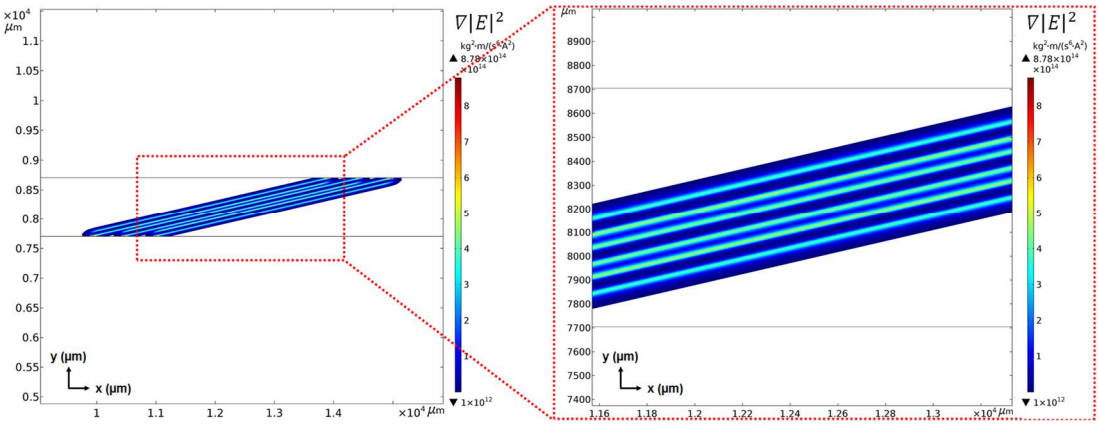


*Figure 4.9.* The change of $\nabla E^2$ for DEP-based enrichment device

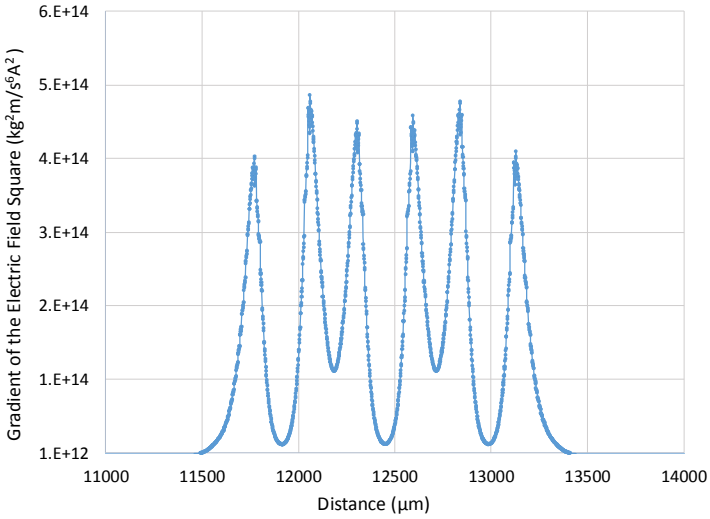


*Figure 4.10.* The graph of $\nabla E^2$ distribution for DEP-based enrichment device

When the given simulation results are examined, it can be seen that the proposed electrode design creates the required electric field gradient to manipulate the cells on the active DEP region. Throughout the active DEP region, the change of the $\nabla E^2$ is greater than $10^{12}$ $kg^2m/s^6A^2$, indicating that the cells will be successfully manipulated across the active DEP zone. Again, regular repetition of variations of the $\nabla E^2$ in the active DEP region indicates that the cells will undergo progressive withdrawal.

### 4.3. Fabrication

In this section, microfabrication techniques used in the fabrication of DEP enrichment devices are presented. As in DEP spectrum devices, surface micromachining techniques have been used to produce DEP enrichment devices. Fabrication flows with the photos showing important stages of fabrication, mask drawings generated through Cadence Layout Editor software, and images of the fabricated device will be presented in the following sections.

DEP enrichment device fabrication is a three mask process. It involves metal sputtering, wet and dry etching, photolithography, polymer (Parylene-C) coating. The

fabrication flow and all necessary constraints are given in the Appendix B. Whole fabrication process for the DEP-based enrichment device is given in Figure 4.11.

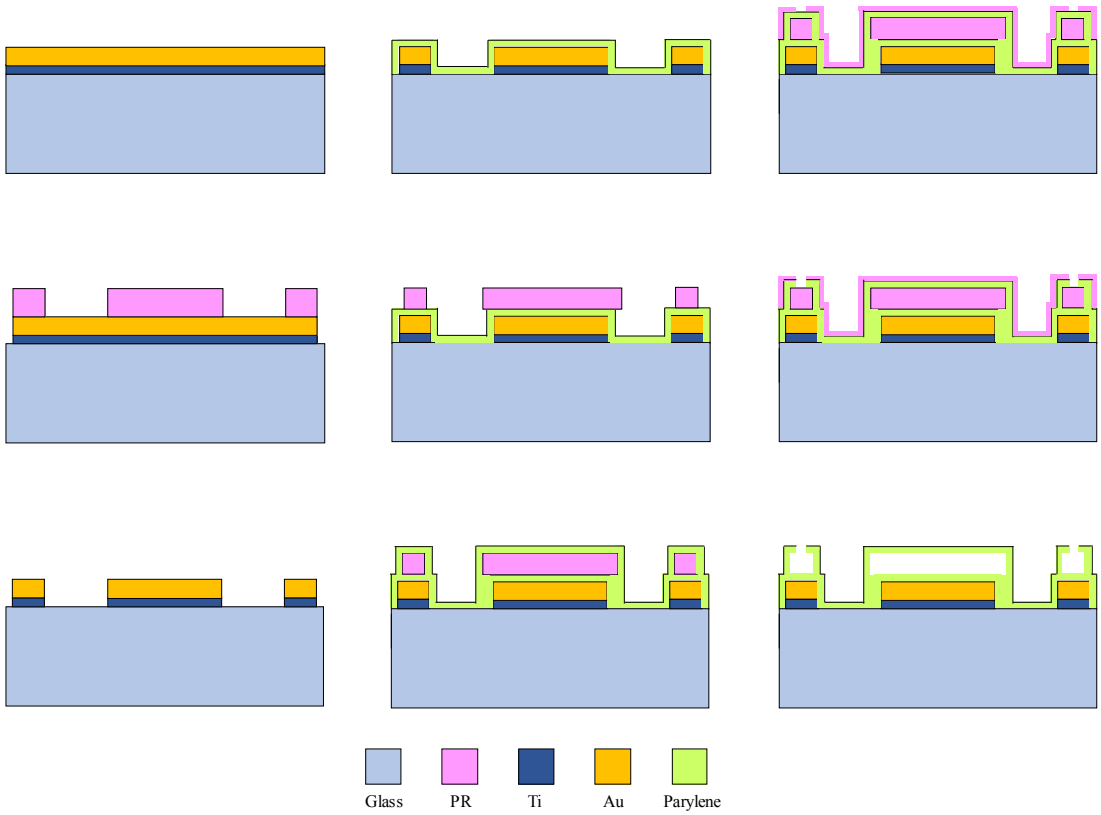


*Figure 4.11.* The fabrication flow of DEP-based enrichment devices

Fabrication started with the preparation of 6" glass wafers. In this context, wafers were pre-cleaned. Initially, the wafers were cleaned for organic residues with the piranha solution, then the wafers were etched with BHF (1: 7) (HF: NH4F) solution. After cleaning steps, Ti (30 nm) and Au (300 nm) were coated on the wafers. Ti is utilized as an adhesive layer for Au. Then, mask 1 (clear field) shown in Figure 4.12 was used for shaping of the metal (Ti/Au) layers. In this lithography step, SPR 220-3 positive resist is used so that electrode edges do not lose their sharpness during wet etching of metals. After shaping the photoresist layer, Ti & Au layers were patterned by using

wet etching. Commercial Au etchants were used for the patterning of Au layer. For Ti etching, a freshly prepared Ti etchant, containing of 20 ml HF, 20 ml $H_2O_2$ and 3960 ml DI water was used. The generated planar electrode structures after metal etching are shown in Figure 4.13.

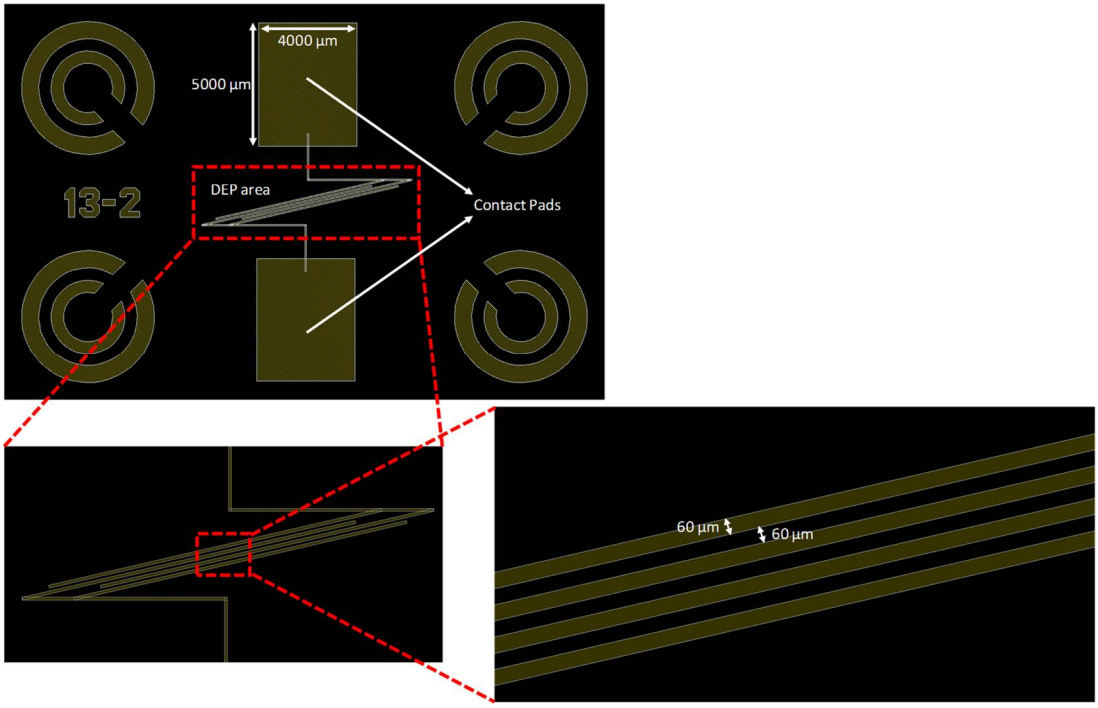


*Figure 4.12.* 1st mask layer of the DEP enrichment devices

After metal patterning, the remaining photoresist was removed from the surface in PR stripping baths. Afterwards, a thin layer of Parylene-C coating (0.5 µm) was made with silane to provide electrical insulation between electrodes and microchannel. Parylene coating with silane allows parylene to stick to the surface. Since there is no photoresist on the surface before the parylene coating in this fabrication flow, the parylene coating is done with silane. As in the case of DEP spectrum device fabrication, all parylene coatings were made at a ratio of 1:2, the thickness of the coated parylene layer in micrometers to parylene weight in grams [51].

*Figure 4.13.* The image of the planar electrodes after wet metal etching step

To pattern inlets, outlets and microchannel 2nd mask (clear field) was utilized. View of the 2nd mask layer is given in Figure 4.14. A thick resist was needed in this lithography to ensure that the microchannel was sufficiently high (~20 μm). Therefore, AZ 40XT photoresist was used by performing single spin. The microchannel structure formed after AZ 40XT patterning is shown in Figure 4.15. For microchannel wall formation on patterned resist, a second Parylene-C coating was done to obtain a thickness of 20 μm.

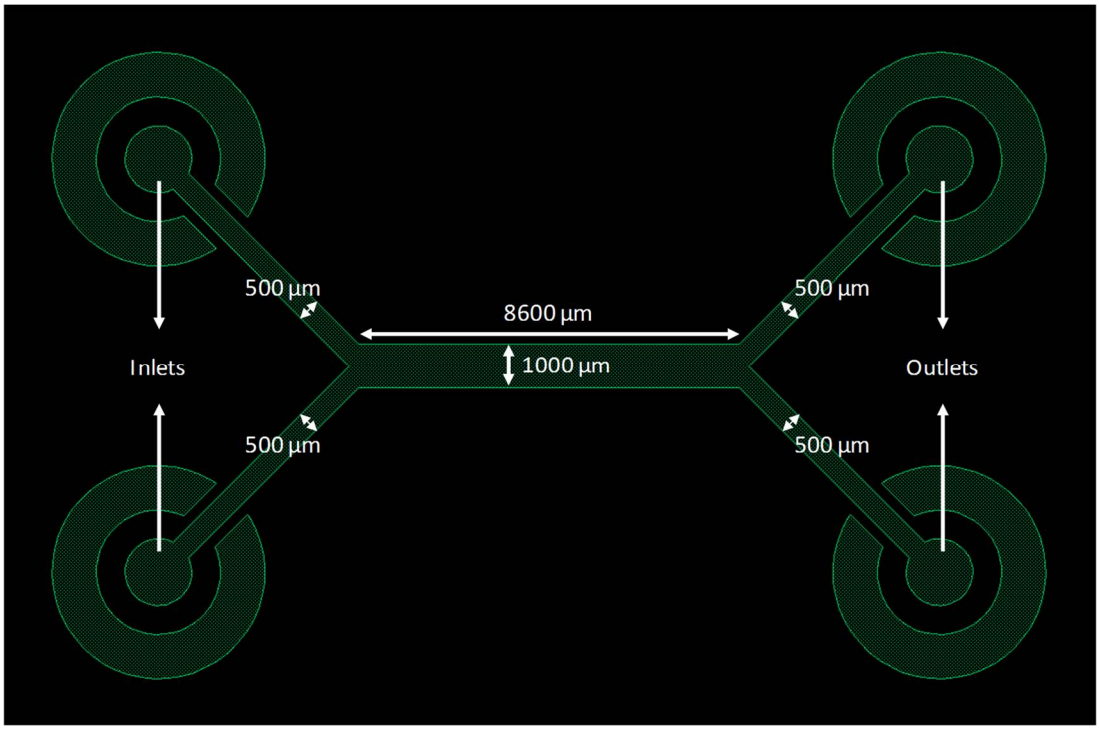


*Figure 4.14.* 2nd mask layer of the DEP enrichment devices

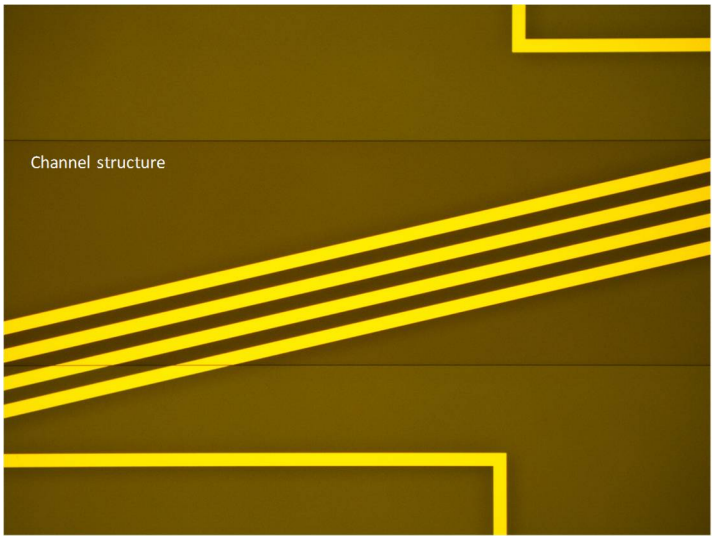


*Figure 4.15.* Channel structure after the AZ 40XT photoresist photolithography

After fabrication of the microchannels, openings for contact pads, inlet and outlet reservoirs were generated by reactive ion etching (RIE). In this content, 3rd mask (dark field) was utilized. View of the 3rd mask layer is given in Figure 4.16. The RIE process was used to open a depth of 20 μm. In order to make these opening processes properly, the applied RIE recipe was 5×20 minutes. Finally, each wafer was diced and 34 devices were obtained per one 6" wafer.

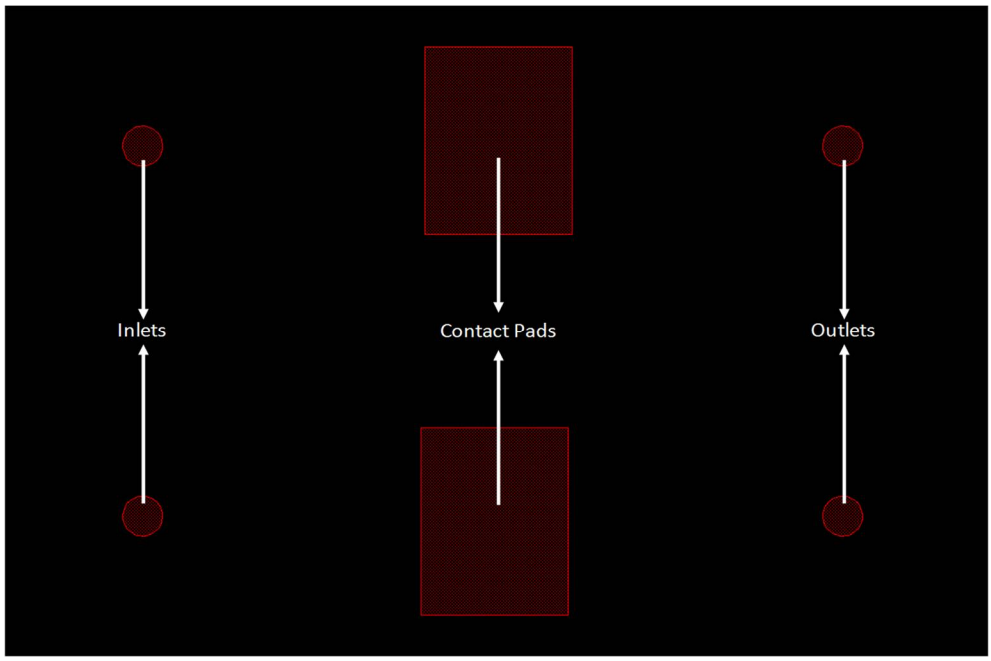


*Figure 4.16.* 3rd mask layer of the DEP enrichment devices

To remove the photoresist used as the sacrificial layer to form microchannel, each chip was placed in acetone for 4-5 days after the dicing step. Figure 4.17 shows the fabricated device.

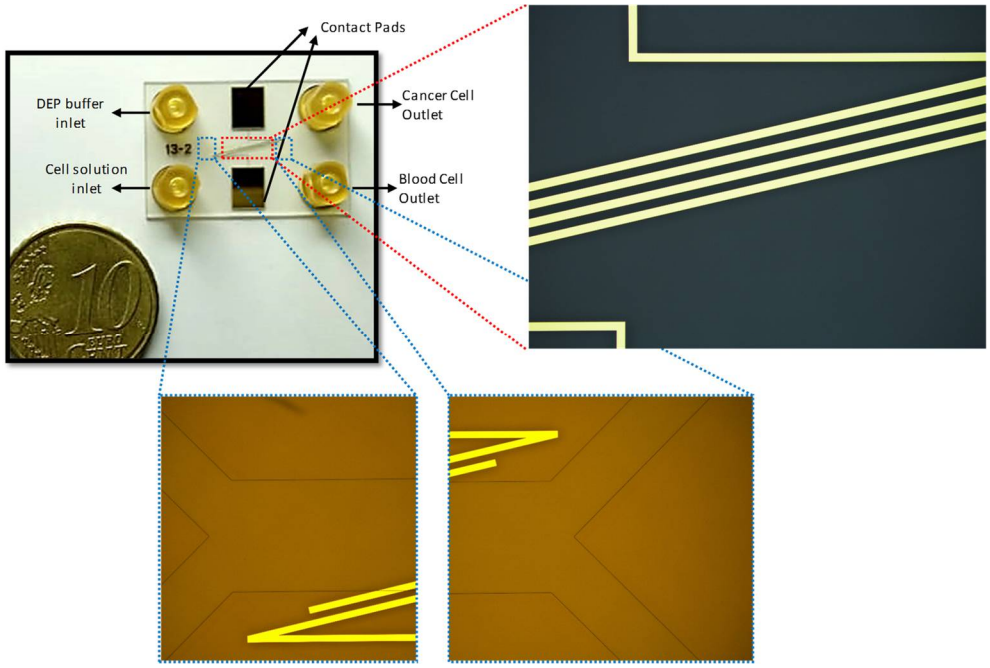


*Figure 4.17.* Fabricated DEP enrichment device

## 4.4. Materials & Method

In this section, cell mixture preparations, experimental setup and rare cell enrichment and recovery rate calculations will be explained.

### 4.4.1. Preparation of MCF7 Breast Cancer Cell & White Blood Cell Mixture

For the testing of DEP-based rare cell enrichment device, MCF7 breast cancer cells and leukocytes were prepared separately and then mixed. Obtained final cell mixture solution was applied to the microchannel.

The preparation steps of MCF7 breast cancer cells followed for the final DEP spectrum experiments in Section 3.2.4.1 were applied in the enrichment experiments. For the WBCs, the preparation steps followed in the final DEP spectrum experiments in Section 3.2.4.1 were applied up to the fluorescent staining part. During the enrichment experiments, in order to observe the MCF7 and WBC movements simultaneously in the microscope the cells were stained with fluorescent dyes of

different colors. In this content, MCF7 cell were stained with fluorescein diacetate (FDA) as explained in Section 3.2.4.1 and were observed as green under fluorescent microscope with the FITC filter after staining procedure was followed. WBCs were stained with CellTracker™ Red CMTPX dye (ThermoFisher Scientific) which is a well suited fluorescent dye for monitoring cell movement or location. To prepare CellTracker™ Red CMTPX dye solution used for staining the cells, the CellTracker™ Red CMTPX dye was dissolved in DMSO (50 µg/72.9 ml DMSO). For the staining of $10^6$ cells 2.5 µl of this solution was applied. Cells were observed as red under fluorescent microscope with the TXR filter after staining procedure was applied. After the cell preparation and staining steps were completed separately, MCF7 and leukocytes were mixed and the cell solution to be given to the channel for enrichment experiments was obtained. Cell viability rates and cell concentration adjustments were made with automated cell counter (BIO RAD, TC20™ Automated Cell Counter).

### 4.4.2. Experimental Setup and Test Procedure

This part presents the developed and used experimental setup for conducting DEP-based enrichment measurements. The schematic presentation of the installed experimental setup is presented in Figure 4.18. For the enrichment of rare cells (MCF7 cells) from WBCs, continuous flow analyses were carried out by using microfluidic flow control system (FLUIGENT, MFCS – EZ Pressure Controller). To provide continuous flow to two inlets (cell solution inlet and DEP medium inlet), a pressure controller (MFCS – EZ) was used. Two outputs of the pressure controller were directly connected to the DEP enrichment device inlets. With the software of pressure controller (MAESFLO™), the flow rates of cell inlet and DEP medium inlet were adjusted separately. Fluidic connections were done from microfluidic flow control system to device via microfluidic peek tubing (LabSmith, LS-TUBE116) with inner diameter 250 µm. The tubing was fitted to port connectors, which were bonded on device to create chip-capillary interface, for each inlet and outlet. Observations were carried out with an inverted fluorescent microscope (Leica, DMi8) under triple band excitation (DAPI-FITC-TRITC filter) option to be able to examine different colored

fluorescent dye-stained MCF7 and WBCs simultaneously. A high-speed camera (Leica, MC190) was used to observe the cell movements under continuous flow. Continuous real-time recording of the enrichment experiments was carried out with the software of the camera and microscope system (Leica, LAS MultiTime – Movie – Timelapse). DEP force required to provide cell movement was created by applying the electrodes with a signal generator (Agilent, 81150A). Two of its four outputs were connected to the two planar electrodes by 50Ω coaxial cables with BNC connections. 180° phase difference sinusoidal signals were applied to each electrode. Voltage and the frequency of the applied signals were determined by taking into account of the presented results in the Chapter 3. The photograph of the experimental setup is presented in Figure 4.19.

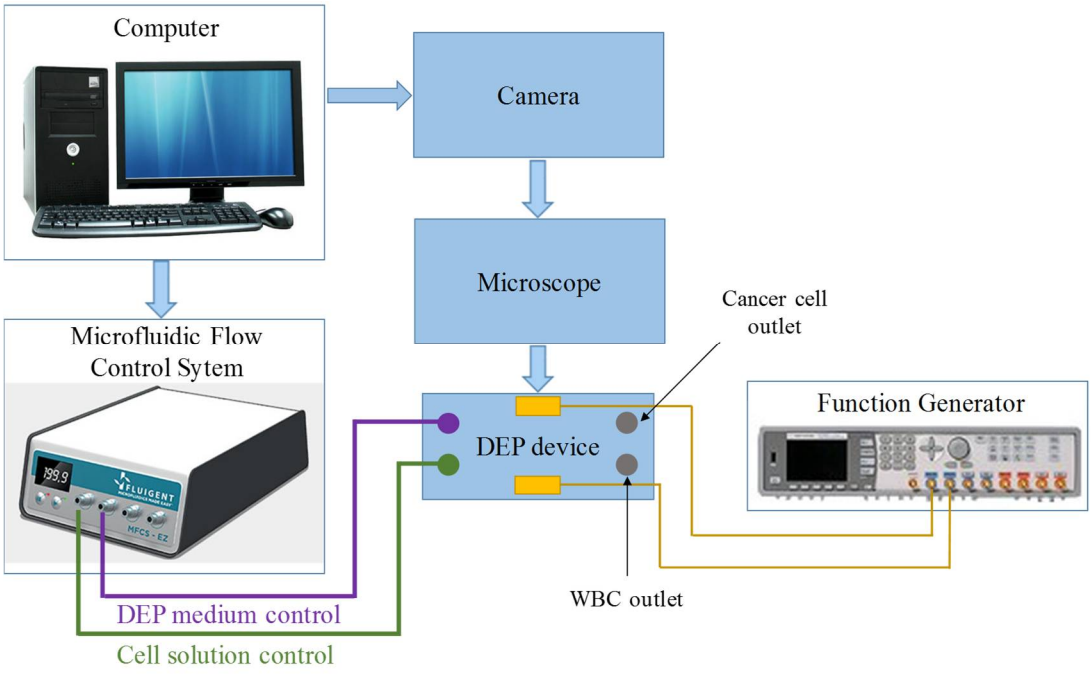


*Figure 4.18.* Schematic presentation of the installed experimental setup used for testing DEP enrichment devices

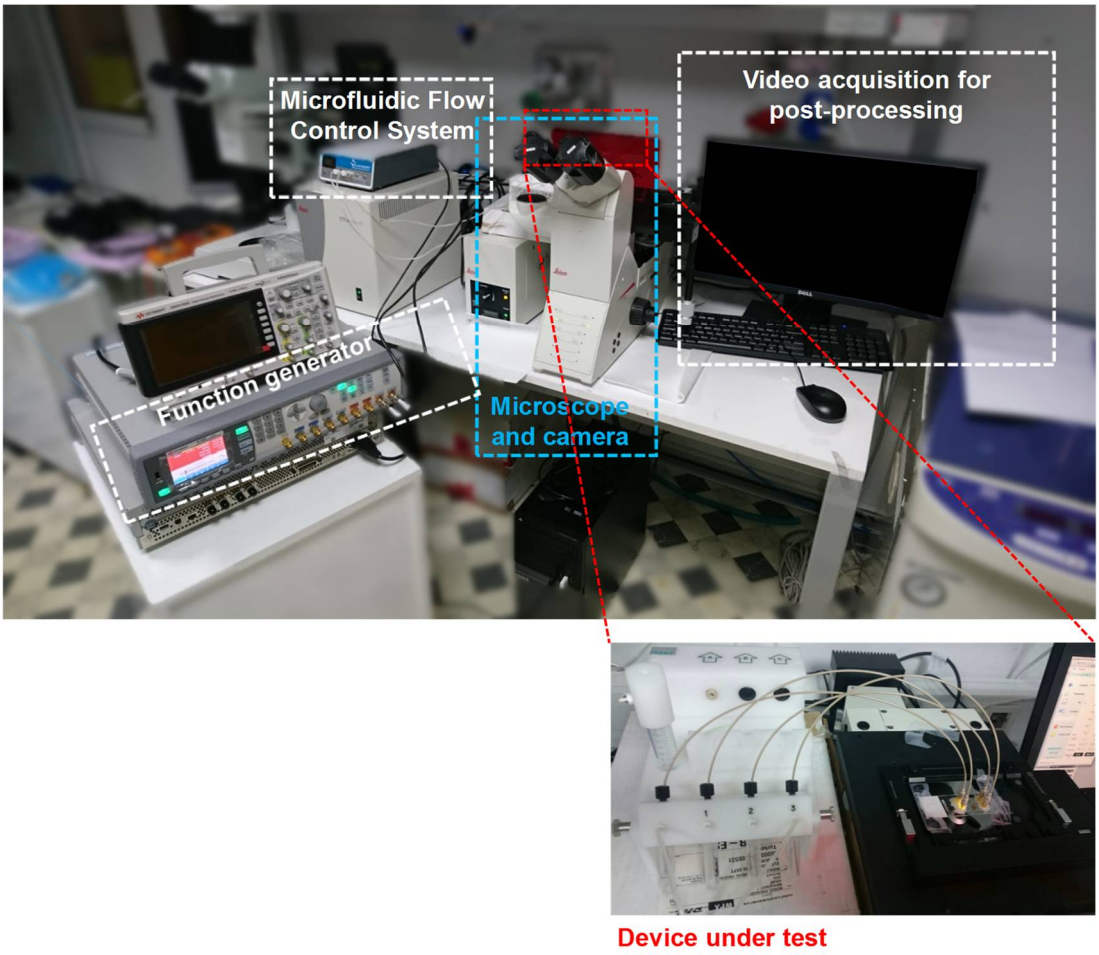


*Figure 4.19.* Image of the experimental test setup with enlarged view of the device under test

### 4.4.3. Experimental Setup and Test Procedure

The recovery rate (yield) in DEP enrichment units is described as the ratio of the number of cancer cells taken from the cancer cell exit to the number of cancer cells given from the channel entrance (Equation 4.1). This ratio should be close to 100%.

$$Recovery\ Rate = \frac{Cancer\ Cells_{cancer\ cell\ outlet}}{Cancer\ Cells_{inlet}} \tag{4.1}$$

Another metric in DEP enrichment units is the enrichment factor (Equation 4.2). This factor is defined as the ratio of the number of cancer cells/blood cells at the cancer cell outlet to the number of cancer cells/blood cells at channel entrance [60].

$$Enrichment\ Factor = \frac{\left(Cancer\frac{Cells}{Leukocytes}\right)_{cancer\ cell\ outlet}}{\left(Cancer\frac{Cells}{Leukocytes}\right)_{inlet}} \quad (4.2)$$

In order to calculate these specified metrics, leukocytes and MCF7 cells directed to the cancer cell and leukocyte outlets should be counted. For this purpose, the obtained enrichment experiment records were analyzed with the cell counter plugin of Fiji and the recovery rate and enrichment ratio were calculated accordingly.

### 4.5. Results

After determination of the frequency at which the MCF7 cells will be enriched from leukocytes at 1 MHz by considering the results presented in Chapter 3, performance experiments of the DEP-based enrichment devices were conducted. For this purpose, a systematic study was performed for the microchannel experiments. In this content, the microchannel experiments to be carried out with the fabricated DEP-based enrichment devices were divided into two stages. In the first stage of the tests, it was planned to perform microfluidic experiments with only liquid or only MCF7 cells. With these experiments, it was aimed to optimize hydrodynamic focusing operation, the CTC density to be used in the cell solution, delivery pressures of cell and DEP solutions from chip inputs and voltage to be applied. In the second stage experiments, enrichment of MCF7 cells from leukocytes was conducted. After successful results were obtained in the first stage tests, CTC enrichment tests were aimed to be done with the optimized data obtained from the first stage experiments by providing the cell solution containing CTC and leukocyte to the devices.

### 4.5.1. Analysis for the Selection of Experimental Parameters

As described above, in the first stage experiments, it is aimed to optimize the fabricated DEP-based enrichment unit using either cell-free liquids or solution containing MCF7 cells alone. Thus, it was ensured that CTC enrichment experiments were performed with optimized data by minimizing the use of blood cells obtained from healthy individuals. Three different steps were determined for the first stage experiments.

#### 4.5.1.1. Verification of Hydrodynamic Focusing

It is aimed to verify the hydrodynamic focusing process used in the proposed DEP-based enrichment structure. In the hydrodynamic focusing process, the objective is to ensure that the cells transmitted into the main channel are focused to the main channel wall at the cell inlet side before the active DEP zone. In order to eliminate the stage of preparation and staining of cells and to obtain verification results in a shorter time, fluorescent dye-stained cell-free DI water solution focusing was made. To prepare the fluorescent dye-stained cell-free DI water solution, the fluorescein sodium salt (in powder form) was dissolved in DI water (1 mg/ml) and used as a fluorescent tracer. The tests were carried out by transmitting the fluorescent dye-stained cell-free DI water solution from one inlet of the microchannel and by transmitting the normal DI water from the other inlet. The hydrodynamic focusing of the fluids, transferred from the side channels, to the main channel walls was tested using different pressures at the channel entrances with the help of the pressure controller. The results are given in Figure 4.20. As can be seen, by adjusting the pressures at the entrances properly, it is possible to focus the solution hydrodynamically on the desired area. Since the pressures at the inputs also affect the speed of the given solution, the minimum and maximum pressure values in which hydrodynamic focusing was successfully performed during the tests were also determined. While the pressure at the entrances was 20 mbar and at the level of 300 mbar, the hydrodynamic focus was achieved successfully.

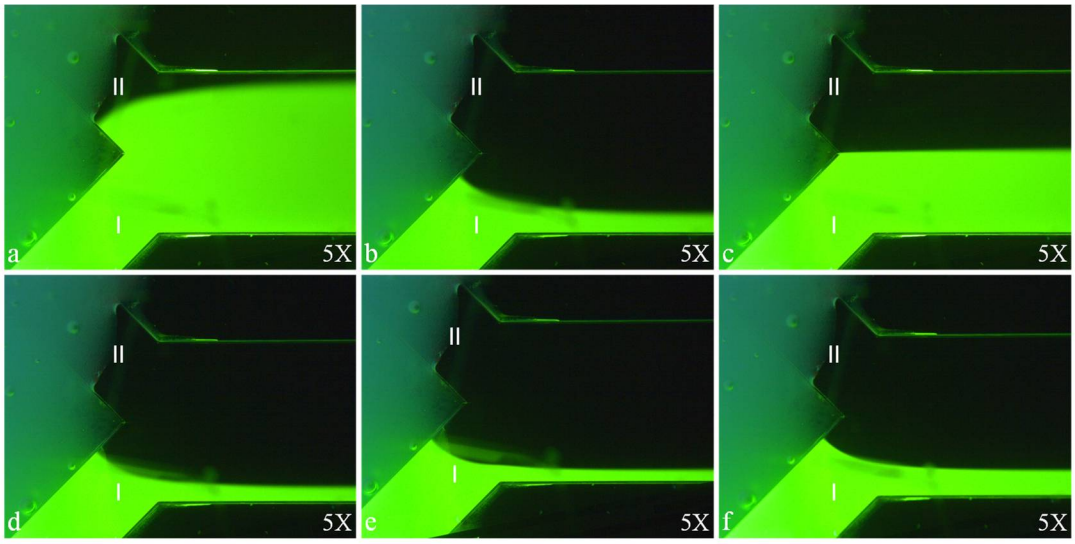


*Figure 4.20.* Hydrodynamic focusing test results obtained by giving different pressures from the microchannel inlets. Inlet pressures, (a) I: 20 mbar, II: 18 mbar, (b) I: 50 mbar, II: 59 mbar, (c) I: 100 mbar, II: 100 mbar, (d) I: 100 mbar, II: 120 mbar, (e) I: 200 mbar, II: 290 mbar, (f) I: 300 mbar, II: 400 mbar

The flow of the hydrodynamic focused fluorescent solution with pressure optimization in the channel is shared in Figure 4.21. As it can be seen, the solution continues to flow in a focused manner without any deterioration as expected.

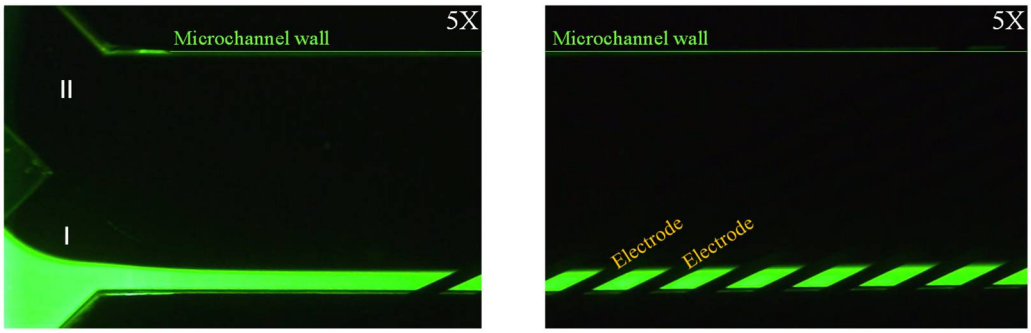


*Figure 4.21.* View of the focused stream at the entrance and along the channel (Inlet pressures, I: 270 mbar, II: 340 mbar)

#### 4.5.1.2. Determination of the Minimum CTC Density to Successfully Complete the Tests

Since the CTC concentration in the blood at the early stages of cancer is low, keeping the cell density to be used in the cell solution in a minimum level is important for the enrichment experiment to achieve its purpose in the advanced stages. For this reason, it was aimed to determine the minimum CTC concentration (to be detected by the microscope) that could be studied in the microchannel fabricated during this test phase. During the experiments, 3 different concentrations of MCF7 cell solutions ($3.42\times10^5$ cells/ml, $4.85\times10^5$ cells/ml and $6.93\times10^5$ cells/ml) were introduced into the microchannel and the flow density of the cells into the channel was observed. Cell concentration adjustments were made with automated cell counter (BIO RAD, TC20™ Automated Cell Counter). In the examinations, $3.42\times10^5$ cells/ml cell concentration was found to be sufficient for enrichment tests and it did not cause any problems for microscopic examination. In the second stage enrichment experiments, CTC and leukocytes will be mixed with each other and given to the microchannel. This will increase the concentration of the cell solution to be prepared. Therefore, it was decided that each cell type should be used at a concentration of $3\times10^5$ cells/ml so that this increase in total cell concentration does not result in blockage at the cell inlet and in the connecting parts that provide access to the chip.

#### 4.5.1.3. Optimization of Pressure and Voltage Values

Since the DEP force providing the separation/enrichment is related to the electric field gradient created by the applied voltage, the maximum CTC collection from the cancer cell output (CTC enrichment) depends on the application of the optimum voltage and pressure values. At this phase of the first stage experiments, the system is tested at different voltage and pressure values and it is aimed to determine the experiment parameters at which the most efficient CTC collection is provided. In this content, the optimum voltage to be applied to the electrodes and pressure values to be applied to the inputs were studied.

As described above, initial experiments were carried out by experiments on the focusing of the fluorescent dye-stained cell-free DI water solution to the channel wall to verify the hydrodynamic focusing principle. In experiments with cancer cells, hydrodynamic focusing was first tested again. For this purpose, the hydrodynamic focusing of the cell solution to the microchannel wall was tested by arranging the pressures in the chip inlets at different values. An example of the hydrodynamic focusing of the cell solution to the microchannel wall is presented Figure 4.22. The test results show that, as in focusing of the fluorescent dye-stained cell-free DI water solution tests, the cell solution is focused on the channel wall by appropriately adjusting the pressure values at the channel entrances.

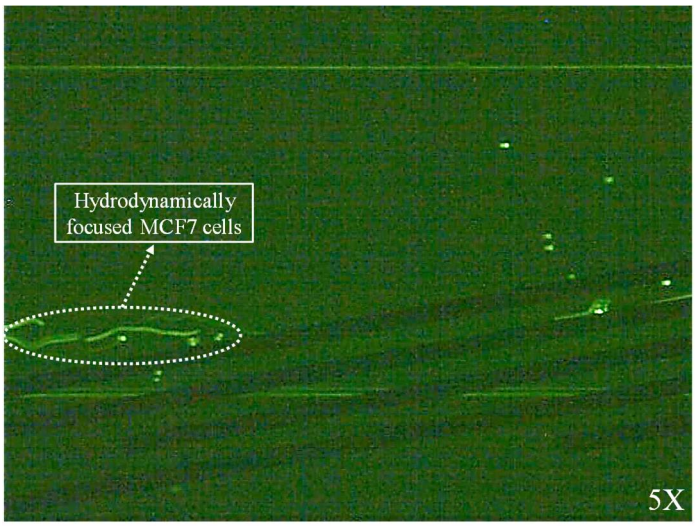


*Figure 4.22.* View of the MCF7 cells that are hydrodynamically focused on the bottom channel wall (voltage = 10 $V_{pp}$, frequency = 1 MHz, cell inlet pressure = 35 mbar, DEP buffer inlet pressure= 50 mbar)

As a result of DEP spectrum study, the separation frequency of leukocytes and MCF7 cells in the DEP-based enrichment unit was determined to be 1 MHz. Since the DEP spectrum experiments of the corresponding cells were performed at 10 $V_{pp}$ and the velocity difference was observed at this voltage, tests for determining the optimum

voltage and flow rate for directing the cells over the active DEP region and collecting from the correct output were started with 10 $V_{pp}$.

In the experiments, different voltage and pressure values were tried and cell movements were observed. When the cells are under high DEP and/or low flow rate conditions, they tend to form pearl chain structures between the electrodes as expected. The channel view in which this case was observed is presented in Figure 4.23.

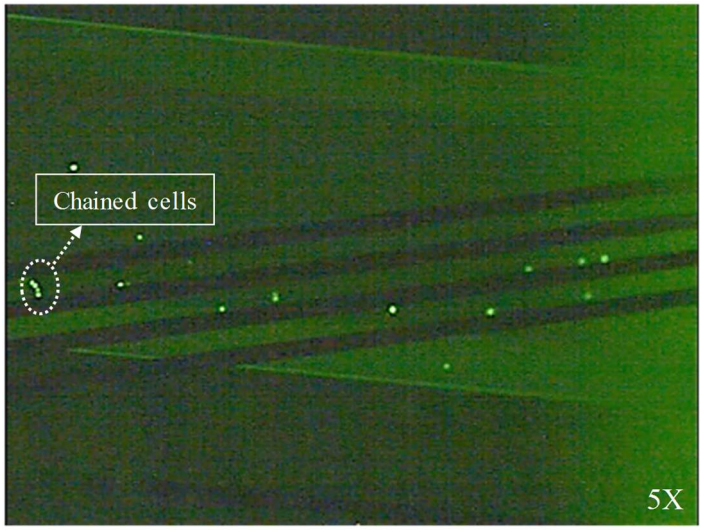


*Figure 4.23.* The appearance of the cells forming the pearl chin structure between the first two electrodes (voltage = 10 $V_{pp}$, frequency = 1 MHz, cell inlet pressure = 25 mbar, DEP buffer inlet pressure = 30 mbar)

In cases where flow rate is high, the pDEP force generated in the active DEP region is inadequate and the cells are unable to be directed towards the cancer cell outlet (the upper outlet). This is also an expected result and the channel view in which this case was observed is presented in Figure 4.24.

After the cells were successfully focused on the bottom wall of the channel, MCF7 cells were able to direct to the cancer cell outlet at optimum voltage and inlet pressures.

The movements of the focused cells in the active DEP region are shown in Figure 4.25 using consecutive images of a record taken during the experiment. As can be seen from the given figure, the cells slide along the electrodes with the flow and leave the main channel through the upper outlet which is cancer cell outlet.

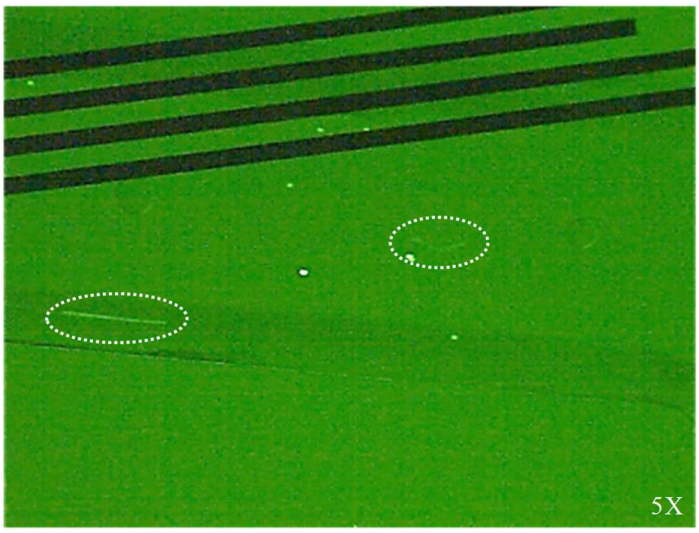


*Figure 4.24.* Image of MCF7 cells that are not directed to the cancer cell outlet (upper outlet) as a result of high flow rate and insufficient DEP force (voltage = 10 $V_{pp}$, frequency = 1 MHz, cell inlet pressure = 30 mbar, DEP buffer inlet pressure = 65 mbar)

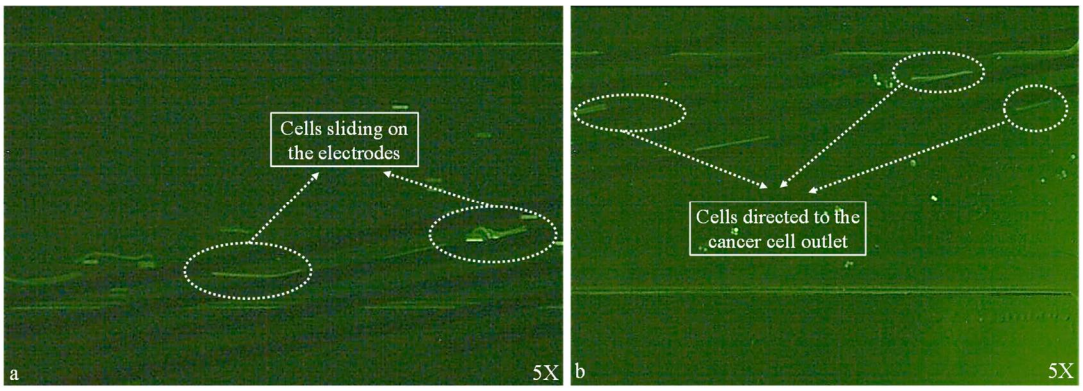


*Figure 4.25.* Views of MCF7 cells sliding along the electrodes (a) and directed to the CTC outlet (b) (voltage = 10 $V_{pp}$, frequency = 1 MHz, cell inlet pressure = 35 mbar, DEP buffer inlet pressure = 50 mbar)

In the first stage tests performed with the MCF7 cells described above, it was observed that the optimum pressure values which provide hydrodynamic focusing and directing the cells to the correct output differ between the tested chips. This is due to the fact that the ports that connect the reservoirs located at the inlets and outlets of the chips to the tubes carrying the solutions are not evenly bonded to the devices. The fact that these ports cannot be precisely matched to the reservoirs makes a difference in the pressure being delivered. For this reason, the pressure values that provide the proper flow within the main channel differed between the devices and even the two inputs in the same device. However, the test results taken at this stage showed that the hydrodynamic focusing is achieved in a short time by adjusting the pressures at the side channels before enrichment (voltage application) for each chip to be tested. Therefore, enrichment experiments were carried out in this way.

### 4.5.2. CTC Enrichment Experiments

After successful results were obtained for the first stage tests, the cell solution containing CTCs and leukocytes with pre-optimized data was transferred to the DEP-based CTC enrichment tests. The devices must undergo a number of pretreatments to be ready for enrichment experiments. These pre-treatments involve passage of some liquids prepared prior to the experiment through the channel in a predetermined order. In this context, the whole channel surface was first wetted with ethanol by providing from inlets and collecting from outlets. It is aimed to prevent the problem of air bubble formation within the channel by wetting the entire channel surface with ethanol. Then, all the ethanol in the channel was cleaned by giving DI water to the microchannel. Thirdly, the PBS (10X, pH 7.4 Gibco) solution containing 5 mM EDTA (Sigma-Aldrich) and 1% BSA (bovine serum albumin, Sigma-Aldrich) was passed through the channel at low pressure and allowed to penetrate the entire channel surface. With this solution given to the channel, the problem of cell adhesion on the channel surface was prevented. The electrical conductivity of the PBS solution is very high and must be completely cleaned from the microchannel prior to the enrichment experiments. For this purpose, DI water was passed through the microchannel again. Then, the cell-

free DEP buffer was passed through the whole side and main channels to bring the system into the standard operating condition.

After completing the priming of the device, prepared cell solution was given from cell inlet and the enrichment experiments was started. The preparation of the cell solution containing both cell types is described in Section 4.4.1. Within the scope of the first stage tests, the concentration specified in the determination of minimum CTC density tests to successfully complete the enrichment experiments was taken into account and in the prepared cell solution, the concentration of both cell types was adjusted to $3\times10^5$ cells/ml. The cell solution prepared in this way was delivered from the cell inlet of the DEP-based enrichment device. Then, hydrodynamic focusing is achieved in a short time by adjusting the pressures at the side channels before enrichment (voltage application) for each chip to be tested. After the cells were focused on the channel wall with hydrodynamic focusing, the voltage was applied to the electrodes and the enrichment experiments were started. With the experiments performed, it was observed that the proposed separation method has been realized as expected, and the cancer cells and leukocytes were successfully directed to the correct outlets. Sequential channel views showing that the leukocyte (red-surrounded cell) and the MCF7 cell (green-surrounded cell) progress to the correct outlets in the successful CTC enrichment test is given in Figure 4.26.

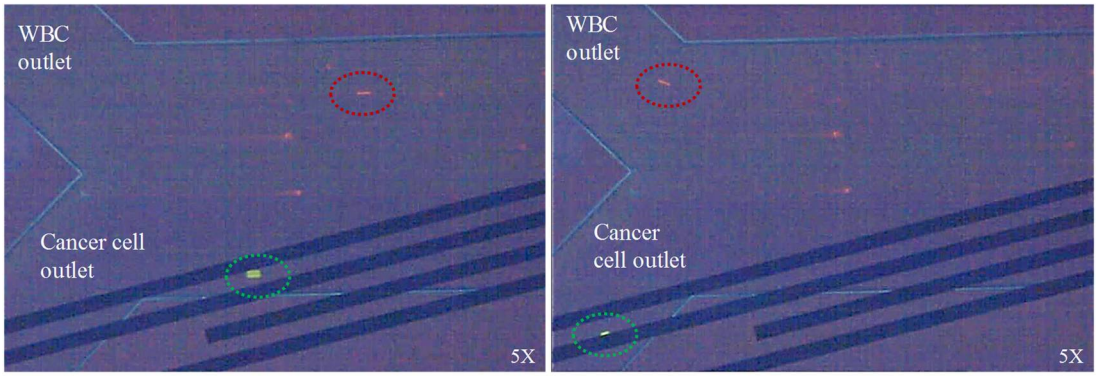


*Figure 4.26.* Sequential channel views showing that the WBC (red-surrounded cell) and the MCF7 cell (green-surrounded cell) progress to the correct outlets in the successful CTC enrichment test.

The results measured from the experiments performed for the three different experimental sets made with the DEP-based CTC enrichment units are presented in Table 4.3. Enrichment factor and recovery rate calculations that are used to determine the level of enrichment were calculated as explained in Section 4.4.3. Table 4.3 gives all related cell counts including the number of WBCs that leave microchannel from wrong outlet (cancer cell outlet).

Table 4.3. *Recovery rate and enrichment factor results calculated from cell counts for three different experimental sets performed with DEP enrichment device*

| **CTC Outlet** | | **WBC Outlet** | | **Total Number of Cells Entering the Channel** | | **Recovery Rate (%)** | **Enrichment Factor** |
|---|---|---|---|---|---|---|---|
| Number of Cancer Cells | Number of WBCs | Number of Cancer Cells | Number of WBCs | Number of Cancer Cells | Number of WBCs | | |
| 17 | 16 | 9 | 136 | 26 | 152 | **65.39** | **6.21** |
| 40 | 59 | 8 | 155 | 48 | 214 | **83.33** | **3.02** |
| 135 | 107 | 3 | 112 | 138 | 219 | **97.83** | **2.00** |

## 4.6. Conclusion

The proposed DEP-based enrichment device was developed within the scope of the conducted TUBITAK project. The project aims to develop a fully integrated MEMS-based microfluidic system for the detection of rare cell in the blood. The proposed system is composed of three functional units:

i. Dielectrophoretic CTC enrichment unit,

ii. Immuno-based CTC capture and gravimetric detection unit,

iii. Integrated closed-loop readout circuit for on-chip quantitative measurement and (Dielectrophoresis) DEP actuation

The aim of DEP-based rare cell enrichment unit is to obtain a CTC-enriched blood sample by separating blood cells from CTCs at a high efficiency, based on the differences in their size and dielectric properties. The unique property of this unit is to transmit relatively increased concentration of CTCs from the sensing unit, thereby increasing the efficiency of the immune-based gravimetric cell detection and counting unit. CTC capture and counting unit is composed of a resonance-based gravimetric mass detection system. The resonator surface was activated with appropriate bioactivation protocols to capture CTCs. In order to provide rapid and sensitive on-chip quantitative CTC detection, without needing any external equipment (optical systems, etc.), the system is integrated with a CMOS closed loop readout circuit.

It is aimed to increase the recovery rate result from the CTC enrichment experiments performed with leukocyte and MCF7 cells mixture within the scope of the above project requirements. In the gravimetric detection unit, the immuno-based CTC capture eliminates the residual blood cells, included in the CTC enriched sample provided from DEP unit, from the system and ensures that they cannot be included in the count. Therefore, the results obtained from the enrichment experiments are evaluated within the scope of these project requirements.

When the enrichment results were examined, it was seen that with the increase of the recovery rate, the enrichment factor decreased, as expected. With the help of immune-based CTC capture, the system needs to work at the optimum recovery rate and the enrichment factor which is 83.33% and 3.02, respectively. These results indicate that approximately 83% of the CTCs from the inlet are directed towards the correct output and the CTC/leukocyte ratio at the cancer cell outlet is 3 times the CTC/leukocyte ratio at the inlet. Reached recovery rate is comparable with other CTC enrichment studies in the literature.

Gupta et al. submitted a DEP-based enrichment for the isolation and recovery of cancer cells from peripheral blood cells, ApoStream$^{TM}$. This device performs its operation without using antibody. Experiments were conducted with the SKOV3 and

MDA-MB-231 cancer cells added into approximately $12\times10^6$ blood cells extracted from 7.5 ml human donor blood sample. Measured recovery rates for this study were 75.4% and 71.2% for SKOV3 and MDA-MB-231 cancer cells, respectively [31]. Huang et al. reported another microfluidic platform for the label-free enrichment of CTCs. In this design dielectrophoretic force is induced optically. Enrichment of PC-3 cells or OEC-M1 cells from WBCs were presented and measured recovery rates were 76–83% for PC-3 cells and 61–68% for OEC-M1 cells 0.1 µl/min flow rate [32]. Huang et al. designed a DEP-based device with circular indium-tin-oxide electrodes to separate HeLa (cervical carcinoma cells) from RBCs for 16 $V_{pp}$ at 1 MHz. The experimental results indicate that the HeLa cells were collected at the center microelectrodes with a recovery rate of approximately 64.5% [33]. Shim et al. reported a continuously run DEP-FFF device. The developed system was able to process 10 ml of patient sample in less than an hour. Recovery rate results for the MDA-MB-435 (human melanoma) and MDA-MB-231 cells spiked into PBMC were around ~75% [34]. Cheng et al. designed a DEP-based microfluidic platform for isolation of AS2-GFP cells. Different flow rates were tested with this system and the corresponding recovery rates were reported. Measured recovery rate values for this cell line at 30 µl/min and 20 µl/min were ~60% and ~85%, respectively [61].

Table 4.4. *Recovery rate results for CTC enrichment available in the literature*

| Reference | Cancer Cell | Recovery Rate (%) |
|---|---|---|
| [31] | SKOV3<br>MDS-MB-231 | 75.4<br>71.2 |
| [32] | PC-3<br>OEC-M1 | 76–83<br>61–68 |
| [33] | HeLa | 64.5 |
| [34] | MDA-MB-435<br>MDA-MB-231 | 75 |
| **[61]** | AS2-GFP | 85 |
| **This study** | MCF7 | 83.3 |

According to the comparisons of enrichment factors and recovery rates, proposed DEP-based enrichment device is promising for the future improvements on this study.

# CHAPTER 5

## CONCLUSION AND FUTURE WORK

The main goal of the thesis is the enrichment of CTCs from blood, through the design, simulation, fabrication and implementation of a MEMS-based dielectrophoretic device. To achieve this goal, DEP spectrum analysis was studied initially. In this content, a DEP spectrum device was developed by utilizing MEMS fabrication technique. Corresponding DEP spectra of these cells were studied and according to the results, DEP-based enrichment device was designed. Fabrication of the DEP-based enrichment device was also done by using MEMS technique. After the fabrication of the proposed devices, enrichment experiments were performed with MCF7 breast cancer cells and leukocytes extracted from healthy donors. Obtained enrichment experiment results were submitted.

The achievements obtained through the research to reach the determined goals can be listed as follows:

1. DEP spectrum analysis was conducted in order to design a successful DEP-based enrichment device through following studies:

- DEP spectrum device was designed for the proof of DEP spectrum investigation of the biological cells with the proposed analysis method and required FEM simulations were done by using COMSOL software.

- A MEMS fabrication flow was developed and MEMS fabrication of the DEP spectrum devices were achieved.

- Experimental setup and procedures were developed for the testing of the proof of concept DEP spectrum devices.

- Testing of the proof of concept DEP spectrum devices was carried out with polymoprhonuclear leukocytes and mononuclear leukocytes obtained from 2 different healthy donors and MCF7 cells (human breast adenocarcinoma cell line) for 15 different frequencies in the range from 100 kHz to 50 MHz at 10 Vpp.

- Post-experiment examination method was developed for the experimental records by utilizing VirtualDub and Meazure$^{TM}$. However, manual analysis became challenging due to experimental problems.

- A significant velocity difference was detected between MCF7 cells (33.99 μm/s) and leukocytes, mononuclear leukocytes (7.9 μm/s) and polymorphonuclear leukocytes (13.82 μm/s), which can be utilized as the working frequency for DEP-based enrichment of MCF7 cancer cells from WBCs.

2. Considering the problems associated with the initial DEP spectrum study, improvements were inserted to the method through the following studies:

- DEP spectrum design was improved by using COMSOL software utilizing FEM simulations.

- DEP spectrum device was fabricated by following the same fabrication flow.

- Development of the new experimental setup and fluorescence staining procedure of the cells were accomplished.

- Testing of the improved analysis was carried out with leukocytes obtained from single donor and MCF7 cells at 10 Vpp for 9 different frequencies in the range from 500 kHz to 10 MHz.

- Post-experiment examination method was improved and automatized by using using TrackMate, Fiji, and generated C++ code compiled/built with Borland Developer Studio.

- The results reveal that there are significant velocity differences occurs between MCF7 cells and leukocytes at 500 kHz, 850 kHz and 1 MHz with the ratios 3.58, 3.37 and 3.12, respectively.

3. A DEP-based MEMS enabled CTC enrichment device was accomplished through following studies:

- According to the DEP spectrum analysis, the design of the DEP-based enrichment device was achieved and electric field analysis was done by using COMSOL software utilizing FEM simulations.

- Fabrication flow of the parylene microchannel was achieved and fabrication of the devices were completed.

- Development of the experimental setup (pressure controller, inverted fluorescence microcopy, high speed camera) and different fluorescence staining procedures of the cells to observe the movement of the leukocytes and MCF7 cells simultaneously inside the microchannel were achieved.

- Testing of the CTC enrichment experiments were performed by applying a number of pretreatments to the microchannel was achieved.

- Successful recovery rate (83%) and enrichment factor (3) were achieved for MCF7 and leukocyte mixture with the proposed DEP-based enrichment units at 1 MHz.

As a future work, it is planned to test other possible enrichment frequencies (500 kHz and 850 kHz) obtained from the final DEP spectrum analysis method. Additionally, the applicability of the complete DEP spectrum analysis method and the DEP-based enrichment unit will be expanded with other cell types. In this content, the DEP spectrum experiments of Huh7 and Hep3B, liver cancer cells and cancer stem cells (CSCs) were already conducted. After examining the experiments carried out, DEP

spectra of the corresponding cells will be determined. As in the case of MCF7 and leukocytes, it is aimed to detect a possible enrichment frequency for enrichment of CSCs from normal cancer cells.

## REFERENCES


[1] A. J. R. L. Siegel, K. D. Miller, "Cancer Statistics, 2017," *CA A Cancer J. Clin.*, vol. 5, no. 6, pp. 1927–1939, 2014.

[2] F. Bray, A. Jemal, N. Grey, J. Ferlay, and D. Forman, "Global cancer transitions according to the Human Development Index (2008-2030): A population-based study," *Lancet Oncol.*, vol. 13, no. 8, pp. 790–801, 2012.

[3] A. Kowalik, M. Kowalewska, and S. Góźdź, "Current approaches for avoiding the limitations of circulating tumor cells detection methods—implications for diagnosis and treatment of patients with solid tumors," *Transl. Res.*, vol. 185, p. 58–84.e15, 2017.

[4] S. A. Joosse, T. M. Gorges, and K. Pantel, "Biology, detection, and clinical implications of circulating tumor cells," *EMBO Mol. Med.*, vol. 7, no. 1, pp. 1–11, 2015.

[5] M. C. Miller, G. V. Doyle, and L. W. M. M. Terstappen, "Significance of Circulating Tumor Cells Detected by the CellSearch System in Patients with Metastatic Breast Colorectal and Prostate Cancer," *J. Oncol.*, vol. 2010, pp. 1–8, 2010.

[6] "Vortex BioSciences." [Online]. Available: https://vortexbiosciences.com/technology/. [Accessed: 05-Dec-2018].

[7] S. Miltenyi, W. Müller, W. Weichel, and A. Radbruch, "High gradient magnetic cell separation with MACS," *Cytometry*, vol. 11, no. 2, pp. 231–238, 1990.

[8] S. Sharma *et al.*, "Circulating tumor cell isolation, culture, and downstream molecular analysis," *Biotechnol. Adv.*, vol. 36, no. 4, pp. 1063–1078, 2018.

[9] D. R. Parkinson *et al.*, "Considerations in the development of circulating tumor cell technology for clinical use," *J. Transl. Med.*, vol. 10, no. 1, 2012.

[10] M. T. Gabriel, L. R. Calleja, A. Chalopin, B. Ory, and D. Heymann, "Circulating tumor cells: A review of Non-EpCAM-based approaches for cell enrichment and isolation," *Clin. Chem.*, vol. 62, no. 4, pp. 571–581, 2016.

[11] C. Alix-Panabières and K. Pantel, "Technologies for detection of circulating tumor cells: Facts and vision," *Lab Chip*, vol. 14, no. 1, pp. 57–62, 2014.

[12] S. A. Joosse and K. Pantel, "Biologic challenges in the detection of circulating tumor cells," *Cancer Res.*, vol. 73, no. 1, pp. 8–11, 2013.

[13] A. M. Sieuwerts *et al.*, "Anti-epithelial cell adhesion molecule antibodies and

the detection of circulating normal-like breast tumor cells," *J. Natl. Cancer Inst.*, vol. 101, no. 1, pp. 61–66, 2009.

[14] A. H. Talasaz *et al.*, "Isolating highly enriched populations of circulating epithelial cells and other rare cells from blood using a magnetic sweeper device," *Proc. Natl. Acad. Sci.*, vol. 106, no. 10, pp. 3970–3975, 2009.

[15] V. Zieglschmid *et al.*, "Combination of immunomagnetic enrichment with multiplex RT-PCR analysis for the detection of disseminated tumor cells," *Anticancer Res.*, vol. 25, no. 3 A, pp. 1803–1810, 2005.

[16] W. Harb *et al.*, "Mutational Analysis of Circulating Tumor Cells Using a Novel Microfluidic Collection Device and qPCR Assay," *Transl. Oncol.*, vol. 6, no. 5, pp. 528–538, 2013.

[17] N. Beije, A. Jager, and S. Sleijfer, "Circulating tumor cell enumeration by the CellSearch system: The clinician's guide to breast cancer treatment?," *Cancer Treat. Rev.*, vol. 41, no. 2, pp. 144–150, 2015.

[18] C. Pösel, K. Möller, W. Fröhlich, I. Schulz, J. Boltze, and D. C. Wagner, "Density Gradient Centrifugation Compromises Bone Marrow Mononuclear Cell Yield," *PLoS One*, vol. 7, no. 12, pp. 1–10, 2012.

[19] Y. Chang, P.-H. Hsieh, and C. C.-K. Chao, "The efficiency of Percoll and Ficoll density gradient media in the isolation of marrow derived human mesenchymal stem cells with osteogenic potential.," *Chang Gung Med. J.*, vol. 32, no. 3, pp. 264–75, 2009.

[20] R. Rosenberg *et al.*, "Comparison of two density gradient centrifugation systems for the enrichment of disseminated tumor cells in blood," *Cytometry*, vol. 49, no. 4, pp. 150–158, 2002.

[21] L. Zabaglo, M. G. Ormerod, M. Parton, A. Ring, I. E. Smith, and M. Dowsett, "Cell filtration-laser scanning cytometry for the characterisation of circulating breast cancer cells," *Cytometry*, vol. 55A, no. 2, pp. 102–108, 2003.

[22] V. De Giorgi, "Circulating Benign Nevus Cells Detected by ISET Technique," *Arch. Dermatol.*, vol. 146, no. 10, pp. 1120–1124, 2010.

[23] C. Dolfus, N. Piton, E. Toure, and J.-C. Sabourin, "Circulating tumor cell isolation: the assets of filtration methods with polycarbonate track-etched filters.," *Chin. J. Cancer Res.*, vol. 27, no. 5, pp. 479–87, 2015.

[24] G. Vona *et al.*, "Impact of Cytomorphological Detection of Circulating Tumor Cells in Patients with Liver Cancer," *Hepatology*, vol. 39, no. 3, pp. 792–797, 2004.

[25] L. Wang, W. Asghar, U. Demirci, and Y. Wan, "Nanostructured substrates for isolation of circulating tumor cells," *Nano Today*, vol. 8, no. 4, pp. 374–387,

2013.

[26] H. W. Hou *et al.*, "Isolation and retrieval of circulating tumor cells using centrifugal forces," *Sci. Rep.*, vol. 3, pp. 1–8, 2013.

[27] Y. Dong *et al.*, "Microfluidics and circulating tumor cells," *J. Mol. Diagnostics*, vol. 15, no. 2, pp. 149–157, 2013.

[28] S. J. Tan, L. Yobas, G. Y. H. Lee, C. N. Ong, and C. T. Lim, "Microdevice for the isolation and enumeration of cancer cells from blood," *Biomed. Microdevices*, vol. 11, no. 4, pp. 883–892, 2009.

[29] W. Qian, Y. Zhang, and W. Chen, "Capturing Cancer: Emerging Microfluidic Technologies for the Capture and Characterization of Circulating Tumor Cells," *Small*, vol. 11, no. 32, pp. 3850–3872, 2015.

[30] F. F. Becker, X. Wang, Y. Huang, R. Pethigt, J. Vykoukal, and P. R. C. Gascoyne, "Separation of human breast cancer cells from blood by differential dielectric affinity," *Natl. Acad. Sci.*, vol. 92, no. January, pp. 860–864, 1995.

[31] V. Gupta *et al.*, "ApoStream$^{TM}$, a new dielectrophoretic device for antibody independent isolation and recovery of viable cancer cells from blood," *Biomicrofluidics*, vol. 6, no. 2, 2012.

[32] S. Bin Huang *et al.*, "High-purity and label-free isolation of circulating tumor cells (CTCs) in a microfluidic platform by using optically-induced-dielectrophoretic (ODEP) force," *Lab Chip*, vol. 13, no. 7, pp. 1371–1383, 2013.

[33] C. Te Huang, T. G. Amstislavskaya, G. H. Chen, H. H. Chang, Y. H. Chen, and C. P. Jen, "Selectively concentrating cervical carcinoma cells from red blood cells utilizing dielectrophoresis with circular ITO electrodes in stepping electric fields," *J. Med. Biol. Eng.*, vol. 33, no. 1, pp. 51–58, 2013.

[34] S. Shim, K. Stemke-Hale, A. M. Tsimberidou, J. Noshari, T. E. Anderson, and P. R. C. Gascoyne, "Antibody-independent isolation of circulating tumor cells by continuous-flow dielectrophoresis," *Biomicrofluidics*, vol. 7, no. 1, 2013.

[35] Thomas B. Jones, *Electromechanics of particles*, vol. 89. 1996.

[36] R. Pethig, "Dielectrophoresis: Status of the theory, technology, and applications," *Biomicrofluidics*, vol. 4, pp. 1–35, 2010.

[37] N. Allahrabbi, "Dielectrophoretic Separation of Biological Cells in Microfluidic Systems," National University of Singapore, 2015.

[38] N. Abd Rahman, F. Ibrahim, and B. Yafouz, "Dielectrophoresis for Biomedical Sciences Applications: A Review," *Sensors (Basel).*, vol. 17, no. 3, pp. 1–27, 2017.

[39] Y. Demircan, E. Özgür, and H. Külah, "Dielectrophoresis: Applications and future outlook in point of care," *Electrophoresis*, vol. 34, no. 7, pp. 1008–1027, 2013.

[40] M. Alshareef *et al.*, "Separation of tumor cells with dielectrophoresis-based microfluidic chip," *Biomicrofluidics*, vol. 7, no. 1, 2013.

[41] S. Shim, K. Stemke-Hale, J. Noshari, F. F. Becker, and P. R. C. Gascoyne, "Dielectrophoresis has broad applicability to marker-free isolation of tumor cells from blood by microfluidic systems," *Biomicrofluidics*, vol. 7, no. 1, 2013.

[42] E. A. Henslee, M. B. Sano, A. D. Rojas, E. M. Schmelz, and R. V. Davalos, "Selective concentration of human cancer cells using contactless dielectrophoresis," *Electrophoresis*, vol. 32, no. 18, pp. 2523–2529, 2011.

[43] J. An, J. Lee, S. H. Lee, J. Park, and B. Kim, "Separation of malignant human breast cancer epithelial cells from healthy epithelial cells using an advanced dielectrophoresis-activated cell sorter (DACS)," *Anal. Bioanal. Chem.*, vol. 394, no. 3, pp. 801–809, 2009.

[44] H. M. Coley, F. H. Labeed, H. Thomas, and M. P. Hughes, "Biophysical characterization of MDR breast cancer cell lines reveals the cytoplasm is critical in determining drug sensitivity," *Biochim. Biophys. Acta - Gen. Subj.*, vol. 1770, no. 4, pp. 601–608, 2007.

[45] H. S. Moon *et al.*, "Continuous separation of breast cancer cells from blood samples using multi-orifice flow fractionation (MOFF) and dielectrophoresis (DEP)," *Lab Chip*, vol. 11, no. 6, pp. 1118–1125, 2011.

[46] G. Özkayar, "Rare Cell Enrichment From Blood by Using Dielectrophoresis," Middle East Technical University, 2015.

[47] F. Yang, X. Yang, H. Jiang, W. M. Butler, and G. Wang, "Dielectrophoretic Separation of Prostate Cancer Cells," *Technol. Cancer Res. Treat.*, vol. 12, no. 1, pp. 61–70, 2013.

[48] Z. Çağlayan, K. Sel, Y. Dermican Yalçın, Ö. Şardan Sukas, and H. Külah, "Analysis of the Dielectrophoretic (DEP) Spectra of Biological Cells," 2017, pp. 1644–1647.

[49] G. Bahrieh, "Assessment of Changes in the Dielectric Properties of Multidrug Resistant Cancer Cells By Electrorotation Technique," Middle East Technical University, 2014.

[50] P. Tech Coating Inc, "Parylene Properties Chart for Parylene N, C, D." [Online]. Available: http://www.parylene.com/pdfs/PTC-Parylene_Properties_Chart.pdf. [Accessed: 05-Dec-2018]

[51] Y. Demircan, "Detection of Imatinib and Doxorubicin Resistance in K562

Leukemia Cells By 3D-Electrode Contactless Dielectrophoresis," Middle East Technical University, 2013.

[52] H. Stark, "GraFix: Stabilization of fragile macromolecular complexes for single particle Cryo-EM," in *Methods in Enzymology*, vol. 481, no. C, Elsevier Masson SAS, 2010, pp. 109–126.

[53] Alere Technologies AS. "OptiPrep Application Sheet C11, Isolation of human polymorphonuclear leukocytes (granulocytes) from a leukocyte rich plasma in a discontinuous iodixanol gradient." January 2018.

[54] Miltenyi Biotec. "Red Blood Cell Lysis Solution (10x)."

[55] J. Y. Tinevez *et al.*, "TrackMate: An open and extensible platform for single-particle tracking," *Methods*, vol. 115, pp. 80–90, 2017.

[56] Jean-Yves Tinevez, "Getting started with TrackMate - ImageJ." [Online]. Available: https://imagej.net/Getting_started_with_TrackMate. [Accessed: 12-Oct-2018].

[57] "Photobleaching in Fluorescence Imaging and Ways to Reduce It." [Online]. Available: https://www.thermofisher.com/us/en/home/life-science/cell-analysis/cell-analysis-learning-center/molecular-probes-school-of-fluorescence/imaging-basics/protocols-troubleshooting/troubleshooting/photobleaching.html. [Accessed: 09-Dec-2018].

[58] S. I. Han, S. M. Lee, Y. D. Joo, and K. H. Han, "Lateral dielectrophoretic microseparators to measure the size distribution of blood cells," *Lab Chip*, vol. 11, no. 22, pp. 3864–3872, 2011.

[59] S. Choi and J. K. Park, "Microfluidic system for dielectrophoretic separation based on a trapezoidal electrode array," *Lab Chip*, vol. 5, no. 10, pp. 1161–1167, 2005.

[60] R. Pethig, *Dielectrophoresis Theory, Methodology and Biological Applications*. Wiley, 2017.

[61] I. F. Cheng, W. L. Huang, T. Y. Chen, C. W. Liu, Y. De Lin, and W. C. Su, "Antibody-free isolation of rare cancer cells from blood based on 3D lateral dielectrophoresis," *Lab Chip*, vol. 15, no. 14, pp. 2950–2959, 2015.

# APPENDICES

## A. Fabrication Flow of DEP Spectrum Device

| | **FABRICATION FLOW OF DEP SPECTRUM DEVICE** |
|---|---|
| **1** | ***Glass wafer x3 (6")*** |
| **2** | ***Piranha (30 min) + BHF (5 min) cleaning*** |
| **3** | ***Dehydration in oven (at 110°C for 20 min)*** |
| **4** | ***Desicator for 5 min*** |
| **5** | ***Lift off process - Photolithography*** |
| ***Mask 1*** | HDMS coating 500 rpm 10 sec + 3000 rpm 30 sec |
| | S220-3 spin 500 rpm 10 sec + 3000 rpm 30 sec |
| | Softbake @ 115°C for 30 sec proximity + 3 min on hotplate |
| | Expose UV for 6 sec (vacuum contact) |
| | Develop in MF24A for 60 sec |
| | DI water rinse 90 sec + 90 sec |
| | Dry by $N_2$ |
| | Inspection |
| **5** | ***Descum 2x2 min (180° wafer turn)*** |
| **6** | ***Ti sputtering as adhesion layer (30 nm) (Bestec-1)*** |
| | 300 W $T_1$:120 sec $T_2$:165 sec Flow:2.5 sccm |
| **7** | ***Au sputtering (400 nm) (Bestec-1)*** |
| | 300 W $T_1$:120 sec $T_2$:440 sec Flow:6.2 sccm |
| **Altern.6** | ***Ti sputtering as adhesion layer (30 nm) (AJA-1)*** |
| | 600 W 270 sec 30 nm |
| **Altern.7** | ***Au sputtering (400 nm) (AJA-1)*** |
| | 350 W 680 sec 400 nm |
| **8** | ***Lift off Process - PR strip*** |
| | In acetone for 180 min |

| | |
|---|---|
| | In acetone for 5×4 min via buzzer (with clean acetone at each step) |
| | Rinse with clean acetone + IPA + DI water (gun) |
| | DI water rinse for 3 cycles |
| | Dry by $N_2$ |
| | Inspection |
| **9** | ***Dehydration in oven (at 110°C for 20 min)*** |
| **10** | ***Desicator for 5 min*** |
| **11** | ***Lithography for chamber formation*** |
| ***Mask 2*** | HDMS coating 500 rpm 10 sec + 2800 rpm 30 sec |
| | AZ40XT spin 500 rpm 10 sec + 2800 rpm 30 sec |
| | Wait for 90 min (horizontal position) |
| | Softbake @ 126°C for 7 min proximity + 5 min on hotplate |
| | Edge bead removal |
| | Expose UV for 35 sec (soft contact) |
| | Wait for 15 min |
| | Post exposure bake @ 105°C for 30 sec proximity + 90 sec on hotplate |
| | Wait for 15 min |
| | Develop in MIF826 for 140 sec |
| | DI water rinse 90 sec + 90 sec |
| | Dry by $N_2$ |
| | Inspection |
| **12** | ***Chamber thickness measurement (Dektak)*** |
| **13** | ***Parylene coating (as insulating layer)*** |
| | with silane |
| | 1 g for 0.5 μm parylene thickness |
| **14** | ***Parylene thickness measurement (Dektak)*** |
| **15** | ***Dicing*** |

## B. Fabrication Flow of DEP-based Enrichment Device

| | **FABRICATION FLOW OF DEP ENRICHMENT DEVICES** |
|---|---|
| **1** | ***Glass wafer x3 (6")*** |
| **2** | ***Piranha (30 min) + BHF (5 min) cleaning*** |
| **3** | ***Dehydration in oven (at 110°C for 20 min)*** |
| **4** | ***Ti sputtering as adhesion layer (30nm) (AJA-1)*** |
| | 600 W 270 sec 30 nm |
| **5** | ***Au sputtering layer (300 nm) (AJA-1)*** |
| | 350 W 520 sec 300 nm |
| **6** | ***Dehydration in oven (at 110°C for 20 min)*** |
| **7** | ***Desicator for 5 min*** |
| **8** | ***Lithography for Au & Ti etch*** |
| ***Mask 1*** | HMDS coating 500 rpm 10 sec + 3000 rpm 30 sec |
| | S220-3 spin 500 rpm 10 sec + 3000 rpm 30 sec |
| | Softbake @ 115°C for 30 sec proximity + 3 min on hotplate |
| | Edge bead removal |
| | Expose UV for 6 sec (vacuum contact) |
| | Develop in MF24A for 60 sec |
| | DI water rinse 90 sec + 90 sec |
| | Dry by $N_2$ |
| | Inspection |
| | Hardbake in oven from 50°C to 120°C and 30 min @ 120°C |
| | Cooling in oven from 120°C to 70°C |
| **9** | ***Descum 2x2 min (180° wafer turn)*** |
| **10** | ***Au etch*** |
| | Commercial Au etchant for 65 sec |
| | DI water rinse for 3 cycles |
| | Dry by $N_2$ |

| | |
|---|---|
| | Inspection |
| **11** | ***Ti etch*** |
| | 20 ml HF + 20 ml $H_2O_2$ + 3960 ml DI water as Ti etchant |
| | Ti etchant for 40 sec |
| | DI water rinse for 3 cycles |
| | Dry by $N_2$ |
| | Inspection |
| **12** | ***Photoresist strip*** |
| | In PRS-bath 1 for 15 min |
| | In PRS-bath 2 for 15 min |
| | DI water rinse for 10 cycles |
| | Dry by $N_2$ |
| | Inspection |
| **13** | ***Dehydration in oven (at 110°C for 20 min)*** |
| **14** | ***Parylene coating*** |
| | with silane |
| | 1 g for 0.5 µm parylene thickness |
| **15** | ***Parylene thickness measurement (Dektak)*** |
| **16** | ***Dehydration in oven (at 95°C for 40 min)*** |
| **17** | ***Desicator for 5 min*** |
| **18** | ***Lithography for microchannel formation*** |
| ***Mask 2*** | HMDS coating 500 rpm 10 sec + 2800 rpm 30 sec |
| | AZ40XT spin 500 rpm 10 sec + 2800 rpm 30 sec |
| | Wait for 90 min (horizontal position) |
| | Softbake @ 126°C for 7 min proximity + 5 min on hotplate |
| | Edge bead removal |
| | Expose UV for 35 sec (soft contact) |
| | Wait for 15 min |
| | Post exposure bake @ 105°C for 30 sec proximity + 90 sec on hotplate |

| | |
|---|---|
| | Wait for 15 min |
| | Develop in MIF826 for 140 sec |
| | DI water rinse 90 sec + 90 sec |
| | Dry by $N_2$ |
| | Inspection |
| **19** | ***Microchannel thickness measurement (Dektak)*** |
| **20** | ***Parylene coating*** |
| | without silane |
| | 40 g for 20 µm parylene thickness |
| **21** | ***Parylene thickness measurement (Dektak)*** |
| **22** | ***Dehydration in oven (at 95°C for 40 min)*** |
| **23** | ***Desicator for 5 min*** |
| **24** | ***Opening lithography*** |
| ***Mask 3*** | HMDS coating 500 rpm 10 sec + 2500 rpm 30 sec |
| | AZ40XT spin 500 rpm 10 sec + 1500 rpm 30 sec |
| | Wait for 60 min (horizontal position) |
| | Softbake @ 126°C for 8 min proximity + 7 min on hotplate |
| | Edge bead removal |
| | Expose UV for 45 sec (soft contact)<br>Interval exposure: 22.5 sec exposure + wait 1 min + 22.5 sec exposure |
| | Wait for 15 min |
| | Post exposure bake @ 105°C for 30 sec proximity + 90 sec on hotplate |
| | Wait for 15 min |
| | Develop in MIF826 for 160 sec |
| | DI water rinse 90 sec + 90 sec |
| | Dry by $N_2$ |
| | Inspection |
| **25** | ***Photoresist thickness measurement (Dektak)*** |
| **26** | ***Parylene etching with RIE*** |

| | |
|---|---|
| | in RIE (5×20 min) |
| | Inspection |
| **27** | ***Dicing*** |
| **28** | ***PR Strip*** |
| | In acetone for 4 days |